STRUCTURE/FUNCTION ANALYSIS OF TYPE IIA RECEPTOR TYROSINE PHOSPHATASES ON *DROSOPHILA* MUSCLE INTEGRITY

A DISSERTATION IN
Molecular Biology and Biochemistry
And
Cell Biology and Biophysics

Presented to the Faculty of the University
of Missouri-Kansas City in partial fulfillment of
the requirements of the degree

DOCTOR OF PHILOSOPHY

by
JESSICA E. KAWAKAMI

A.A., Longview Community College, 2001
B.S., University of Missouri, Kansas City, 2005
M.S., University of Missouri, Kansas City, 2011

Kansas City, Missouri
2018

STRUCTURE/FUNCTION ANALYSIS OF TYPE IIA RECEPTOR TYROSINE PHOSPHATASES ON *DROSOPHILA* MUSCLE INTEGRITY

Jessica E. Kawakami, Candidate for the Doctor of Philosophy Degree

University of Missouri – Kansas City, 2018

ABSTRACT

The Lar-family of receptor protein tyrosine phosphatases (RPTPs); including Lar, RPTPσ and RPTPδ, are utilized in signal transduction pathways during neural development. Fundamentally, the processes of axon guidance and synaptogenesis are carried out by rearrangements of the actin cytoskeleton for extension and maturation of structures. To determine whether this regulation is conserved in other tissues, we utilized interdisciplinary approaches for a structure/function analysis of Lar-RPTPs in the *Drosophila* musculature. We find that the single fly ortholog, Dlar, is localized to the muscle costamere in wandering L3 larvae. The costamere has important functions in muscle integrity and force transmission during contractions. Further, depletion of Dlar in the musculature causes aberrant sarcomeric actin patterning and mislocalization of the major transmembrane receptor of the costamere, integrin dimers. Ablation of two additional proteins from the musculature; including the guanine nucleotide exchange factor, Trio, and the basement membrane protein, Glutactin (Glt), results in similar disruptions to the muscle architecture. Thus, Trio and Glt provide links to actin through the Rho family of small GTPases and the BM membrane which is intimately involved in integrin signaling. We show that the actin cytoskeletal aberrations cause deficits in

larval locomotor function. Additionally, we find that the cytosolic domains of Dlar are particularly important for muscle function and have implications in integrin signaling versus physical receptor/ligand interactions which agree with x-ray crystallographic analysis of the FN4-6 repeats. A proteomic approach was utilized to find novel binding partners and resulted in identification of basement membrane proteins as conserved Lar-RPTP ligands. Finally, we offer a model for Dlar signaling that results in the low affinity integrin conformation induced by inside-out signals arising from actin remodeling.

APPROVAL PAGE

The faculty listed below, appointed by the Dean of the School of Graduate Studies, have examined a dissertation titled "Structure/Function Analysis of Type IIa Receptor Tyrosine Phosphatases on *Drosophila* Muscle Integrity," presented by Jessica E. Kawakami, candidate for the Doctor of Philosophy degree, and certify that in their opinion it is worthy of acceptance.

Supervisory Committee

Samuel Bouyain, DPhil, Committee Co-Chair
Molecular Biology and Biochemistry

Erika Geisbrecht, Ph.D., Committee Co-Chair
Cell Biology and Biophysics

Brian Geisbrecht, Ph.D.
Cell Biology and Biophysics

Jeffrey Price, Ph.D.
Molecular Biology and Biochemistry

Xiaolan Yao, Ph.D.
Molecular Biology and Biochemistry

CONTENTS

LIST OF ILLUSTRATIONS

Figure Page

LIST OF TABLES

Table Page

ABBREVIATIONS

Central nervous system	CNS
Chondroitin sulfate proteoglycans	CSPGs
Drosophila Lar	Dlar
Dystroglycan	Dg
Ectodomain	ECD
Extracellular matrix	ECM
Fibronectin type III domain	FNIII
Filamentous actin	F-actin
Focal adhesion	FA
Glutactin	Glt
Heparan sulfate proteoglycans	HSPGs
Human Embryonic Kidney 293 cells	HEK293
Immunoglobulin-like domain	Ig
Inflated	if
LamininW	WB
Lysine-glycine-aspartate	KGD
Leukocyte antigen-related tyrosine phosphatase	LAR
Myospheriod	mys
Netrin-G ligand-3	NGL-3
Neuromuscular junction	NMJ

Peripheral nervous system	PNS
Phosphotyrosine	P-Tyr
Protein tyrosine phosphatase	PTP
Receptor Protein Tyrosine phosphatases	RPTPs
Arginine-glycine-aspartate	RGD
Thin	tn
Thrombospondin	Tsp
Tiggrin	Tig
Tyrosine kinase	TK

ACKNOWLEDGMENTS

I would like to thank my co-PIs, Dr. Samuel Bouyain and Dr. Erika Geisbrecht for supporting me through all the phases of graduate education. Their expertise, enthusiasm and kindness are the driving force behind this endeavor. In addition, the members of my committee were instrumental in evaluating my progress and offering advice: Dr. Brian Geisbrecht, Dr. Jeffrey Price and Dr. Xiaolan Yao.

I would like to thank the members of the Bouyain lab: Roman Nikolaienko, Boadi Agyekum, Rana Zalmai, Victor Broerman, Sebastian Karuppan and Laurie Ray; in addition to the members of the Geisbrecht lab: David Brooks, Bridget Biersmith, Nicole Green, Zong-Heng Wang and Cindy Liu. I received additional support from the fly lab of Dr. Leonard Dobens and members: Liz Dobens, Anna Shipman, Zach Fischer, and Chris Nauman.

I would like to acknowledge the excellent facilities and resources utilized from the UMKC and OSU Mass Spectrometry Facilities, the Developmental Studies Hybridoma Bank, the Bloomington Stock Center and the Southeast Regional Collaborative Access Team beamlines at the Advanced Photon Source, Argonne National Laboratory.

Support for this work comes from the National Institutes of Health (R21AR066264) to S.B., the American Heart Association Predoctoral Fellowship Midwest Affiliate (14PRE18850079) to J.K., and the UMKC Women's Council Graduate Assistance Fund.

DEDICATION

This dissertation is dedicated to: my mother and father, Teri Iris and Alan; my family and loves, Eric, Caden and Logan; my siblings, Melissa, Derek, Robin, Jeffery, and Dini (RIP, sweetheart); and my friends and confidantes, Sandi, Jilly and Megan.

CHAPTER 1

INTRODUCTION

Tyrosine phosphorylation in metazoans

The reversible phosphorylation of tyrosine is a post-translational modification utilized for signal transduction and mediated by the opposing actions of protein tyrosine kinases (PTKs) and protein tyrosine phosphatases (PTPs). In broad terms, the role of phosphotyrosine (P-Tyr) is to provide a docking site for Src homology 2 (SH2) or phosphotyrosine-binding (PTB) domains. These domains are found in signaling proteins ranging from enzymatic kinases, phosphatases and GTPases; to small adaptor or scaffolding proteins [1,2]. Tyrosine phosphorylation is particularly important to metazoans, as it plays a central role in growth and developmental pathways [3]. Accordingly, aberrant tyrosine phosphorylation can lead to human diseases, such as cancer and diabetes [4].

The first tyrosine-specific kinase activity was discerned in the Rous Sarcoma virus protein, Src kinase (v-Src) [5,6]. Pioneering studies on cellular Src kinase (c-Src) in chicken were driven by the revelation that v-Src is similar to c-Src but with constitutively active kinase activity [7,8]. Comparison of these kinases led to two major discoveries: (1) identification of conserved mechanisms of activation and regulation for kinases as a whole and (2) recognition of tyrosine kinases as proto-oncogenic proteins [9,10]. Briefly, two major phosphorylation sites control Src activity. First, autophosphorylation of a tyrosine residue in a highly conserved region called the

activation loop causes displacement from the substrate pocket, thereby allowing the active site access to substrate [11]. Second, a carboxy-terminal P-Tyr site in c-Src that is absent from v-Src, negatively regulates kinase activity by providing an intramolecular docking site to an amino-terminal SH2 domain [11,12].

The activation state of c-Src is determined by the P-Tyr balance, and is therefore regulated by both PTKs and PTPs. Due to the cellular localization of c-Src to the plasma membrane, a number of receptor PTPs (RPTPs) have been found to dephosphorylate c-Src *in vitro;* including, RPTPα (PTPRA), RPTPλ (PTPRL) and leukocyte common antigen-related molecule (LAR/PTPRF) [9]. RPTPs are members of the Class I or classical PTPs, which include the cytoplasmic PTPs and the RPTPs. Class I PTPs have a highly conserved active site CX_5R sequence where the catalytic Cys acts as a nucleophile and Arg participates in phosphate binding [13]. RPTPs are single-pass transmembrane proteins that combine the adhesive properties of a cell adhesion molecule (CAM) to the catalytic activity of either single or tandem phosphatase domains. Typically, the membrane proximal domain (D1) is catalytically active and the membrane distal (D2) is a pseudophosphatase that plays a regulatory role. This structure allows for coupling of ligand binding to downstream signaling.

The Lar-RPTP family

RPTP research in mammals is complicated by the diversity of their extracellular domain features, with the 22 human RPTPs subdivided into eight groups (Fig. 1B). Many RPTPs are orphan receptors and the known ligands encompass a range of

proteins including: ECM proteins, CAMs and growth factors. One example of this diversity is seen in the type IIa family, or Lar-RPTPs, which are arguably the best characterized RPTPs. The Lar-RPTPs are capable of binding several structurally distinct ligands (summarized in Table 1), which will be discussed further below. The three vertebrate family members: Lar/PTPRF, RPTPδ/PTPRD and RPTPσ/PTPRS share ~ 90% amino acid sequence identity in their PTPase domains and ~75% sequence identity with the invertebrate ortholog, *Drosophila* Lar (Dlar). Overall, Lar, RPTPσ and RPTPδ share 75% residue conservation across their receptor and PTPase domains (Dlar - 50%) (Supplementary Table 1) [14]. The ectodomains of Lar-RPTPs resemble CAMs and include three immunoglobulin-like (Ig) domains followed by four to nine fibronectin type III (FNIII) repeats [15]. Further diversification is achieved through alternative splicing of four mini-exons A-D (meA-meD) which encode short peptides (Fig. 1A). The receptor is expressed as a proprotein and is cleaved by endoproteases that recognize a site in the C-terminus of the extracellular domain, the cleavage products associate at the membrane non-covalently [16]. Additional proteolytic processing results in shedding of the ectodomain, internalization of the tandem phosphatase domains and regulation of downstream protein-protein interactions [17–20].

Structural insights into the type IIa ectodomains (ECDs) have revealed highly flexible inter-domain regions, with the exception of the Ig1 and Ig2 domains, which adopt a rigid horseshoe conformation [21,22]. The ligands of the Ig1 and Ig2 domains are heparin sulfate proteoglycans (HSPGs) and chrondroitin sulfate proteoglycans

(CSPGs), which elicit antagonistic effects on the developing nervous system [23–26]. The ligand-binding site resides on a highly positively charged region of the Ig1 domain via the negatively charged HS and CS chains. This region has the same binding affinity to both HSPGs and CSPGs (K_d 10-20 nM). However, the physiological effects of these proteoglycans differ: CSPGs inhibit neurite outgrowth through trans interactions whereas HSPGs act in cis to cause receptor oligomerization and increased local phosphatase activity [22].

The interdomain region between Ig2 and Ig3 displays both heterogeneity and flexibility by alternative splicing. Inclusion of meA inserts an additional six residues into the Ig2 domain and meB increases the Ig2/Ig3 linker by an additional four residues. The mini-exons modulate trans-synaptic binding to a number of post-synaptic adhesion molecules including: dendritic neurotrophin receptor tyrosine kinase C (TrkC), IL-1-receptor accessory protein-like 1 (IL1RAPL1), Interleukin-1 receptor accessory protein (IL1RAcP), Slit- and Trk-like receptors 1-5 (Slitrks1-5) and synaptic adhesion-like molecule 5 (SALM5) and SALM3 (Table1) [27–34]. An additional trans-synaptic Lar interaction involves a tripartite complex composed of trans-synaptic NGL-1/Netrin G1 which allows for a Netrin G1/Lar cis interaction on the pre-synapse. This interaction requires both the Ig and FNIII domains of Lar and promotes synapse formation [35]

Similar to the Ig domains, the FNIII domains are alternatively spliced. Isoforms include deletions of entire FNIII domains or inclusion of meC which adds nine residues to the FN5 domain [14,36]. The additional nine residues disrupt the binding of laminin-

nidogen to Lar during cell spreading in Hela cells (Pauline O'Grady, Thai, & Saito, 1998). A secreted isoform of Lar (LarFN5C) includes an amino-terminus absent from full-length Lar, inclusion of meC and the C-terminus of the FN5 domain. LarFN5C promotes neurite outgrowth by its homophilic association with full-length Lar [37]. RPTPδ is also capable of homophilic interactions which modulate synapse formation [38]. Lastly, the post-synaptic membrane receptor, Netrin-G ligand-3 (NGL-3), binds Lar-RPTPs via FN1-2 domains at excitatory synapses (Table 1) (Kwon, Woo, Kim, Kim, & Kim, 2010; Woo et al., 2009). As organizers of synaptic formation and maturation, Lar-RPTPs and their ligands are implicated in a number of human neuropsychiatric disorders including autism spectrum disorders and schizophrenia [39].

RPTP Research in Flies

The implication that RPTPs function in neural development came from characterization of expression patterns in nervous tissue in the early 1990s, including: Dlar, PTP99A, PTP10D and PTP69D in *Drosophila*; chick RPTPσ (CRYPα); and human RPTPζ and RPTPδ [40–45]. However, the functional significance of this expression was elucidated by work in the *Drosophila* embryo. *Drosophila* is an amenable model organism for RPTP research, with eight RPTPs in the genome compared to 22 in mammals (Fig. 2) [46]. The "neural specific" *Drosophila* RPTPs mentioned above, including PTP52F characterized in 2001, are highly expressed in both central and peripheral nervous tissue [47]. *Dlar*, *Ptp69D* and *Ptp52F* single mutants display motor axon pathfinding defects during innervation of body wall muscle targets [47–49]. In

contrast, mutants of *Ptp99A* and *Ptp10D* lack a phenotype unless in combination with mutants of *Dlar*, *Ptp69D* and *Ptp52F*. Double, triple or quadruple mutants reveal intricate interactions that can be synergistic or antagonistic. Specifically, motor neurons exit the CNS and defasciculate into five nerve branches: ISN, SNa, SNb, SNc and SNd, which innervate specific muscle targets. *Dlar* single mutants display ISN truncations which increase in severity and penetrance with the concomitant loss of PTP99A and/or PTP69D. Loss of PTP10D in addition to the *Dlar Ptp69D Ptp99A* triple mutant suppresses ISN defective guidance cues (Qi Sun, Schindelholz, Knirr, Schmid, & Zinn, 2001). Additionally, *Dlar* mutants display aberrant SNb and SNd branches, but concomitant loss of PTP99A will suppress the *Dlar* phenotype in the SNb branch [50]. *Ptp69D* single mutants also disrupt SNb guidance cues but display a phenotype distinct from the *Dlar* SNb phenotype. In this instance, concomitant loss of PTP99A enhances the *Ptp69D* SNb phenotype instead of suppressing it [50]. In the SNa branch, *Ptp69D Ptp99a* or *Ptp69D Ptp10D* double mutants display aberrant axon guidance [48,51]. *ptp10 Ptp69D* double mutants also reveal RPTP function in the CNS with aberrant axon crossing at the midline, the additional loss of *Dlar* and/or *Ptp99A* (triple or quadruple) mutants exacerbates the phenotype [52].

The remaining neural phosphatase, PTP52F, is unique in that it displays defects to both the motor axons and the CNS with a single null mutation [47]. Similar to *Dlar* single mutants, *Ptp52F* mutants display truncations to the ISN branch that are exacerbated by the removal of either PTP69D or PTP10D. However, there is not a

synergistic effect in *Dlar Ptp52F* double mutants. In the SNb branch, *Ptp52F* in combination with either *Ptp10D* or *Ptp69D* double mutants result in a stall phenotype distinct from the Dlar SNb phenotype. Again, *Dlar Ptp52F* double mutants do not display synergistic effects in the SNb. In the SNa branch, PTP52F alone or in combination with Dlar, PTP69D or PTP10D (but not PTP99A) increases the SNa stall phenotype. Finally, in the CNS, loss of PTP52F results in a novel phenotype in the longitudinal tracts that can be suppressed by the concomitant loss of Dlar [47].

The mechanisms underlying axon extension are still poorly understood but are known to involve rearrangements of the actin cytoskeleton resulting in growth at the leading edge [53]. Several lines of evidence implicate Lar-RPTP family members participate in actin regulation through a number of proteins. Examples include the intracellular Abelson tyrosine kinase (Abl), *abl* loss-of-function suppresses the Dlar SNb and SNd phenotype while gain-of-function mimics *Dlar* mutants [54]. The Abl substrate Enabled (Ena), a member of the Ena/vasodilator-stimulated phosphoprotein (VASP) family, is a regulator of actin dynamics. *Ena* mutants mimic *Dlar* mutants. Both Abl and Ena are Dlar substrates, and Dlar is a substrate for Abl [54]. Additionally, the actin binding protein Profilin (*chickadee*) binds directly to Ena and genetically interacts with Abl in *Drosophila* neural development [55,56].

An additional link between Lar-RPTPs and cytoskeletal dynamics and actin assembly is through the Rho family of GTPases. *Drosophila* Trio is a guanine nucleotide exchange factor (GEF) with two Dbl homology domains that activate both

Rho and Rac GTPases. Loss of Trio or Rac exacerbates the Dlar SNb bypass phenotype [57]. Trio genetically interacts with Abl/Ena in the CNS where heterozygous *trio* and *abl* mutants display synergism in the developing longitudinal tracts and commissures, while heterozygous *ena* mutants can partially rescue *trio* mutants [58]. Trio, Ena and Dlar genetically interact in the developing visual system where photoreceptor neurons (R7-R8) form synapses with specific regions of the optic lobe in the brain [59]. Utilizing a *Dlar* mutant background, single copies of either *ena* or *trio* mutants were assessed for dosage sensitive interactions, both exacerbate the Dlar phenotype [59].

Experimentation in the *Drosophila* visual system has highlighted the complexity of Dlar signaling pathways. Additional subsets of photoreceptor neurons (R1-R6) are targeted to the optic lobe through distinct Dlar binding proteins, N-cadherin and Dliprin-α [60,61]. N-cadherin is a homophilic CAM that interacts with the cytoskeleton through the actin binding protein, β-catenin. The domain requirements for Dlar in R1-R6 targeting include both the Ig and FNIII domains; however, N-cadherin and Dlar interact via their intracellular regions. Liprin-α is a scaffolding protein that co-localizes with Lar at focal adhesions and binds to the Lar D2 domain [62]. Dlar and Dliprin-α also modulate synapse formation at the neuromuscular junction (NMJ) whereby NMJ size is sensitive to the gene dose of Dlar and Dliprin-α functions downstream of Dlar [63].

Studying RPTP function in the *Drosophila* musculature

Despite high expression of the mammalian Lar-RPTPs in neuronal tissues, the overlapping expression patterns obfuscate their function in motor axon guidance. While RPTPσ and δ single mutant mice are viable, RPTPσ/δ double mutant mice die at birth from respiratory failure. This is attributed to defective late stage extension of motor neurons, which causes abnormally thin skeletal muscle in the diaphragm and limbs [64]. The authors note that Lar-RPTP expression is not limited to nervous tissues. Northern blot analysis reveals that mRNA of human Lar/σ/δ is differentially expressed in heart, kidney, brain, muscle, and other tissues [43]. A similar study in rodent utilizing RNA *in situ* hybridization localized RPTPσ and RPTPδ mRNA to tissues of neuronal and mesodermal origin, including the striated musculature [65]. However, characterization in non-neuronal tissue in both vertebrates and invertebrates is sparse due to early lethality caused by defective neural development [49].

To determine if RPTPs function in skeletal muscle tissue, we utilized the UAS/GAL4 system to examine tissue specific knockdown by RNAi in *Drosophila* muscle [66]. In muscle tissue, the main components of the contractile machinery and the accessory proteins that stabilize and relay signals are conserved between flies and humans. Specifically, our studies focus on a specialized site in striated muscle called the costamere. The costamere is composed of transmembrane complexes that physically stabilize the internal architecture, as well as transmit signals between the internal and external environments. The vertebrate costamere contains two adhesive

protein complexes, the dystrophin-associated protein complex (DPC) and the integrin-mediated adhesion complex [67]. Patients with muscular dystrophies, such as Duchenne Muscular Dystrophy, present mutations in DPC proteins and an upregulation of integrins, while patients with cardiomyopathies display both aberrant expression and localization of integrin subunits [68,69]. The specific function of each of these adhesive complexes remains unclear. Our research has found a role for Dlar in integrin organization at the larval costamere.

Integrin adhesion complexes in muscle

Integrins are a major class of cell adhesion molecules responsible for cell-cell and cell-matrix interactions in metazoans. Transmembrane integrin receptors are heterodimers comprised of α and β subunits. Each integrin subunit has a large ECD, a single transmembrane helix and a short cytoplasmic tail. The human genome includes 18 α and 8 β subunits and 24 distinct heterodimers have been identified as of yet [70,71]. Eight of the 24 known vertebrate integrin dimers recognize RGD-containing ligands [72]. In *Drosophila* there is evidence for just four heterodimers: αPS1, αPS2, or αPS3 with βPS and αPS3βυ [73]. The αPS2βPS dimer interacts with two RGD-containing proteins, laminin W and Tiggrin (Tig) [74,75], in addition to the KGD-containing Thrombospondin (TSP) [76].

The composition of the heterodimer is determined by temporal and spatial specificity, allowing for distinct extracellular (fibronectin, collagen and laminin) and intracellular (kinases and adapter proteins) integrin-binding partners. Integrin adhesion

is usually indirect because binding occurs through the ECM. The ECM is composed of proteoglycans, including: perlecan and agrin, and fibrous proteins, such as: laminin, collagen and fibronectin [77]. Links to the actin cytoskeleton are through proteins that bind to integrin tails, including: talin, vinculin and paxillin [78].

Besides providing a structural link between the ECM and the actin cytoskeleton, integrin receptors function as a hub for inside-out and outside-in signaling. Integrin receptor activity is determined by the ability to engage in adhesive interactions based on receptor conformation. An active conformation is extended and the inactive conformation is bent (Fig. 3) [79,80]. These conformational shifts can be induced by intracellular binding partners or by the chemical environment of the ECM to promote or terminate processes such as cell survival or growth [81,82]. In striated muscle, integrin receptors are found at the myotendinous junction (MTJ), the intercalated disc (ICD), the neuromuscular junction (NMJ), and the costamere. These integrin receptors in the fly musculature are composed of αPS1βPS and αPS2βPS heterodimers [83,84]. Ablation of the common βPS subunit or the αPS2 subunit causes embryonic lethality, muscle detachment from tendon cells and disruption of the costamere [85]. Ablation of the αPS1 subunit causes larval lethality, but does not present defects in muscle attachment or costamere function [86]. Due to this early lethality associated with the αPS2βPS complex, studying their long-term functions in muscle homeostasis is challenging.

Organization and structure of dissertation

We sought to determine the role of Dlar in muscle maintenance during the *Drosophila* late larval L3 stage by genetic and biochemical methods. The first results section, Chapter 3: *Genetic Investigation of Dlar Function in Muscle Tissue*, characterizes Dlar localization and loss of function by histochemical examination of larval muscle tissue. We utilized rescue assays to attempt to determine the domains required for function in the muscle. Next, *Structural Analysis of RPTP Type IIa FN Domains 4-6* examines the sequence conservation of specific FNIII domains and utilizes x-ray crystallography to undertake a structure/function relationship of Dlar loss of function on integrin localization in larval muscle. Last, *Detecting Physical Interactions of Lar-RPTPs* examines the results of co-immunopreciption (co-IP) and pull-down experiments from both larval and mammalian cell lysates.

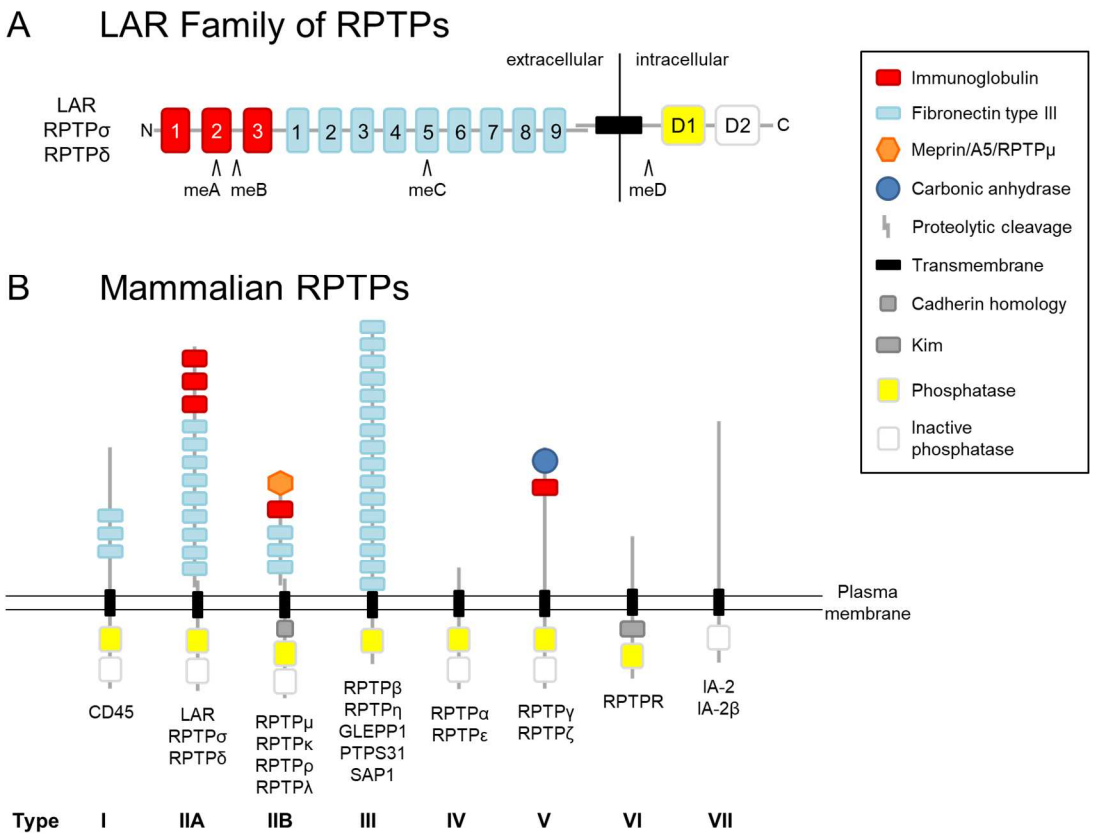

Figure 1. Schematic representation of Receptor Protein Tyrosine Phosphatase domain structure. (A) The Lar-RPTP domains with alternative splice sites of mini-exons. (B) The human genome contains 22 RPTPs subdivided into eight groups. Key to the right.

TABLE 1

LIGANDS OF THE TYPE IIA FAMILY

Ligands	**Cis/ Trans**	**RPTP**	**+/- miniexon**	**Domains**	**Functional significance**
HSPGs	Cis	LAR/σ/δ	-	Ig1-2	Axonal growth
CSPGs	Trans	LAR/σ/δ	-	Ig1-2	Axonal growth
TrkC	Trans	σ	- meA/ - meB	Ig1-3	Synapse formation
IL1RAPL1	Trans	δ	+ meA	Ig1-3	Synapse formation
IL1RAcP	Trans	δ > LAR/σ	+ meA/ + meB	Ig1-3	Synapse formation
Slitrk1-5	Trans	LAR/σ/δ	+ meB	Ig1-3	Synapse formation
SALM5	Trans	LAR/σ/δ	- meB	Ig1-3	Synapse formation
SALM3	Trans	LAR/σ/δ	+ meB	Ig1-3	Synapse formation
NGL-1/ Netrin-G1	Trans/ Cis	LAR	-	ECD	Synapse formation
Laminin-nidogen	Trans	LAR	- meC	FN5	Cytoskeletal reorganization
LARFN5C	Trans	LAR	+ meC	FN5	Neurite outgrowth
δ	-	δ	-	ECD	Synapse formation
NGL-3	Trans	LAR/σ/δ	-	FN1-2	Synapse formation
Syndecan (HSPG)	Cis	Dlar		Ig1-2	NMJ
Dallylike (HSPG)	Trans	Dlar		Ig1-2	NMJ

The known ligands of mammalian and *Drosophila* Lar-RPTP family orthologs. The binding affinity between RPTPδ and IL1RAcP is much stronger than the Lar/σ and IL1RAcP affinity (δ > Lar/σ). Lar-RPTP domains involved in binding including the presence or absence of mini-exons. Functional significance of Lar-RPTP binding.

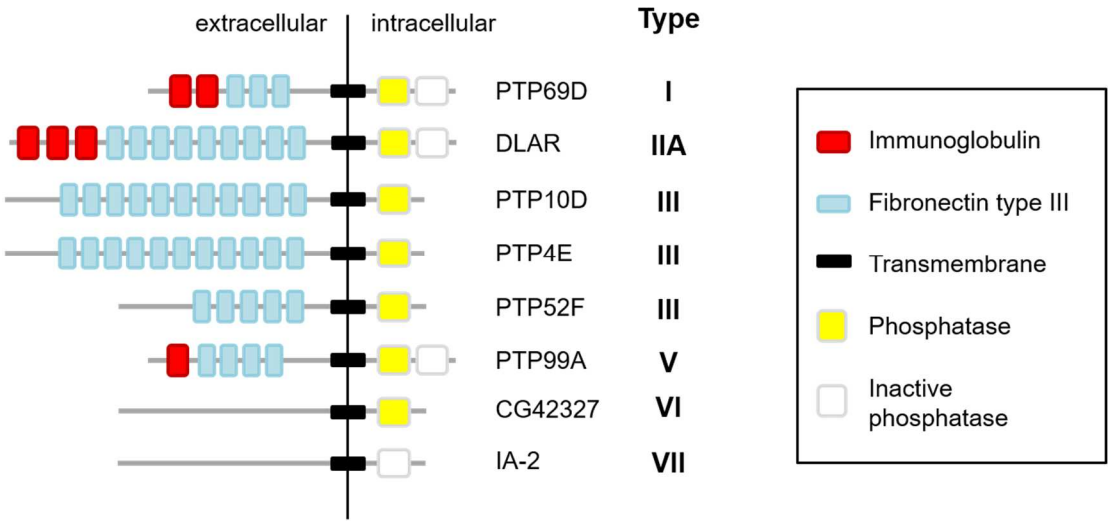

Figure 2. Schematic representation of *Drosophila* Receptor Tyrosine Phosphatase domain structure. There are eight RPTPs in the *Drosophila* genome. Type designated by orthology relationship to human RPTPs [46]. Key to the right.

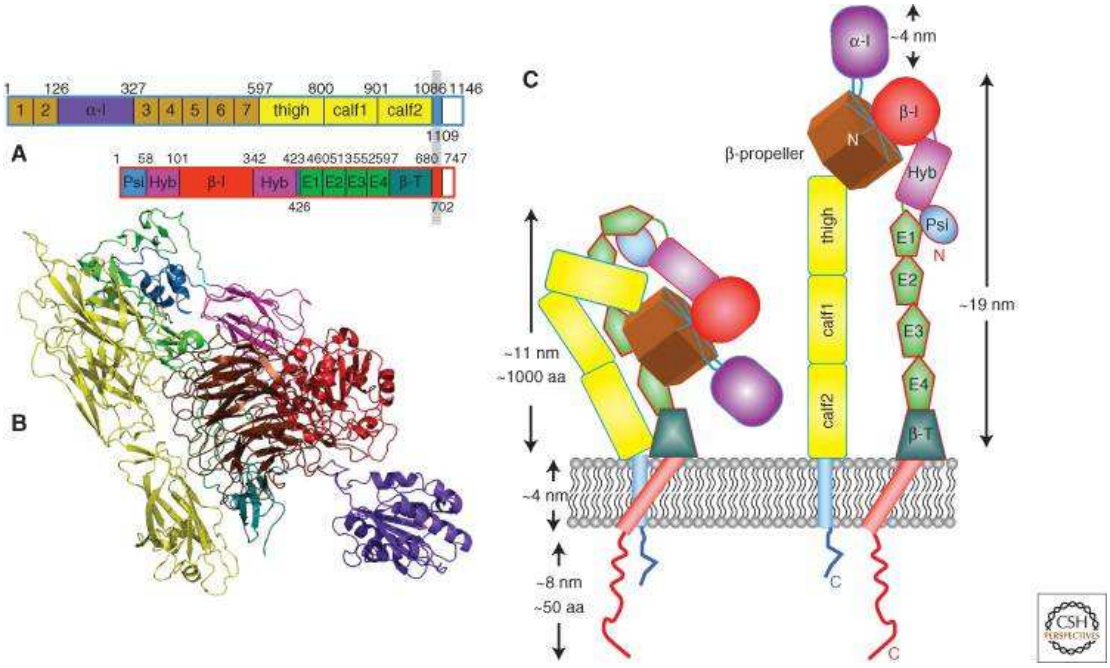

Figure 3. Activation of integrin dimers [79]. (A) Schematic representation of domains of the α (top) and β (bottom) subunits. (B) Ribbon diagram representing the bent conformation from (PDB: 3K6S). (C) Cartoon of bent (inactive) and upright (active) conformations.

CHAPTER 2

MATERIALS AND METHODS

Fly husbandry

The following stocks were obtained from the Bloomington *Drosophila* Stock Center (BDSC): *wild-type* (*WT*) strain refers to w^{1118} (BL-3605) or $y,^{1}$ w^{1118} (BL-6598) (also GAL4 driver line alone or crossed to *WT*); *Dlar13.2/CyO* (BL-8774); wg^{Gla-1}*/CyO, twi-2xEGFP* (BL-6662); *24B-Gal4* (BL-1796), *mef2-Gal4* (BL-27390); $elav^{c155}$*-Gal4* (BL-8760); *da-Gal4* (BL-55850); *UAS-Lar.K* (BL-9149); *UAS-Dlar* $RNAi^{349}$ (BL-34965); *UAS-Dlar* $RNAi^{409}$ (BL-40938); *UAS-Dlar* $RNAi^{439}$ (BL-43979); *UAS-trio* $RNAi^{277}$ (BL-27732); *UAS-trio* $RNAi^{435}$ (BL-43549); *UAS-Ptp10D RNAi* (BL-39001); *UAS-Ptp69D RNAi*; *UAS-Ptp99A RNAi*; *UAS-mys RNAi* (BL-27735); *UAS-if RNAi* (BL-27544). The following stocks were obtained from the Vienna *Drosophila* Resource Center (VDRC); *UAS-Dlar* $RNAi^{107}$ (107966kk), *UAS-Glt* $RNAi^{154}$ (v15428GD), *UAS-Glt* $RNAi^{101}$ (v101918KK). *Dlar5.5/CyO* was a generous gift from Kai Zinn. Stocks and fly crosses were raised at 25°C on standard cornmeal medium unless otherwise indicated. *Dlar13.2* and *Dlar5.5* alleles were balanced over GFP-marked balancer chromosome and mutant larvae were selected by the absence of GFP using a Nikon M165 fluorescent stereomicroscope or a Fluorescence Adapter and Filter Kit (Nightsea, Lexington, MA).

Cloning for *Dlar* transgenic fly lines utilized a pUC57 + Dlar full-length construct. A G-block containing the PTPD1 C→A active site mutation flanked by

restriction sites was digested and cloned into the pUC57 + Dlar cut vector. Additionally, the FN5 KGD→AAD mutation was cloned in the same manner. The Dlar constructs were then moved into the pUASTattB vector and their sequences verified before sending to Rainbow Transgenic Flies, Inc. (Camarillo, CA) for micro-injection. The remaining stocks for generation of rescue fly lines were obtained from BDSC: *yw*, *UAS-Dlar(ΔFn4-6)* (BL8588); *yw*, *UAS-Dlar(ΔPTPD2)* (BL8590); and *UAS-trio(III)* (BL9513). Dlar13.2 and Dlar5.5 were maintained over CyO-tm6-tb balancer. The *24B-Gal4* and *UAS-Dlar* constructs were placed over a CyO-GFP balancer.

qPCR analysis

To verify knockdown of UAS-RNAi lines, we utilized quantitative real-time PCR (qPCR). Crosses were set with the ubiquitous *da-Gal4* driver and reared at 29°C to maximize expression of RNAi. Between 1 and 5 larvae were homogenized for each biological replicate and total RNA was extracted and purified using the RNeasy Mini Kit (Qiagen). 150 ng – 600 ng of RNA was used to make single stranded cDNA using the SuperScript III First-Strand Synthesis System Kit (Invitrogen). The cDNA solution was diluted 1:10, 1:25 or 1:50 and mixed with iQ SYBR Green Supermix (Bio-Rad). Primers for the qPCR reactions were synthesized by Integrated DNA Technologies (IDT, Coralville, IA) (Table 1). qPCR assays were carried out on the CFX96 Touch Real-Time PCR Detection System with CFX Manager Software (Bio-Rad). Three

technical replicates for each biological sample were averaged to generate Ct values. The differential normalized fold change was performed using the ΔΔCt method.

TABLE 2

PRIMERS USED FOR QPCR

Gene	Forward primer	Reverse primer
rp49	5'-GCCCAAGGGTATCGACAACA-3'	5'-GCGCTTGTTCGATCCGTAAC-3'
Dlar	5'-CCCAGATGGTCGACAATAGCG-3'	5'-CCGGCTCCCATCGATGTGTA-3'
Glt	5'-AGCCTCACTAGCCACCAAC-3'	5'-CTTCCAGAGGCGGTGCTC-3'
trio	5'-TGAAACCCATCCAAGAGCCG-3'	5'-GATTGCCGTCCATTTTGCCG-3'

Immunohistochemistry and imaging

L3 larvae were collected from the side of a food vial, filleted and fixed, as previously described [87]. The following primary antibodies were obtained from Developmental Studies Hybridoma Bank (DSHB); anti-Dlar (1:10), anti-PTP10D (1:5), anti-PTP99A (1:5), anti-PTP69D (1:5), anti-αPS2 (1:50), anti-βPS (1:50), anti-Trio (1:10), anti-talin (1:5), anti-enabled (1:50), and anti-spectrin (1:5). Anti-vinculin (1:200) was purchased from Santa Cruz Biotechnology.

Custom Dlar antibodies were raised in rabbits against extracellular Dlar domain fragments; Ig12 and FN5. The purified proteins were sent to Pocono Rabbit Farm and Laboratory, following their 70-day protocol. We purified the exsanguination on an affinity chromatography column created by covalent attachment of antigen to Pierce™ NHS-activated agarose. Custom integrin antibodies were generated by GenScript (Piscataway, NJ). Briefly, peptides were used as antigens in rabbits, followed by affinity chromatography purification. The following peptides were used as antigens:

anti-αPS2 intracellular peptide CRNRPTDHSQERQPL, anti-βPS-1 intracellular peptide CKERMNAKWDTGENP, and anti-βPS-2 extracellular peptide QSMRLALRVNEKHNC. Glutactin (Glt) antibodies were raised in rabbits against peptides and affinity purified by GenScript. The following peptides were used as antigens: anti-Glt-1 n-terminal peptide SVGLRPDYNDYSDEC, anti-Glt-2 n-terminal peptide 2 PELDRLRLSESRGEC, and anti-Glt-3 c-terminal peptide CQQHPEQSLPEEQPT.

For fluorescence microscopy, phalloidin, DAPI, and Alexa Fluor® secondary antibodies were used [1:400 (Thermo Fisher Scientific)], as previously described [88]. Additionally, tyramide staining was utilized for Dlar and Trio signal enhancement (Vector Labs, Burlingame, CA). Confocal images were collected on an Olympus Fluoview 300 (UMKC) or a Zeiss 700 (KSU) and processed in ImageJ.

Phenotypic quantitation and analysis

For quantitation of sarcomeric actin defects, crosses were reared as above at 25°C. L3 larval fillets were fixed and stained with phalloidin. Larvae were scored as percent defective based on a total of 80 muscles per larvae omitting hemisegments near the anterior and posterior, as well as dorsal muscles to circumvent quantitation of artifacts from dissection. Percent defective for each cross was analyzed for 20 larvae in GraphPad Prism 6.0 by comparing the mean of each group to wild-type using the Man-Whitney t-test. For rescue, we utilized the GAL4/UAS system to drive Dlar or

Trio expression in muscle in a *Dlar13.2/Dlar5.5* mutant background. Rescue crosses were carried out at 25°C and non-GFP L3 larvae were collected for dissection.

Larval locomotion was analyzed as previously described [89]. Briefly, L3 larvae were reared as above, collected from the side of a food vial and placed on apple juice agar medium containing bromophenol blue for contrast enhancement. After 30 s acclimatization, larval movement was recorded with a Kodak EasyShare C195 camera (14 megapixels; 640 × 480 video capture resolution) for 30 – 360 s. Videos were analyzed in an ImageJ Plugin wrMTrck (ImageJ: http://imagej.nih.gov/ij/ and wrMTrck: http://www.phage.dk/plugins/wrmtrck.html). Parameters to subtract background and filter light are as follows: rolling ball radius of 0.7, boxes corresponding to 'light background' and 'sliding paraboloid' were checked; Kalman Stack, acquisition noise variance estimate = 0.05, bias to be placed on the prediction = 0.97. The measured pixels/s was converted to mm/s. 20 larvae per cross were analyzed using a one-way ANOVA in GraphPad Prism 6.0.

Immunoprecipitation and pull-down

L3 larvae were harvested from either w^{1118} or $y,^{1}\ w^{1118}$ fly lines. Larvae were homogenized with a glass homogenizer in 50 mM Tris pH 7.5, 150 mM NaCl, 0.1% Triton X-100, 1 mM PMSF, 20 µM leupeptin, 10 µM pepstatin A and +/- of the following; 1 mM EDTA, 1 mM EGTA, 1 mM $CaCl_2$ and 1 mM $MgCl_2$. Lysates were centrifuged at high speed for 5 minutes. Supernatant was pre-cleared with either of the following; Rat IgG and protein A-agarose (Sigma-Aldrich) or Rat IgG attached to

NHS-activated agarose. Coupling efficiency was assessed by SDS-PAGE and coomassie stain. After pre-clear, immunoprecipitations were carried out with monoclonal antibodies against αPS2, βPS and Dlar (DSHB). The antibodies were incubated in supernatant and subsequently precipitated with protein A-agarose. Protein was eluted with 4x SDS + β-mercaptoethanol gel running dye and run on a 7.5% SDS-PAGE gel. Bands of interest were excised, reduced and alkylated, then subjected to in-gel trypsin digestion by standard methods. Extracted peptides were analyzed by capillary LC-tandem mass spectroscopy (LCMS) by Dr. Andrew Keightley (UMKC). The mass spectrometer (Thermo Finnigan Linear Ion trap LTQ) was operated in data dependent mode, with 8 dependent scans per survey scan. Protein identifications were made using Mascot protein identification software (Matrix Science) searching against Swiss-Prot release 57.15 database (3-02-2010, 515,203 sequences) or a custom *Drosophila*-only database downloaded from NCBI. Mass tolerances for database searches were 1.6 Da for peptide mass (precursor m/z), and 0.9 Da for peaks in the MS/MS scans. Protein identifications were considered acceptable when peptide matches exceeded the threshold for 95% confidence [90]. Additionally, purified rabbit anti-Dlar Ig12 antibodies were utilized as above, except the gel was shipped to the Recombinant DNA/Protein Resource Facility, Oklahoma State University (OSU, Dr. Steve Hartson), for identification using LC–MS/MS and run on either an Oribtrap Fusion Tribrid or an LTQ Oribtrap XL Hybrid Fourier Transform Mass Spectrometer (Thermo Scientific). Alternatively, rabbit antibody was covalently attached to NHS-

activated agarose for IP and subsequent MS analysis of the resin (OSU). Pull-down experiments were performed with Dlar Ig12 and Dlar FN5 over-expressed in *Escherichia coli*, purified and covalently attached to NHS-activated agarose. DlarEcto and Glt were expressed as Fc fusion proteins in HEK293 cells, purified and either precipitated with protein A-agarose or attached to NHS-activated agarose. Either purified proteins or NHS-attached proteins were incubated in pre-cleared larval lysates. Polyacrylamide gel or NHS agarose were analyzed by MS at OSU. For LC-MS/MS on the LTQ Oribtrap XL, peptide and protein identification was carried out in Scaffold version 4 (Proteome Software), Benjamini-Hochberg $p < 0.05$.

Protein expression and purification

Dlar FN5 (residues 706-812) was amplified by PCR from a *Drosophila* cDNA library and cloned into a pT7HMP vector. Protein expression in *Escherichia coli* BL21(DE3) cells resulted in a hexahistidine fusion protein with a human rhinovirus 3C protease cleavage site. Following homogenization and lysis of cells, protein was purified by batch binding on nickel sepharose resin. After proteolytic cleavage of the hexahistidine tag, protein was purified by immobilized-metal affinity and ion exchange chromatography. Dlar FN4-6 (residues 611-907) was purified as above, except the construct was obtained from IDT as a gBlock™. Dlar Ig12 (residues 32-237) was expressed and purified as previously described [21]. Briefly, the obtained clone comprises a modified pET32 vector (Novagen), called pET32HP, expressing a thioredoxin tag, a hexahistidine tag and a human rhinovirus 3C protease cleavage site (Bouyain et al.

2010). Expression in *Escherichia coli* Origami2(DE3) cells (Novagen) allows for proper formation of disulfide bonds. Purification of the cleaved protein was achieved by immobilized-metal affinity, ion exchange and size-exclusion chromatography. The remaining constructs were cloned into pET32HP and purified as above; Dlar FN4-5 (residues 608-812) was cloned by PCR and Mlar FN5 (residues 710-810) was purchased from GeneScript.

Transient expression of proteins in HEK293 cells from a pHLSEC2Fc vector results in a fusion protein of Human IgG Fc. Conditioned media is dialyzed against 20 mM Tris pH 7.5, 150 mM NaCl and affinity purified on protein A-agarose [91]. Alternatively, Fc fusion proteins can be dialyzed against 10mM Hepes pH 7.5, 150 mM NaCl for subsequent AlphaScreen™ (Perkin Elmer) or against Hank's Balanced Salt Solution (HBSS) for cell binding assay. For AlphaScreen™, additional proteins were transiently expressed in HEK293 cells from a pFcYTS vector comprising fusions of chicken IgY Fc, which does not bind to protein A, followed by a Twin-Strep-tag® (tandem Strep-tags joined by a linker sequence (WSHPQFEKGGGSGGGSGGSAWSHPQFEK)) [92]. Conditioned media is dialyzed against 10mM Hepes pH 7.5, 150 mM NaCl. The following proteins were transiently expressed in HEK293 cells; DlarEcto, Dlar Ig12, Dlar FN46, Dlar FN5, Glt (full-length), Gltn1, Gltn2, Gltc3, Dally and Cd98Hc. Western blotting with rabbit anti-human IgG Fc or Strep-Tactin®-AP (Iba Lifesciences Goettingen, Germany) confirmed expression of fusion proteins.

X-ray crystallography

Crystals were grown by hanging drop diffusion at 20°C. Conditions of crystallization and cryoprotection are listed in Table 2. X-ray diffraction data was collected at the Advanced Photon source of Argonne National Laboratory from the Southeast Regional Collaborative Access Team (SER-CAT) beamlines 22-BM and 22-ID. Data processing was done with HKL2000 software [93]. Structure solutions were obtained using the PHENIX suite software [94], models were manually built in COOT software and refined by PHENIX [95]. For graphical representations of structures PyMol software (www.pymol.org) was utilized. The model for Dlar FN5 was obtained by single-wavelength anomalous diffraction (SAD) from Zn^{2+} ions bound to the KGD motif. PHENIX AutoSol and AutoBuild routines gave a BAYES correlation coefficient of 40 ± 11 and figure of merit of 0.517. The initial model was used for molecular replacement-SAD, new BAYES correlation coefficient of 75 ± 3.35 and figure of merit of 0.733. Both HPTPRD(FN4-6) and Mlar(FN5) were solved by molecular replacement in PHASER PHENIX utilizing the Dlar FN5 as the initial model.

TABLE 3

CRYSTALLIZATION AND CRYOPROTECTION CONDITIONS

Protein	Conc. (mM)	Crystallization conditions	Cryoprotection conditions
Dlar FN5	1	100 mM HEPES pH 7.0, 200 mM Ammonium acetate, 3mM Zinc acetate, 25% (w/v) PEG 3350	100 mM HEPES pH 7.0, 200 mM Ammonium acetate, 5mM Zinc acetate, 25% (w/v) PEG 3350, 10% (w/v) PEG 400
Human PTPRD FN4-6	1	200 mM Magnesium formate, 20% (w/v) PEG 3350,	200 mM Magnesium formate, 20% (w/v) PEG 3350, 15% (v/v) glycerol
Mouse Lar FN5	1	100mM Na-cacodylate pH 6.5, 1.4 M Na-citrate tribasic dehydrate	100mM Na-cacodylate pH 6.5, 1.4 M Na-citrate tribasic dihydrate, 30% (w/v) sorbitol

Binding assays

The PerkinElmer AlphaScreen (Amplified Luminescent Proximity Homogeneous Assay) technology is used to detect interactions between fusion-tagged proteins. We utilized StrepTactin-coated donor beads, an engineered streptavidin and protein A-coated acceptor beads to detect binding between Fc-fusion and FcYTS-fusion proteins. Upon excitation at 680 nm, the donor bead containing phthalocyanine converts ambient oxygen to a reactive form of O2, singlet oxygen. An acceptor bead within 200 nm of singlet oxygen transfers energy to thioxene derivatives, resulting in a luminescent signal at 520-620 nm. In a 96-well conical bottom plate (Thermo Fisher Scientific) fusion proteins are incubated together for one hour, followed by a one-hour incubation with acceptor beads. After addition of donor beads, the reaction is transferred to an opaque 96-well microplate (PerkinElmer Life Sciences) and allowed to equilibrate for an additional 1 hour. Signal detection takes place in an EnSpire multimode plate reader (PerkinElmer Life Sciences). Control reactions contained Fc-only and Rb anti-Dlar Ig12 (or FN5) antibodies.

For cell binding assays with Human IgG Fc fusion proteins, HEK293 cells were trypsinized from a confluent T-25 plate and resuspended in 10 mL of media, then diluted 1:10 with media. Acid washed, autoclaved 18-mm coverslips were placed into each well of a 12-well plate and covered with 1 ml of media plus 0.5 mL of the diluted cell solution. Cells were transfected with 0.5 – 1 μg of pHLSEC2 vector containing DlarEcto with an Emerald-tagged transmembrane sequence. Cells are ready for binding

assay in two days. To 1 mL of dialyzed Fc fusion protein in HBSS add 10 µL of normal goat serum and 0.5 µl of goat anti-human Fc – AlexaFluor 568 and incubate on ice for 30 m in the dark. Media was aspirated from wells, washed with HBSS, followed by addition of the Fc fusion protein conjugated to AlexaFluor to each well and incubated for 30 m in the dark. After incubation, conjugate was removed then coverslips were washed with HBSS and fixed in 4% (v/v) paraformaldehyde and DAPI for 15 – 30 m. After PBS wash, coverslip is removed from the well with forceps, washed with water, blotted dry on a kimwipe and mounted onto a glass coverslip with 1 drop of Aqua Poly/Mount solution (Polysciences, Inc. Warrington, PA).

Specific contributions

Jessica Kawakami: Fly husbandry, immunohistochemistry, phenotypic quantitation and analysis. Antibody purification, IPs and pull-downs. Expression and purification of Dlar Ig12, Dlar FN5, Dlar FN4-6, Mlar FN5. Crystallization and structural determination of Dlar FN5 and Mlar FN5.

Samuel Bouyain: Crystallization and structural determination of human PTPRD(FN46). Mammalian cell expression of fusion proteins, and purification of Fc fusion proteins for AlphaScreens and cell binding assays. Design of βPS custom antibodies.

Erika Geisbrecht and David Brooks: Fly husbandry and molecular biology including generation of rescue lines and qPCR. Immunohistochemistry, phenotypic quantitation and analysis, and locomotion assays. Design and characterization of Glt custom antibodies.

Rana Zalmai: Larval dissection and phenotypic quantitation.

CHAPTER 3

GENETIC INVESTIGATION OF DLAR FUNCTION IN MUSCLE TISSUE

Overview

Focal adhesions (FAs) are comprised of integrin dimers that link the ECM to the actin cytoskeleton. Skeletal muscle fibers form two distinct FA complexes, one at the myotendinous junction (MTJ) and the other at the costamere. *Drosophila* myofibers are attached through the ECM at both ends to tendon cells which contact the epidermis. The contractile unit of a muscle fiber is the sarcomere, which spans from Z-disc to Z-disc. The sarcomere is made up of thin filaments, filamentous actin (F-actin), and is interdigitated by thick filaments, myosin. The contractile force of actin and myosin are transmitted laterally by the costamere at Z-discs to the MTJ which translates to movement via tendon cell attachment to the exoskeleton, comparable to muscle-tendon-bone force transmission in vertebrates. I present data that show heterodimers of the larval muscle costamere are perturbed by Dlar depletion.

Dlar functions in larval muscle integrity

To determine if *Drosophila* RPTPs function in muscle tissue, the GAL4/UAS system was utilized for muscle-specific knockdown of RPTPs by RNA interference (RNAi) (Brand 1993). In neural development, *Dlar* and *Ptp69D* are classed as lethals and *Ptp10D* and *Ptp99A* are viables, displaying no phenotype upon deletion [46]. Therefore, crosses to the ubiquitous *da-GAL4* driver act as a control to confirm that only the *UAS-Dlar^{349} RNAi* and *UAS-Ptp69D RNAi* crosses are lethal (Fig. 4,D). Next, crosses to the muscle-specific drivers, *24B-GAL4* and *mef2-GAL4*, resulted in pupal

lethality in *UAS-Dlar*^{349} *RNAi* (Fig. 4,D). The remaining RNAi lines crossed to *24B-GAL4* and *mef2-GAL4* were viable as determined by the presence of adults eclosing indicating that lethality was specific to Dlar ablation and not to RPTP ablation in general (Fig. 4,D).

Pupal lethality resulted in no adults for analysis; therefore, examination of muscle tissue was carried out on late larval third instar (L3) stage. The larval muscle pattern is established during embryogenesis. The abdominal segments (A2-A7) have a stereotyped pattern of 30 muscles per hemisegment (Fig. 5A, superficial muscles only) [96]. *24B-Gal4 > UAS-Dlar*^{349} *RNAi* larvae are smaller in size but display normal muscle patterning and intact muscle-muscle attachments compared to *WT* (size difference of *Dlar*-depleted flies will be discussed further below) (Fig. 5A,B). Closer examination reveals sarcomeric patterning defects and overall decreased muscle integrity marked by split, broken or tearing myofibers, and enlarged spaces between adjacent myofibers (Fig. 5D). In addition, wildtype muscles have regularly spaced nuclei whereas knockdown displays irregular nuclear spacing, an additional indicator of muscle disease (Fig. 5D) [97].

Immunofluorescene with anti-Dlar FN5 antibodies show Dlar localization in larval body wall muscles, specifically in the sarcolemma, near the costamere (Fig. 6). The presence of the costamere complex in the *Drosophila* larval musculature was recently confirmed [67,92]. Mammalian Lar associates with FAs in the breast cancer cell line, MCF7 [62]. Additionally, on the basal surface of the *Drosophila* follicular

epithelium, Dlar is localized to the junction of three cells, which is the basal membrane iteration of FAs [98].

Ablation of Dlar results in costameric integrin mislocalization

The integrin dimers of the *Drosophila* larval costamere are comprised of βPS encoded by *myospheroid* (*mys*) and αPS2 encoded by *inflated* (*if*). In follicular epithelia, *Dlar* and *mys* mutant clones display loss of F-actin polarity and βPS mislocalization resulting in a round egg phenotype. Further, decreasing the *mys* gene dosage by half in a *Dlar* null background increases the penetrance of the phenotype [98,99]. To determine if this interaction is conserved in the larval muscle costamere, we utilized immunofluorescence to visualize βPS integrin localization in *Dlar*-depleted muscle (Fig. 7). In *WT* larval muscle, βPS is found at MTJs (Fig. 7A) and circumferentially where the membrane aligns with Z-discs (Fig. 7C). Dlar knockdown larvae display normal βPS distribution at the MTJ (Fig.7B), consistent with the absence of Dlar protein there (Fig. 6A). However, the costameric association of βPS is lost and instead is broadly distributed across the sarcolemma (Fig. 7D). To control for off-target effects of Dlar RNAi, we examined the larval muscle of two additional *UAS-Dlar RNAi* lines (BL40938 and BL43979) crossed to the *24B-GAL4* and *mef2-GAL4* driver. F-actin staining of muscle in all *Dlar*-depleted larvae show hypercontraction indicated by a shortening of sarcomeres (Fig. 8B,C) and mislocalization of βPS at the costamere (Fig. 8A'-C',A"-C"). Additionally, αPS2 immunofluorescence phencopies βPS localization in all *UAS-Dlar RNAi* lines crossed to muscle drivers (not shown). Moreover, the actin and integrin defects are caused by Dlar depletion specifically as

24B-GAL4 < UAS-Ptp69D RNAi larvae exhibit normal integrin distribution at both MASs and costamere (Fig. 8A,B).

Examination of integrin depletion in larval muscle requires utilization of the temperature sensitive muscle driver, *mef2-GAL4/GAL80,* because integrin knockdown is lethal before larval hatching [100]. Careful rearing at 18°C until 1st instar larvae hatch followed by incubation at 29°C for staging allows *mys*- and *if*-depleted larvae to reach L3 stage. Severe muscle detachment in the *mys*-depleted muscle show either complete loss of sarcomeric patterning or intense Z-disc staining (Fig. 9A). Examination of Dlar localization by immunofluorescence in and *mys*-depleted muscle shows a similar pattern: the protein is mislocalized in muscles with severe sarcomeric patterning defects but remains associated with Z-disc in muscles that maintain normal sarcomeric patterning. Previous characterization of integrin null mutants revealed that the muscle detachment phenotype of *if* occurs later in development and is less severe than *mys* mutants (discussed in Chapter 1) [101]. Hence, the ablation of *if* results in a hypercontraction phenotype that is more similar to the hypercontraction phenotype observed after Dlar depletion (Fig. 9B). The localization of Dlar in *if*-depleted muscle is partially disrupted, with some Z-disc association as well as accumulation on the lateral surface (Fig. 9B). Taken together, severe disruption of the actin cytoskeleton results in Dlar mislocalization; however, we cannot determine whether Dlar localization is dependent on integrin localization from these experiments.

Integrin adhesion complexes (IACs) include cytosolic proteins that link integrin to the actin cytoskeleton and participate in signaling. The proteins that make up the

integrin adhesome and their downstream functions are specific to the cellular context of the IAC. One protein found to be indispensable to the IAC in all cellular contexts thus far is Talin (*rhea*), a large homodimer composed of an N-terminal "head" and C-terminal "rod" [102,103]. The head region contains a four-point-one, ezrin, radixin, moesin (FERM) domain that binds to an array of proteins incuding: βPS tails, the plasma membrane and actin [104]. The rod domain has additional actin binding sites and tension reveals ancillary sites; namely for vinculin, another actin binding protein [105–107]. Integrin activation is negatively regulated by tyrosine phosphorylation which decreases Talin binding affinity and results in decreased integrin ligand binding (inside-out signaling) [108–110]. In *Drosophila*, *mys* or *if* mutant embryos lose Talin localization at muscle membranes indicating early Talin recruitment is integrin dependent [111]. *rhea* mutant embryos have strong muscle detachment, but integrin localization does not require Talin. We next examined Talin localization in Dlar knockdown larvae and found Talin retains a wildtype localization at the costamere and MTJ (Fig. 10). This differs from previous work in *Drosophila* where mutations in genes that influence costamere integrity, results in mislocalization of Talin in conjunction with βPS [92]. This is also interesting because if βPS was a substrate for Dlar, dephosphorylation should result in increased Talin binding; whereas, it appears that Talin localization is maintained despite βPS mislocalization. Talin has integrin independent functions, but this may indicate that Dlar helps maintain integrin localization but does not disrupt early recruitment of costamere proteins [112].

Dlar-interacting proteins in muscle maintenance

To determine if known Dlar-interacting proteins functioned with Dlar in the larval musculature, we utilized a reverse genetic approach. The widely expressed Dlar-interacting protein called Trio is a Rho guanine nucleotide exchange factor (GEF) protein consisting of spectrin-like repeats, tandem Dbl homology (DH) and Pleckstrin homology (PH) sequences and a src homology 3 (SH3) domain [57]. Mammalian Trio has a C-terminal serine/threonine kinase and Ig-like domains that are absent in fly Trio [113]. Trio was identified by a yeast interaction-trap assay and binds to Lar-PTPD2, the non-catalytic PTPase domain [15,113]; however, *Drosophila* Trio is phosphorylated on tyrosine residues and could be a Dlar substrate [114]. *In vivo*, Trio and Lar co-localize at FAs [113]. In mice mutants, *trio* knockout causes abnormal muscle and neural development [115]. *Drosophila trio* mutants display abnormal muscle patterning in the embryo, in addition to axon guidance defects in the CNS, PNS, and visual system [116,117]. In the *Drosophila* embryo, loss of Trio or Rac function (but not Rho) in a *Dlar* mutant background exacerbates the Dlar phenotype in motor axon guidance [116].

To determine Trio localization in the larval muscle, we dissected *WT* L3 larvae for immunolocalization and find that Trio protein localizes to Z-discs (Fig. 12C). Larval muscle tissue from *UAS-trio^{277} RNAi* and *UAS-trio^{435} RNAi* crossed to *mef2-Gal4* drivers display hypercontracted muscle (Fig. 11B,C,E,F) and mislocalization of integrin subunits at the costamere (Fig. 11B',C',E',F'). To determine if the localization of Dlar was dependent on Trio, examination of *24B-GAL2 > UAS-trio RNAi* was assessed with anti-Dlar FN5 antibodies (Fig. 12A,B). Additionally, *mef2-GAL4 > UAS-*

Dlar^{349} *RNAi* L3 larave were stained with Trio antibodies (Fig. 12C,D). Neither protein is required for the localization of the other. Surprisingly, Talin is absent from Z-discs in Trio knockdown (Fig. 13) and Trio is mislocalized in αPS2 knockdown. These observations suggest that Trio may function in a Dlar-independent pathway. Alternatively, Trio may have multiple inputs at the costamere which results in the additional mislocalization of Talin.

Genetic analysis of Glt in larval muscle

Our initial proteomics experiments identified a basement membrane (BM) protein called Glutatactin (Glt) in the Dlar and integrin immunoprecipitates (Chap. 5). Glt is a tyrosine sulfated glycoprotein first identified in the *Drosophila* embryo as a component of BMs surrounding both neural and muscle tissue. Glt is a member of a family of cell surface glycoproteins that have an acetylcholine esterase domain that lacks a functional catalytic site, which includes: neuroglians, gliotactin, neurotactin and thyroglobulin [118,119]. These proteins participate in cell adhesion through interactions with the cholinesterase domain. Glt acts as a repulsive signal for a subset of motor neurons [120]; but most recently, Glt was identified as a costamere associated protein by the Vigoreaux Lab (unpublished data).

To examine localization of Glt in larval muscle tissue, we used custom antibodies raised against peptides found in the N- and C-terminal regions of Glt (see materials and methods). These reagents show Glt localizes to the BM surrounding larval muscles (not shown). Glt is synthesized in the fat body and muscles for incorporation into BMs [118,120]. Importantly, muscle-specific depletion of *UAS-Glt*^{154}

RNAi and *UAS-Glt^{101} RNAi* phenocopies Dlar knockdown displaying hypercontraction, costameric integrin mislocalization and aberrant nuclear positioning (Fig. 14A,B). Dlar is mislocalized in Glt knockdown (Fig. 14C,D) but appears normal in Trio knockdown despite loss of sarcomeric patterning (not shown). This may indicate that Dlar is downstream of Glt and upstream of Trio. Alternatively, Trio may function independently of Dlar and Glt. Finally, disruption of the BM may result in Dlar mislocalization independent of a specific Dlar/Glt interaction.

αPS2βPS integrin mislocalization results in decreased muscle function

To determine the functional significance of hypercontraction and integrin mislocalization we utilized a locomotion assay optimized by our lab to measure the speed of larval crawling [89]. Decreased locomotor activity in L3 stage was described for dystrophic *tn* mutants displaying sarcomeric patterning defects and βPS mislocalization [87,121]. Results of the locomotion assay are represented in Figure 16. First, we analyzed *Dlar13.2/Dlar5.5* and *trio^{6A}/trio^{1}* mutants. Larval crawling is a complex behavioral outcome that is a coordinated response of the neuromuscular system to stimuli. Therefore, decreases in larval crawling speeds can be attributed to muscle integrity or injury, but also to cognitive impairment or improper innervation. *Dlar* and *trio* mutants display defective neural development in embryogenesis. We find impairment of larval crawling (Fig. 15A), with the largest decrease in *trio* mutants consistent with previous findings in the neural system and in our muscle phenotypic results indicating that Trio likely receives multiple inputs. The three *UAS-Dlar RNAi* lines (BL34965, BL40938, BL43979) crossed to the *24B-GAL4* driver show decreased crawling speeds compared

to the driver line crossed to *WT* (Fig. 15B). Similar to our characterization of muscle defects, all *trio* and *Glt RNAi* lines crossed to the *24B-GAL4* driver display decreased larval crawling speeds (Fig. 15C,D). It is necessary to note that Trio depletions in both the neural and muscular systems result in aberrant synaptogenesis, so it is impossible to attribute the decreases in crawling speeds solely to muscular defects. Likewise, muscular expression of Glt influences innervation of target muscles; however, depletion of Glt protein was not assessed [120].

Muscle-specific depletion of Dlar results in smaller pupae

The "thin" pupal phenotype characterized by Ball *et. al.*, comprises an inability of the larval muscles to shorten and this results in pupae which are long and thin [121]. Examination of the larval musculature revealed aberrant striations that were later shown to be progressive muscle wasting from breakdown of the costamere [92]. In contrast, the muscles and pupae of *24B > Dlar^{349}RNAi* flies appeared smaller overall (Fig. 5C, 16A,B). To characterize the size phenotype and to rule out off-target effects of the RNAi line, we took pupal case measurements (Fig. 16). Briefly, *Dlar13.2/Dlar5.5* pupae are smaller in both length and width resulting in a length/width ratio similar to *WT* (Fig. 16C). The early muscle driver, *mef2-Gal4*, crossed to three *UAS-Dlar RNAi* lines results in decreases to both length and width compared to *WT* or *mef2 > GltRNAi* (Fig. 16D). *24B-Gal4 > GltRNAi* results in the greatest decreases in both length and width compared to *WT* (Fig. 16E). Importantly, the neural driver, *C155-Gal4 > UAS-Dlar^{349}RNAi* pupae that have no significant change in length or width compared to *WT*. Thus, the changes in size are most likely attributed to the

muscle-specific function of Dlar. Additionally, the pupal size of both *mef2 > Dlar^{349}RNAi* and *24B > Dlar^{349}RNAi* are slightly smaller than *Dlar* mutant pupae possibly due to lethality in earlier stages in mutant flies which would have both neural and muscular defects. The size phenotype of Dlar knockdown pupae are not observed in Glt or Trio (not shown) depleted flies; indicating, that in muscle, Dlar has an additional function or functions independently.

Structure/function analysis of Dlar in muscle integrity

To determine if the muscular expression of Dlar could rescue hypercontracted muscle we expressed *UAS-Dlar* lines using a *24B-Gal4* driver in a *Dlar*-/- background (*Dlar13.2/Dlar5.5*). The hypercontraction phenotype was quantitated as described in Chapter 2 and reported as percentage defective. Overall, a statistical increase in percentage defective is observed for *Dlar13.2/Dlar5.5*, *24-Gal4 > UAS-Dlar RNAi*, *24-Gal4 > UAS-Trio RNAi* and *24-Gal4 > UAS-Glt RNAi* (Fig. 18). However, the percentage defective only reaches ~25% as a maximum whether ablation was of Dlar, Trio or Glt and is not significantly increased in all RNAi lines. This may represent a threshold where a higher number of defects results in lethality at an earlier stage. Conversely, the percentage defective may indicate a low penetrance of the actin phenotype.

For rescue, *UAS-Dlar WT* as a control for muscle-specific expression with *24B-Gal4* in a *Dlar-/-* mutant background. These results were compared to the following UAS- lines to determine the domain requirements of Dlar in muscle tissue: *UAS-Dlar ΔFN4-6*, *UAS-Dlar$^{KGD\rightarrow AAA}$*, *UAS-Dlar^{C1638A}* and *UAS-Dlar ΔPTPD2*. First, all UAS-

Dlar constructs expressed with a muscle driver cannot rescue the lethality of the D*lar*-/- background. The *UAS-Dlar ΔFN4-6* and *UAS-Dlar*$^{KGD\rightarrow AAA}$ were constructed to test the hypothesis that the FN4-6 domains have a ligand binding site specific for the Dlar/integrin genetic interaction in muscle and in the follicular epithelia (further discussed in Chapters 1 and 4) [98,122]. Further, that this may represent a physical interaction between Dlar and integrins with the conserved KGD tripeptide found in the fifth FNIII domain of Dlar (further discussed in Chapter 4). The remaining two lines will determine whether Dlar phosphatase activity is important in muscle function. We compared *Dlar13.2/Dlar5.5; 24B-Gal4* to the *Dlar13.2/Dlar5.5; 24B-Gal4 > UAS-* lines. We found that the mutant line with *24B-Gal4* alone decreases from ~20% to ~10% making it similar to the driver crossed to *WT*; although, still statistically more defective than *WT* alone (Fig. 18). This may indicate a variability in the actin defect in the mutant line. Regardless, a modest rescue for the following *UAS-Dlar* constructs was observed: *UAS-Dlar WT*, *UAS-DlarΔFN4-FN6*, and *UAS-Dlar*$^{KGD\rightarrow AAA}$, indicating that muscle expression of Dlar can partially rescue hypercontration of the *Dlar*-null. It also indicates that the FN4-FN6 domains and the KGD motif is not required for Dlar function, as the KGD→AAA substitution rescued similar to *WT* while removing the entire FN4-FN6 region only accounted for a slight decrease in the ability to rescue.

The phosphatase activity of Dlar is limited to the membrane proximal, D1 domain. We utilized an active site mutation in the D1 domain where the cysteine residue of the CX_5R site is mutated to an alanine to abolish catalytic activity. The *UAS-Dlar*^{C1638A} expression driven by *24B-Gal4* results in a decrease in percent defective but

it is not statistically relevant, indicating that phosphatase activity may not be necessary for Dlar function in muscle integrity (Fig. 19). This is correlative to previous studies utilizing a neural driver to express a *UAS-Dlar^{C1638S} mutant* for rescuing the lethality of *Dlar-/-* mutant flies. However, the *C155-Gal4* expression rescued nearly to *UAS-DlarWT* levels [122]. Further, truncation of the PTP D2 domain, *UAS-DlarΔPTPD2*, resulted in earlier lethality with no 3rd instar larvae for dissection. The D2 domain lacks catalytic activity but has a regulatory function as removal of the D2 domain causes an *in vivo* increase of PTPase activity compared to Dlar wildtype [122]. We surmise that an important cytosolic Dlar-binding partner is necessary for muscle function or that the unregulated PTPase activity causes a recessive gain-of-function when expressed in the muscle. To discern between the two possibilities, it would be necessary to test another construct involving the PTPD2 truncation in addition to the C1638A point mutation in the D1 domain. Reiteratively, experiments utilizing a *UAS-DlarPTPD2* truncation and neural driver in the Dlar-/- background cannot rescue lethality [122]. Additionally, a gain-of-function occurs when a neurally-expressed *UAS-DlarD2C1929S* in Dlar-/- background increases the SNb bypass phenotype (discussed in Chapter 1) [122].

Conclusions

The most striking finding of the work presented here is that the receptor phosphatase Dlar localizes to costameres of *Drosophila* larval muscles. This result is in stark contrast to earlier published works from which Dlar appeared to be almost exclusively found in neural tissues. Furthermore, knocking down the expression of Dlar using a muscle-specific driver results in hypercontraction, mislocalization of

costameric integrin subunits and decreased locomotor activity in the L3 stage. Thus, these experiments suggest that Dlar plays a role in the maintenance of muscle tissues. The signaling properties of Dlar on cytoskeletal rearrangements has been well documented during neural development as well as during oocyte elongation [56,61,98]. We primarily focused on the mechanism of Dlar during oocyte elongation because of the demonstrated genetic interaction between Dlar and integrins during this process. Integrins interact with ligands that include the RGD – and to a lower extent KGD – peptides and the FN5 domain of Dlar includes one such stretch of amino acids that is conserved in vertebrate homologs of Dlar. Thus, we speculated that the FN5 domain of Dlar serves as an integrin-binding site. The results of the rescue experiments and structural analysis (Chapter 4) indicates that these proteins likely do not physically interact. Other regions of the Dlar ECD have been implicated in axonogenesis and synaptogenesis in the neuromuscular system (Ig12) and the developing visual system (FN7-9), and there are now more than ten distinct ligands identified for the verterbrate orthologs which interact with regions encompassing the entire ECD (discussed in Chapter 1). Consequently, further deletions of the ECD should enable identification of the region involved in muscle integrity. An important finding is the earlier lethality imparted by the expression of the *UAS-DlarΔPTPD2* in *Dlar-/-* background, indicating a necessary function on PTPase regulation or unknown cytosolic binding partner in the L3 musculature.

One problem we encountered was the variability of the hypercontraction defect which makes it difficult to assess the results of rescue experiments. Going forward it

may be necessary to use a different phenotypic measure. For neural expression, Krueger *et. al*. utilized lethality as a measure of rescue; however, our assays indicate that muscular expression cannot rescue lethality of *Dlar-/-* [122]. However, we could compare the pupae of mutants to knockdowns using both *24B-Gal4* and *C155-Gal4* drivers to determine which pupal stage they are not able to progress past. We could follow lethality more carefully to determine if the pupal stage is the only lethal stage and determine the timing of stage progression, as delayed puparium formation was ascribed to muscular dystrophic larvae [121]. Further, we could determine the locomotor function of the *C155 > DlarRNAi* larvae to see if a difference can be measured between the muscular and neural contributions for locomotor function and utilize this for rescue experiments. Additional locomotor experiments could measure length of stride to ascribe locomotor defects more closely to muscle dysfunction.

Another important result of this analysis is seen in the pupal case measurements. Mutations that cause either muscle wasting or hypercontraction typically results in an elongated pupal cases due to failed muscle-dependent morphogenic movements [87,123]. We do not see the characteristic increase in axial ratio (length/width) in any of the mutant or RNAi pupae despite gross mislocalization of costameric integrin subunits. Additionally, our sarcomeric patterning defects are less severe than the dystrophic *tn* mutants and *Dlar*-depleted muscle do not display talin mislocalization. Further examination of the costameric and Z-disc associated proteins should be carried out in *Dlar*-, *trio*- and *Glt*-depleted muscles to determine which proteins are affected. Additionally, pupal examination may lead to important information about the lethality

of both Dlar-/- and Dlar RNAi. The Dlar-specific decrease in size is another interesting finding and will be discussed further in the Final discussion (Chapter 6).

The other costameric complex is the DPC, disruption of this complex in vertebrates results in muscular dystrophies. Dystroglycan is a transmembrane receptor of the DPC. In flies, *Dg*-depleted muscle results in hypercontraction similar to *Dlar*-depleted muscle; however, locomotor defects were not reported for *Dg*-depleted larvae [124]. Dosage sensitive interactions of a single *Dlar* mutant alleles in combination with DPC components, IAC componenets or *trio/Glt* transheterozygotes should allow definitive answers about the genetic interactions of these proteins at the costamere.

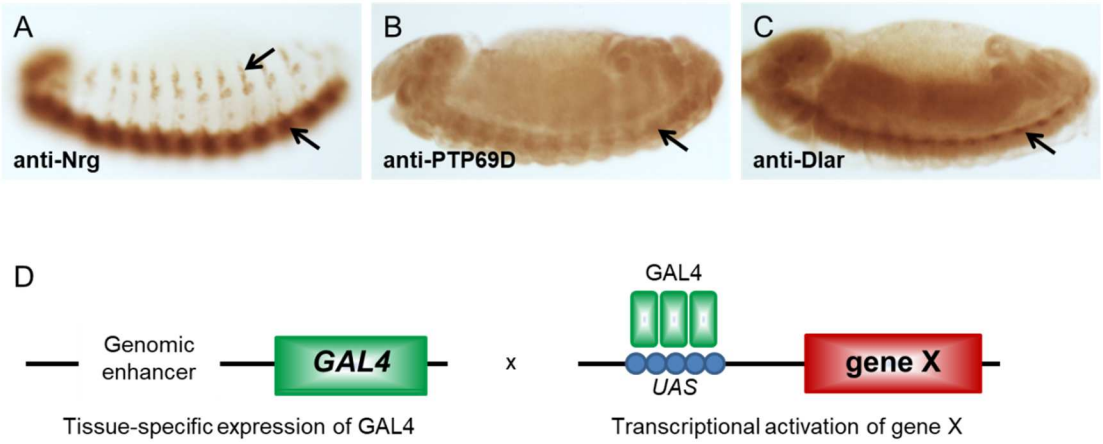

GAL4	tissue	*WT*	*UAS-Dlar RNAi*	*UAS-Ptp10D RNAi*	*UAS-Ptp69D RNAi*	*UAS-Ptp99A RNAi*
Da	ubiquitous	viable	pupal lethal	viable	pupal lethal	viable
24B	early muscle	viable	pupal lethal	viable	viable	viable
mef2	late muscle	viable	pupal lethal	viable	viable	viable

Figure 4. RPTPs are broadly distributed proteins. (A-C) Immunohistochemical stainings of *wildtype* stage 13 embryos. Arrows indicate nerve cord and peripheral neurons. (B) PTP69D and (C) Dlar are found in neural and other tissues compared to the neural-specific receptor (A) Neuroglian (Nrg). (D) Schematic representation of GAL4/UAS knockdown experiments by RNAi and results of crosses at 29°C. A cross was considered viable by the presence of adults eclosing after pupation.

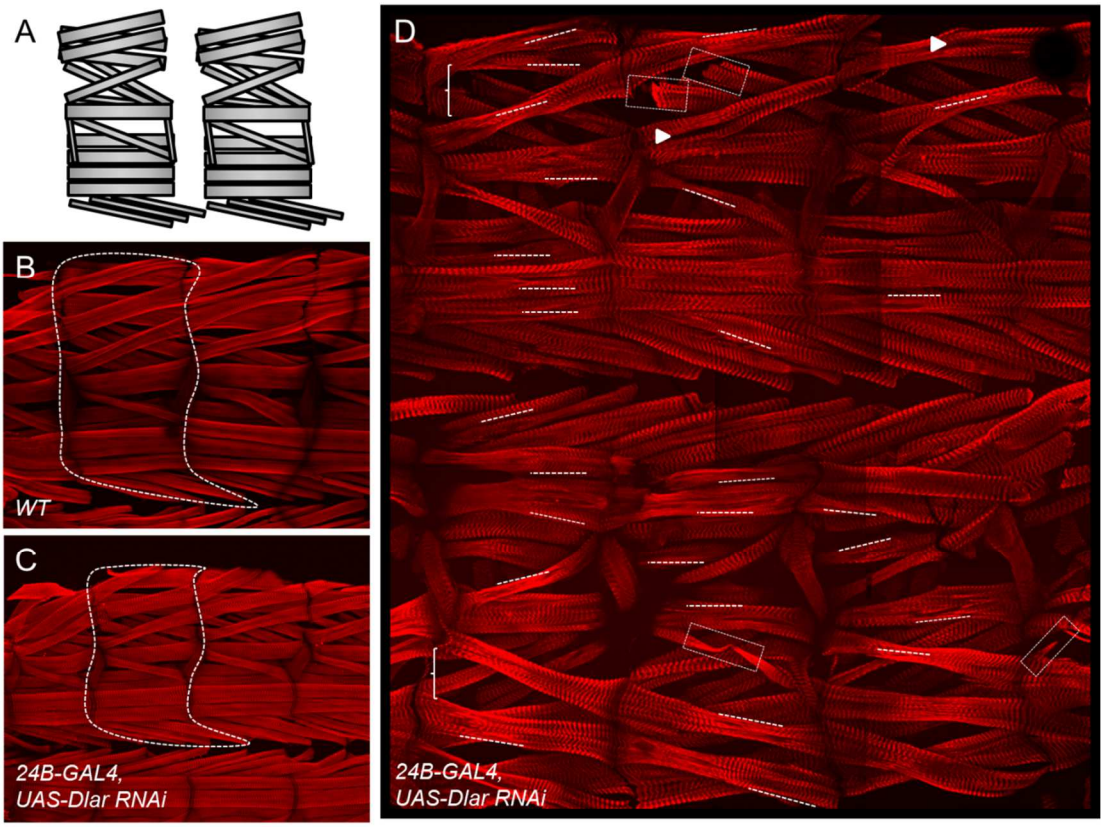

Figure 5. Dlar is required for sarcomeric patterning and muscle integrity in L3 stage. (A) Schematic representation of the interior view of the superficial muscles in two larval hemi-segments. Top is dorsal, left is anterior. (B-D) Immunofluorescence of F-actin in L3 muscle. (B) *WT* 10x image of two hemisegments. Dashed line to highlight relative size of single hemisegment. (C) 24B-Gal4 > UAS-Dlar349 RNAi 10X image. Overall muscle patterning is normal. (D) Composite image from six 20x images depicting six hemisegments of *24B-GAL4 >UAS-Dlar*^{349} *RNAi* muscle. Overall muscle patterning is maintained. Sarcomeric patterning defects (dashed line), splits in myofibrils (arrowhead), broken or tearing muscle (boxes), increase in distance between adjacent dorsal myofibers (solid braces).

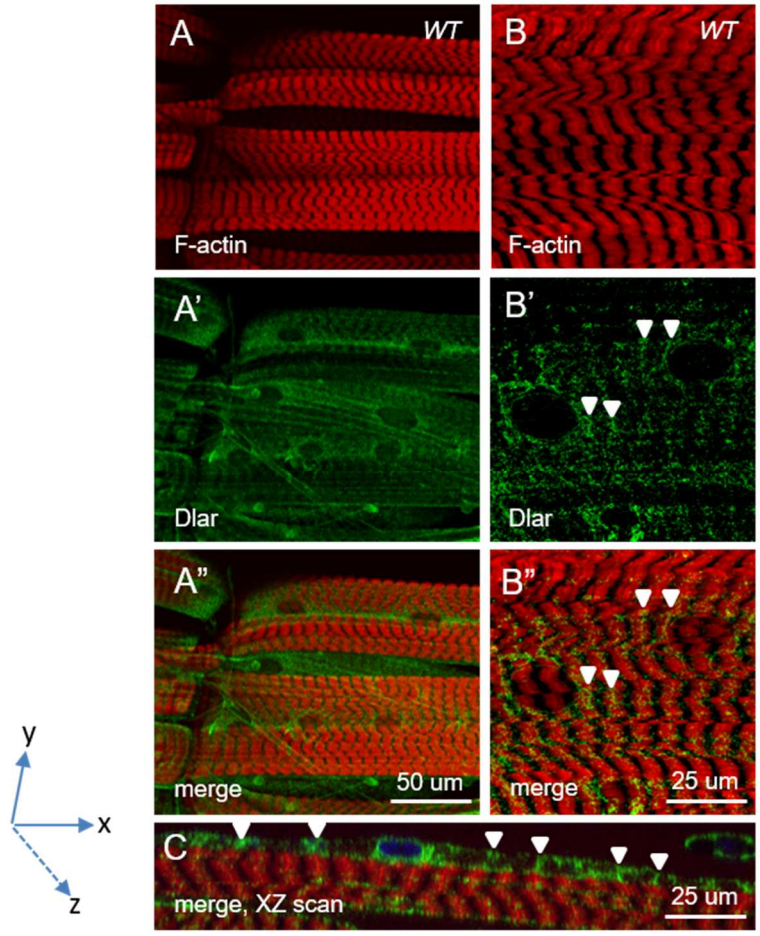

Figure 6. Dlar is localized to the larval muscle membrane at Z-discs. (A-C) *WT* L3 larval body wall muscles. Dlar (affinity purified Rb anti-Dlar FN5) imaged by immunofluorescence in (A-A") 20x images of ventral lateral muscles and (B-B") 60X images indicating Dlar localization loosely associated with Z-discs (white arrowhead). (C) 60x XZ image of perinuclear and membrane staining of Dlar at Z-discs (white arrowhead).

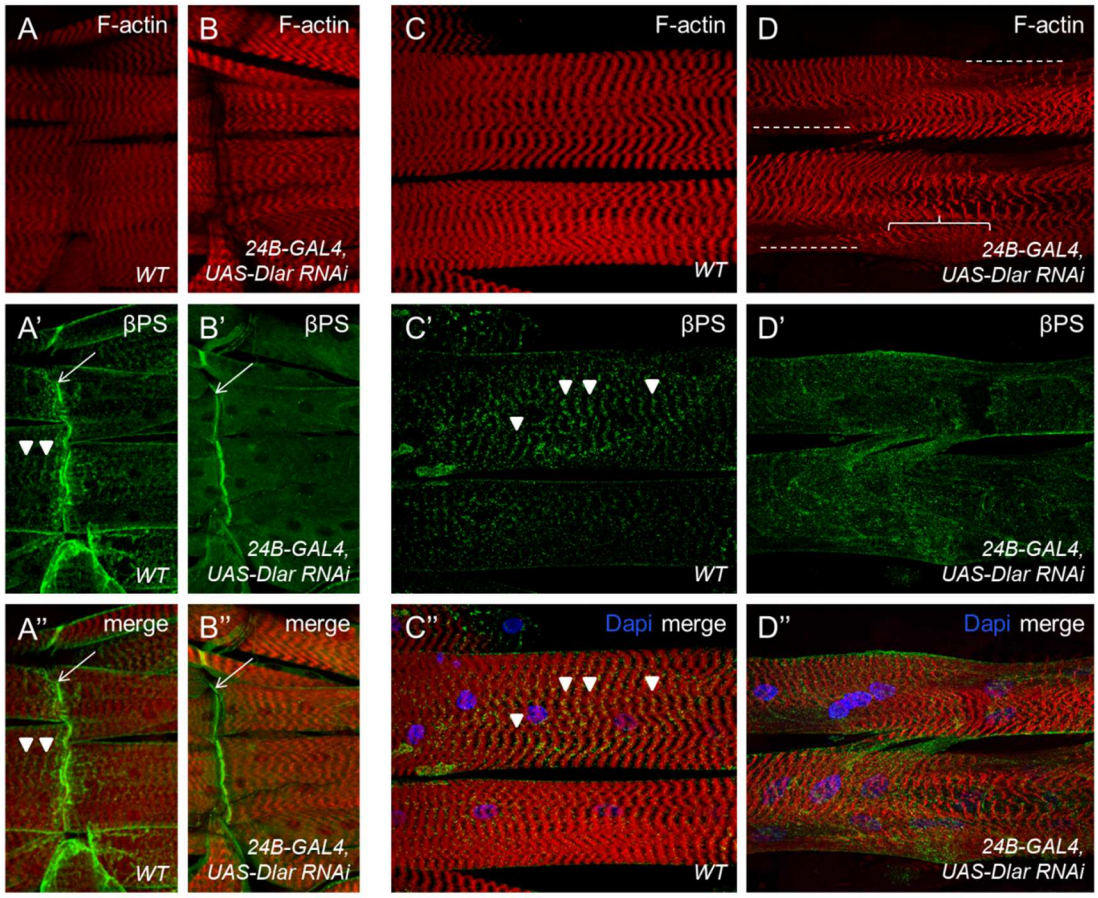

Figure 7. Dlar is required for the localization βPS integrin at costameres. (A-B) 20x images of ventral lateral muscles in L3 stage. (A', A") *WT* and (B', B") *24B-GAL4 > UAS-Dlar^{349} RNAi* display characteristic βPS localization by immunofluorescence at MASs (white arrow). (C-D) 60x images. F-actin staining in (C) *WT* compard to (D) knockdown muscle displays loss of sarcomeric patterning (dashed line) and shortening of sarcomeres (solid brace). βPS co-localizes with Z-disc (arrowhead) in (C', C") *WT* muscle compared to (D', D") *24B-GAL4 > UAS-Dlar^{349} RNAi* muscle.

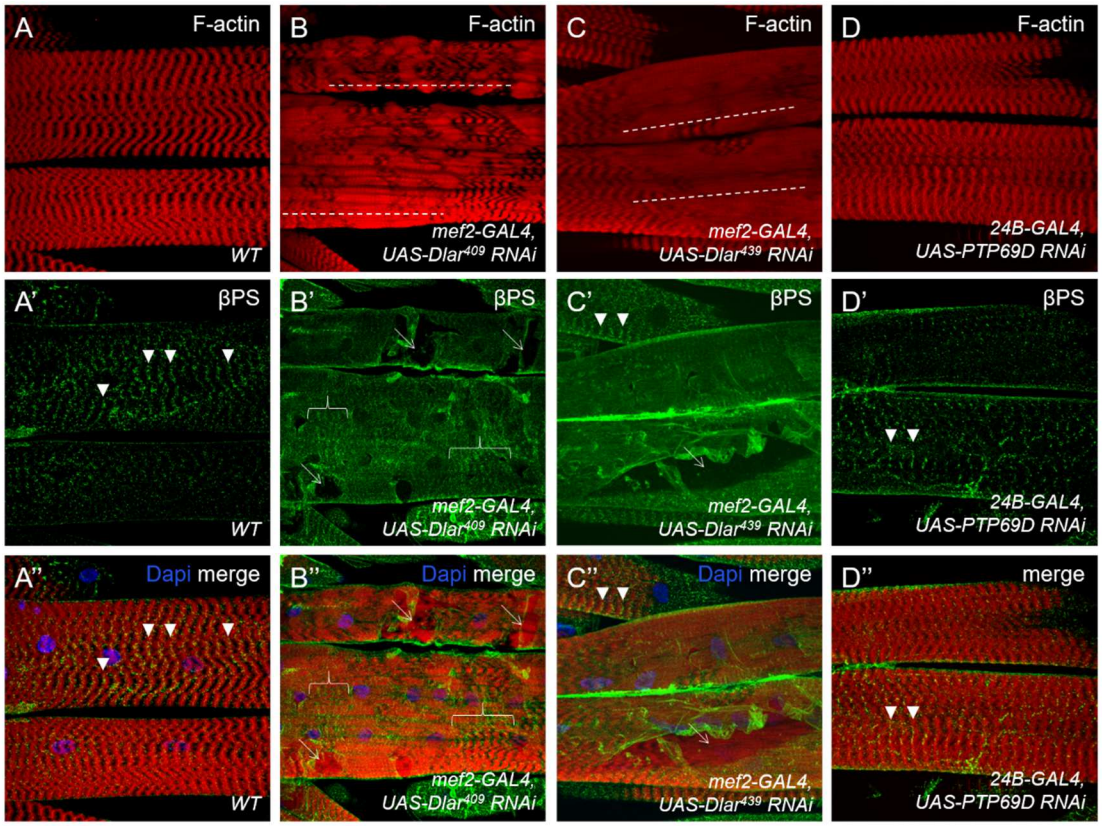

Figure 8. βPS is mislocalized in additional Dlar RNAi lines. (A-D) Confocal images of ventral lateral muscles. F-actin staining in (A) *WT* compared to loss of sarcomeric patterning (dashed line) in knockdown muscle of two additional Dlar RNAi lines, (B) *mef2-GAL4 > UAS-Dlar*^{409} *RNAi* and (C) *mef2-GAL4 > UAS-Dlar*^{439} *RNAi* (A) *WT* βPS localization at Z-disc (arrowhead). The integrin mislocalization phenotype is not 100% penetrant with some muscles in Dlar RNAi (C',C") showing wildtype βPS localization (arrowhead) and some muscles showing areas of less severity (B',B") (braces). The integrity of the sarcolemma is disrupted in both RNAi lines (B',B",C',C") (arrows). (D) *24B-Gal4 > UAS-Ptp69D RNAi* have wildtype sarcomeric patterning and βPS integrin mislocalization.

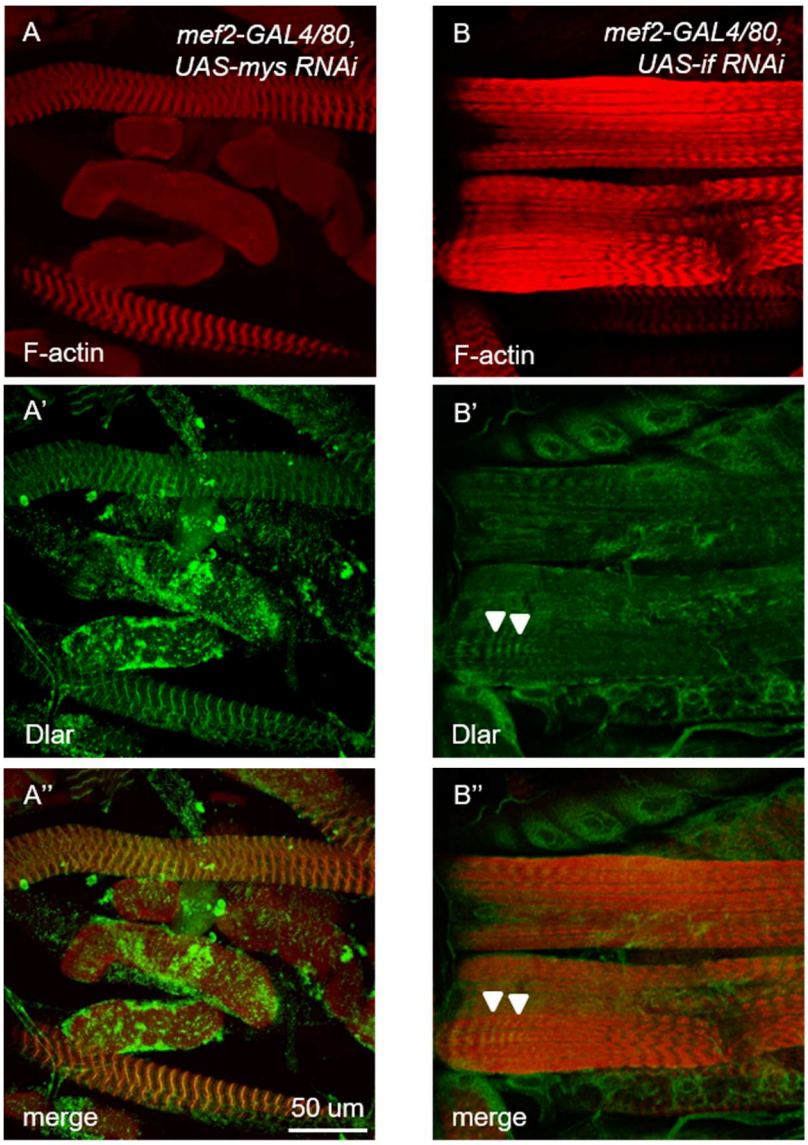

Figure 9. Dlar localization in integrin knockdown. (A-C) Immunolocalization of Dlar by immunofluorescence. (A-B) βPS knockdown shows muscle detachment resulting in complete loss of Dlar localization at Z-discs. (C) αPS2 depleted larvae display moderate Dlar mislocalization.

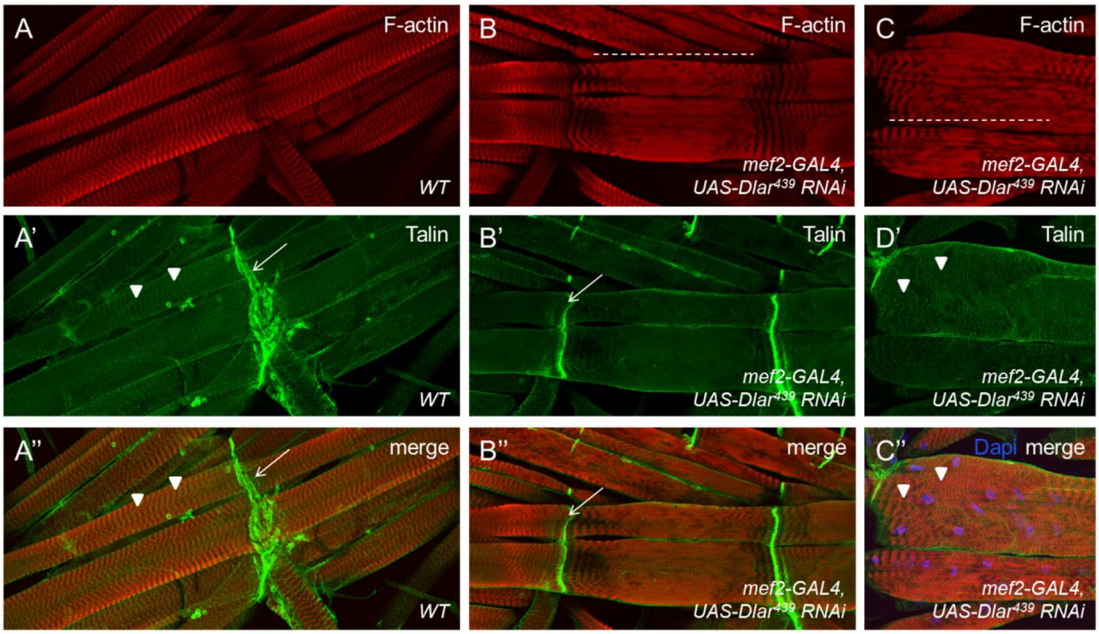

Figure 10. *Dlar*-depleted larvae display wildtype Talin localization. (A-B) Immunolocalization of talin in *mef2-gal4 > Dlar^{439} RNAi* 3rd instar larval vental lateral muscles 6 and 7. (A) 20x image shows normal talin distribution at MAS (boxed). (B) 60x image shows talin maintains Z-disc association in hypercontracted muscle (arrowhead).

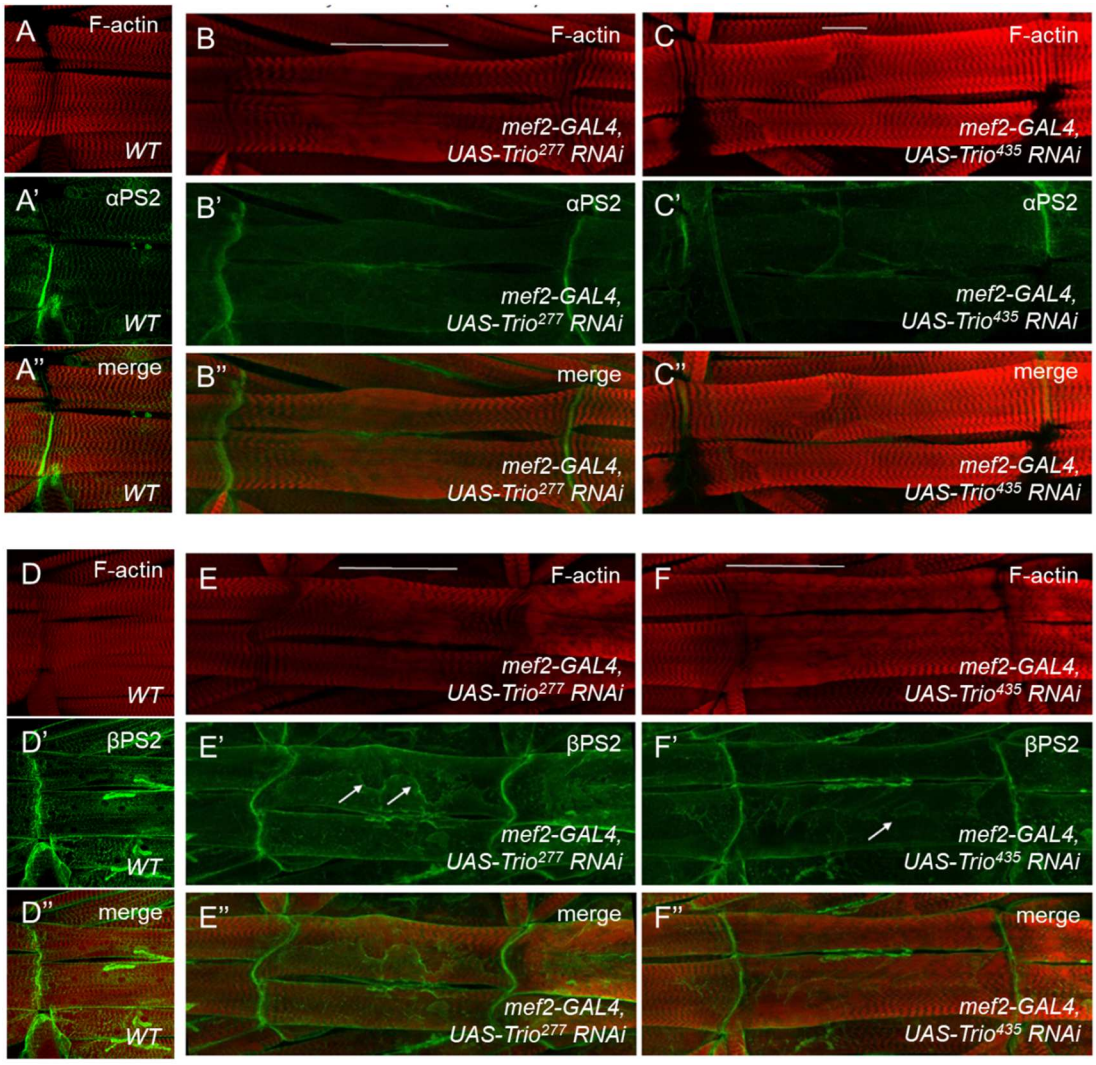

Figure 11. Integrin is mislocalized in *trio*-depleted L3 musculature. (A,D) Immunofluorescence of αPS2 (A) and βPS (B) localization in *WT* L3 muscle. Both *mef2-Gal4 > UAS-Trio^{277} RNAi* (B,E) and *mef2-Gal4 > UAS-Trio^{439} RNAi* (C,F) have aberrant sarcomeric actin patterning (B,C,E,F) and mislocalization of costameric integrin (B',C',E',F').

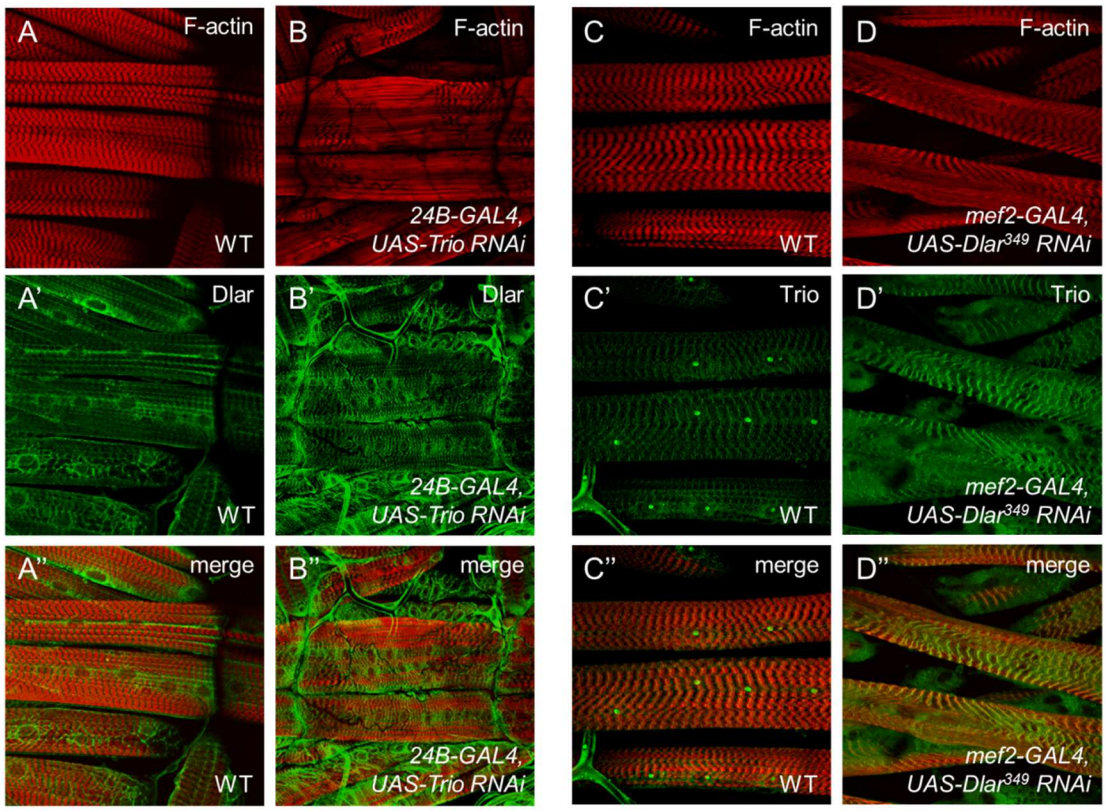

Figure 12. Dlar and Trio localize independently in L3 muscle. (A-B) Immunofluorescence of Dlar in *WT* (A) and *24B-Gal4 > UAS-Trio RNAi* (B) L3 musclulature. Immunofluorescence of Trio in *WT* (C) and *mef2-Gal4 > UAS-Dlar^{349} RNAi* (D).

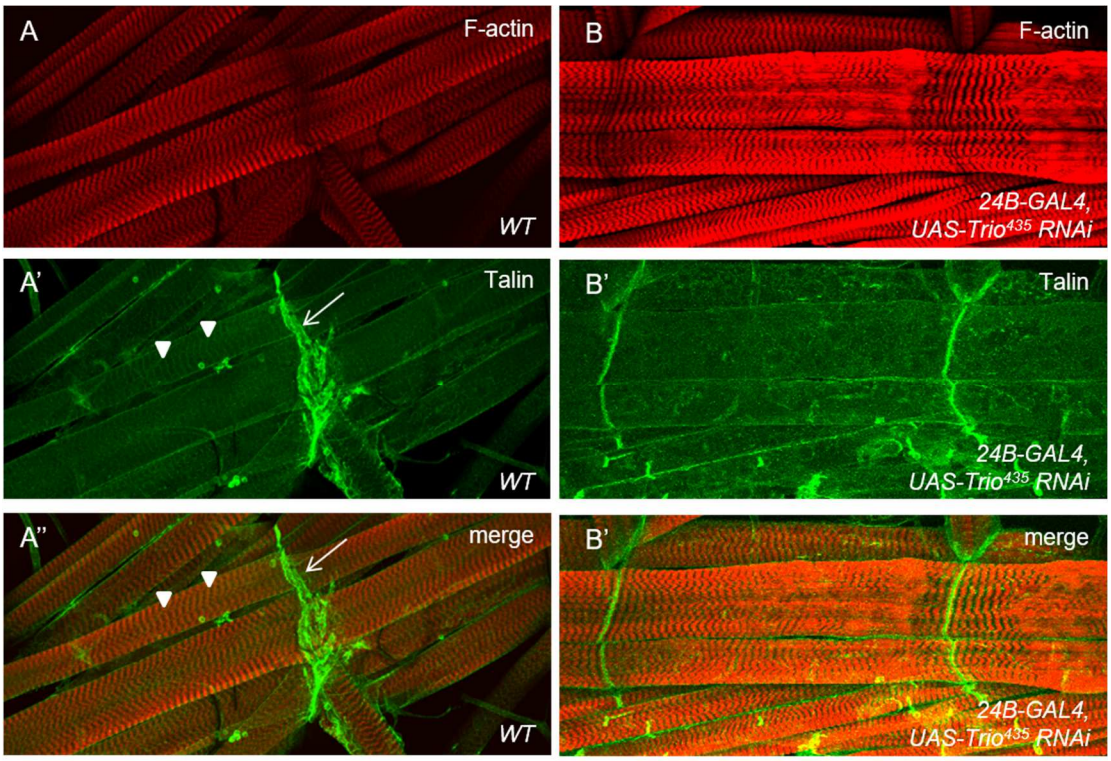

Figure 13. Talin is mislocalized in Trio knockdown. Immunofluorescence of Talin in WT (A) and 24B-Gal4 > UAS-Trio435 RNAi (B) L3 musculature. Talin patterning is lost at Z-discs (B') compared to WT (A').

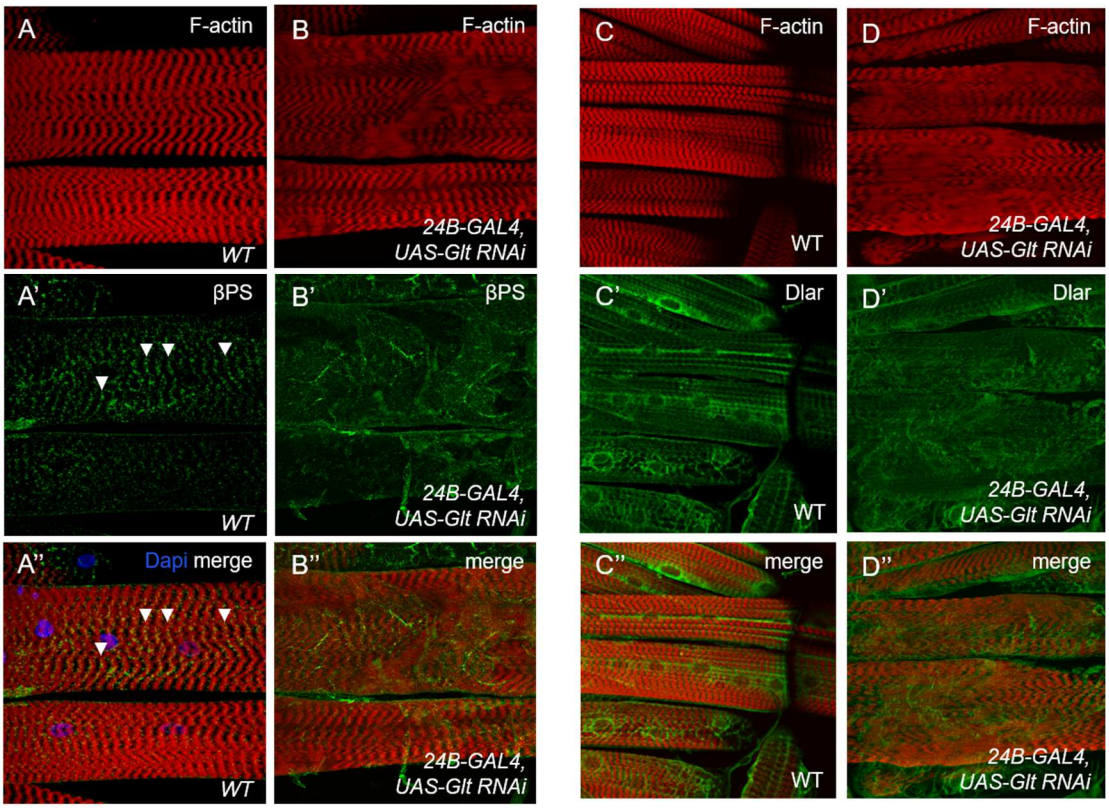

Figure 14. βPS and Dlar are mislocalized in *Glt*-depleted muscle. (A-B) Immunofluorescence of βPS in *WT* (A) and *24B-Gal4 > UAS-Glt RNAi* (B) L3 musculature. (C) Immunofluorescence of Dlar in *WT* (C) and *24B-GAL4 > UAS-Glt RNAi* muscle.

TABLE 4

ANTIBODY STAINING OF DISSECTED L3 MUSCLE

	αPS2	**βPS**	**Dlar**	**Trio**	**Talin**	**F-actin**
Elav-GAL4						
UAS-Dlar RNAi^{349}		○				○
24B- or mef2-GAL4						
UAS-Dlar RNAi^{349}	●	●		◒		●
UAS-Dlar RNAi^{439}		●			○	●
UAS-Dlar RNAi^{409}		●				●
UAS-Glt RNAi^{109}	●	●	●		○	●
UAS-Glt RNAi^{154}	●	●				●
UAS-trio RNAi^{435}	●	●	○		●	●
UAS-trio RNAi^{277}	●	●				●
UAS-Dlar	○	○				○
UAS-Ptp69D RNAi	○	○				○
UAS-if RNAi			◒	◒		●
Mutant line						
Dlar$^{13.2}$/Dlar$^{5.5}$	●	●				●

Elav-GAL4 is a neural specific driver compared to muscle drivers *24B-GAL4* or *mef2-GAL4* and the heterozygous knockout $Dlar^{13.2}/Dlar^{5.5}$. Symbols: ○, ●, ◒ for wild type, aberrant, or partial localization of protein by immunolocalization with the following antibodies; anti-αPS2 (1:50), anti-βPS (1:50), anti-Dlar FN5 (1:50, Rb 29293), anti-Trio (1:10), anti-Talin (1:5). F-actin staining with phalloidin (1:400) is either wild-type (○) or aberrant (●) where aberrant represents hypercontracted myofibrils.

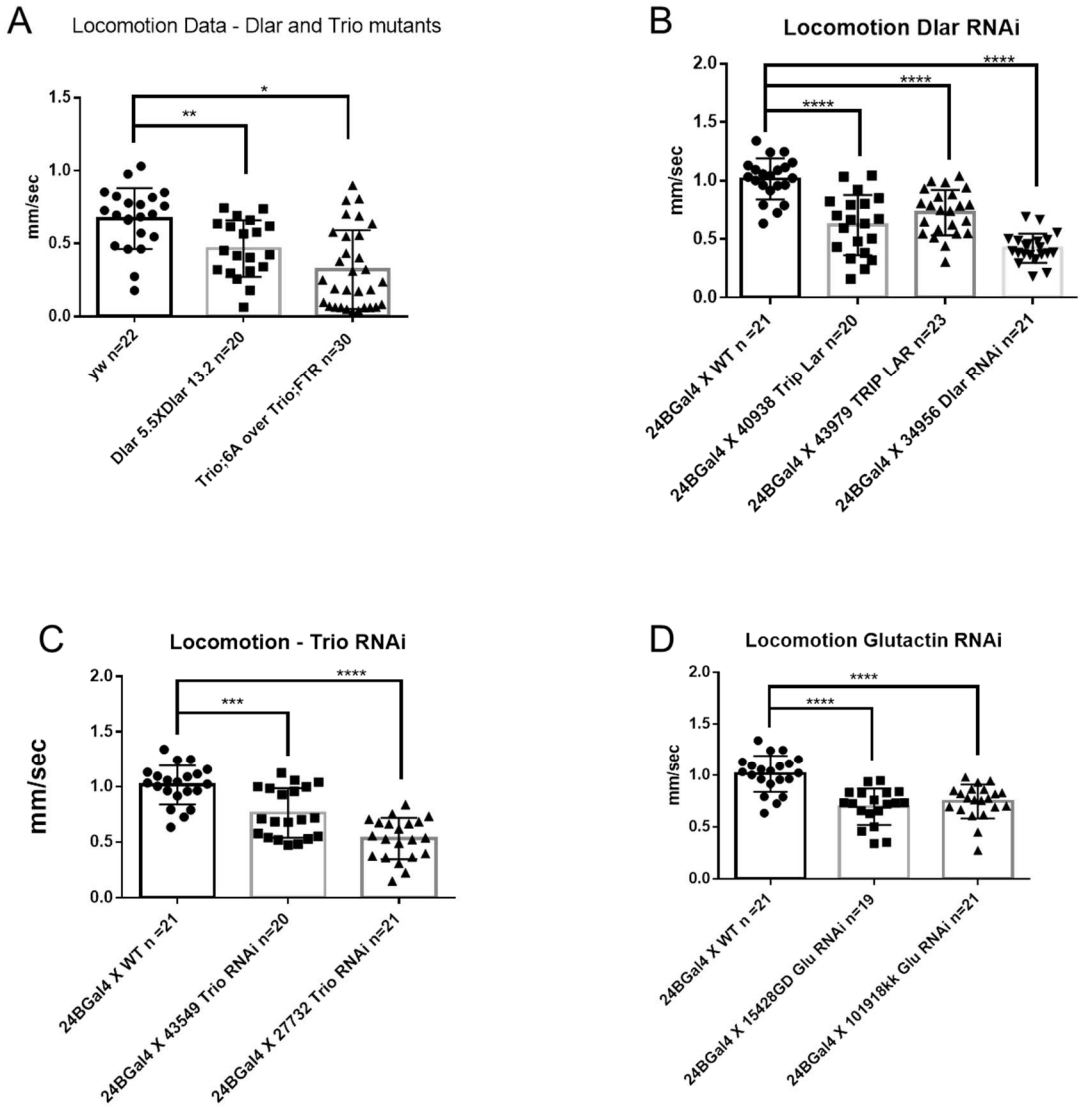

Figure 15. Decreases in larval crawling speeds are associated with neural and muscular defects. (A-D) Measurement of *Drosophila* L3 larval crawling speeds in mm/sec. Detection and analysis in the ImageJ Plugin wrMTrck (ImageJ: http://imagej.nih.gov/ij/) and wrMTrck: http://www.phage.dk/plugins/wrmtrck.html). (A) *Dlar* and *trio* L3 mutants display significant decreases in larval crawling speed compared to *WT*. (B-D) All muscle-specific knockdowns by RNAi of (B) Dlar, (C) Trio and (D) Glt display significant impairment of larval crawling compared to the driver line crossed to *WT*.

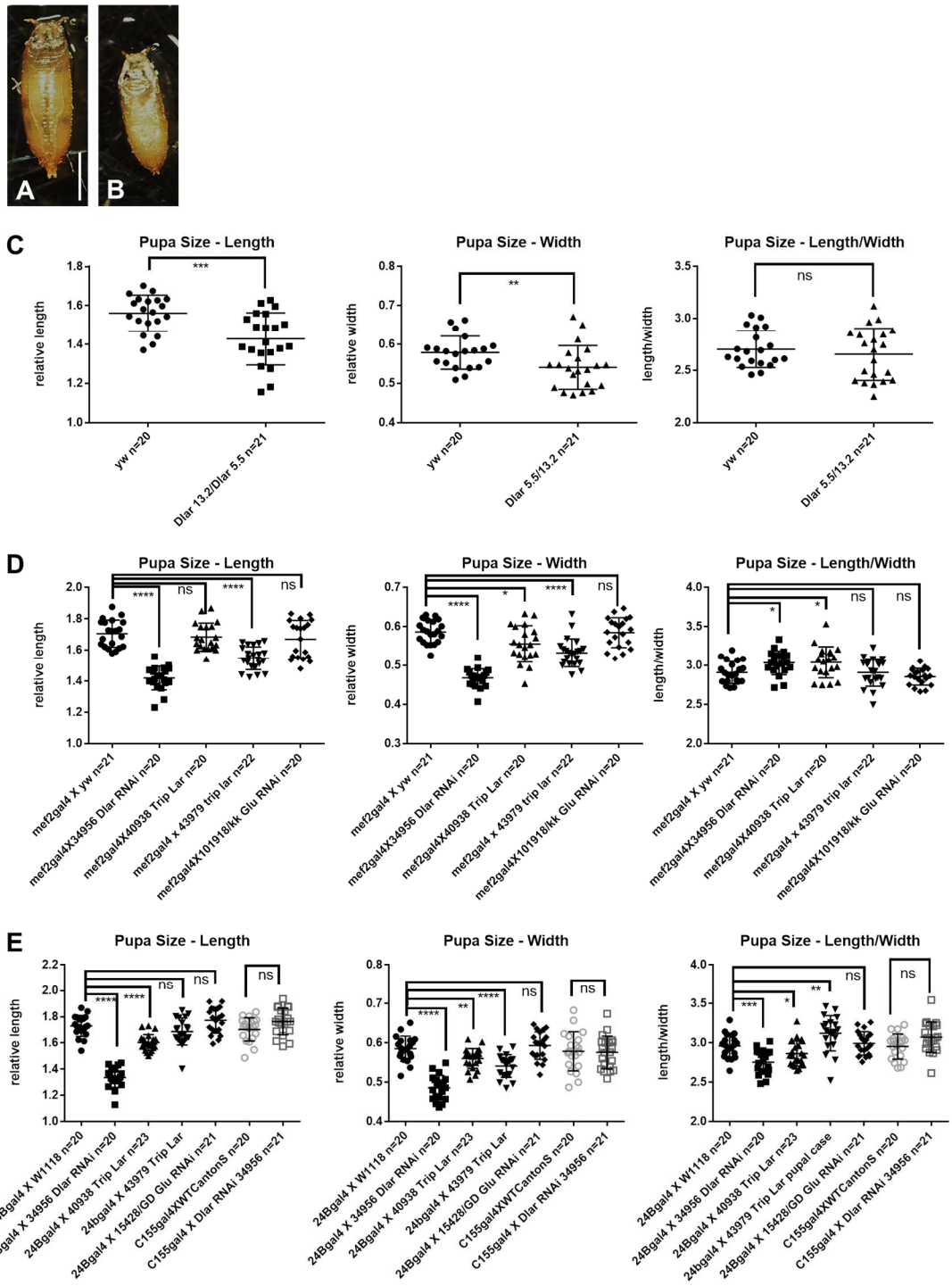

Figure 16. Smaller pupae are a result of the muscle-specific ablation of Dlar. Representative images of *WT* (A) and *24B > Dlar349RNAi* (B) shows a decrease in both length and width. (C) Pupal case measurements of *Dlar13.2/Dlar5.5* show overall decrease in size indicated by the change in length and width but not in length/width

ratio compared to *WT*. (D) The ablation of Dlar by the late muscle driver, *mef2-Gal4*, results in decreases in both length and width with the largest decreases attributed to the greatest decrease in Dlar protein (qPCR results of BL34965 line) compared to *WT* (*24B > W1118*) or *mef2 > GltRNAi*. (E) Ablation with the early muscle driver, *24B-Gal4*, results in greater decreases in size. Additionally, ablation of Dlar with the neural driver, C155-Gal4, does not cause a change in pupal size despite the lethality of the cross indicating that the decrease in size is likely due to the muscle specific function of Dlar.

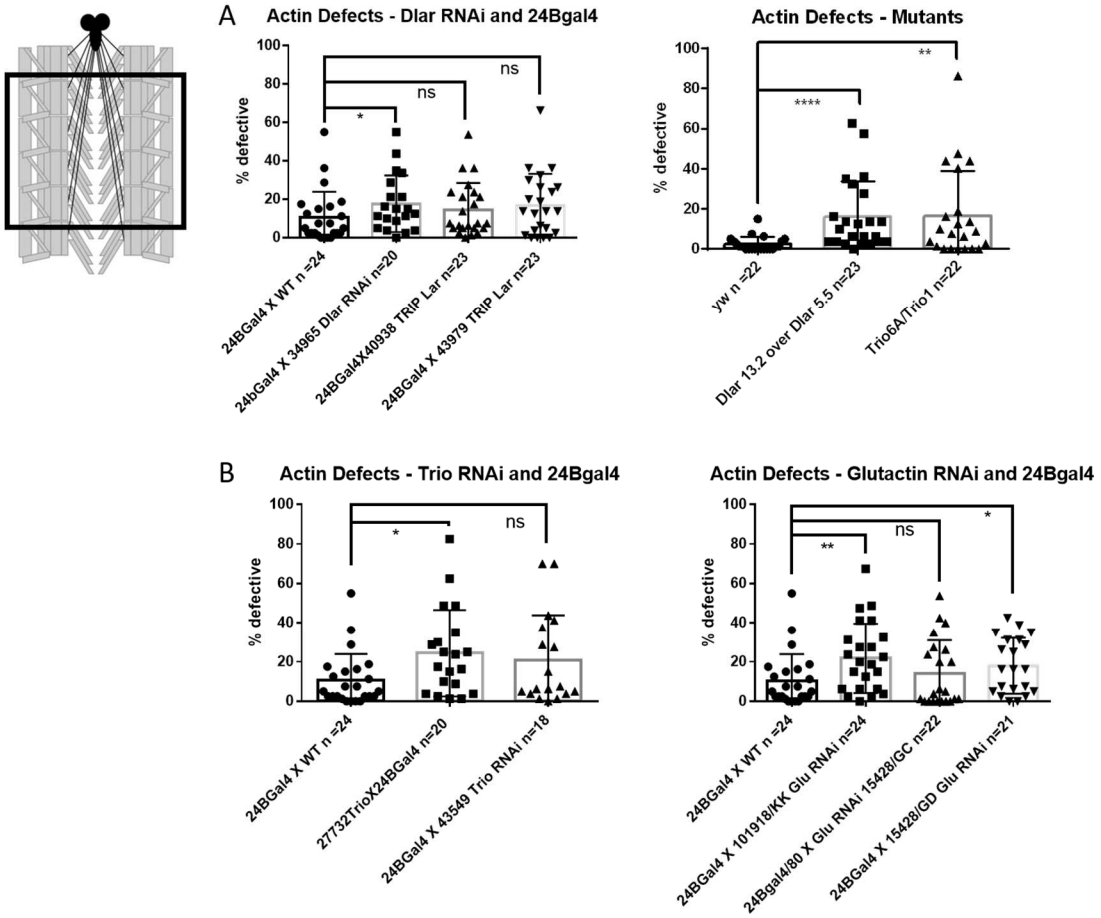

Figure 17. Mutants and muscle specific knockdowns display actin defects in L3 musculature. Schematic of muscles per larvae quantitated for percentage defective to the left. (A) *Dlar*-depleted and *Dlar* mutant L3 musculature display increased number of sarcomeric patterning defects compared to *WT*. (B), Trio and Glt knockdown by RNAi with *24B-Gal4* results in an increase in aberrant sarcomeric patterning compared to driver line crossed to *WT*.

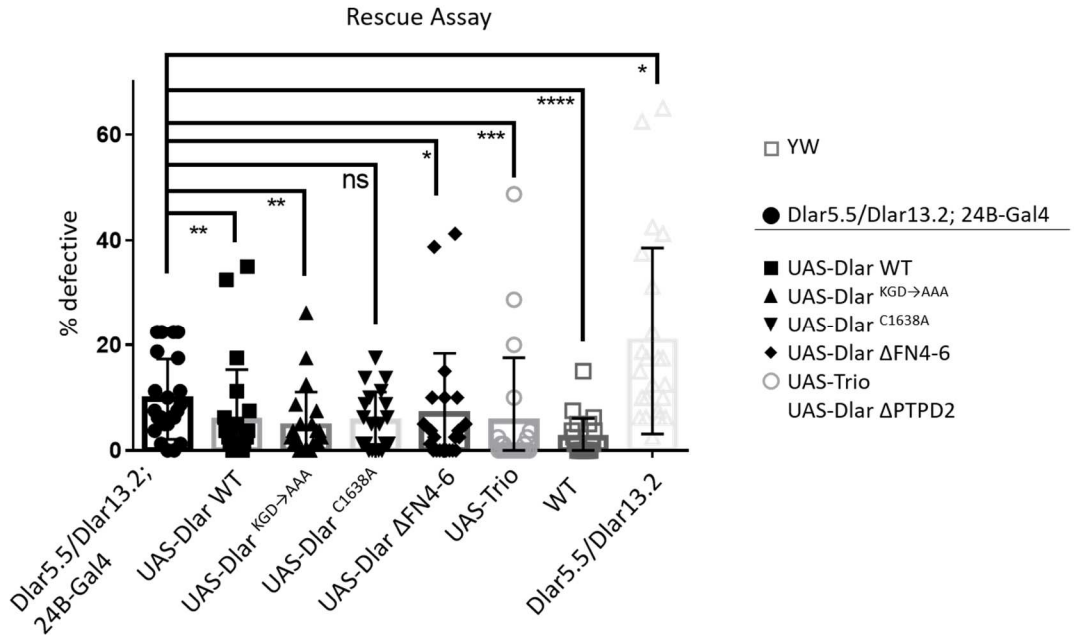

Figure 18. Strucutre/function analysis of Dlar in muscle. The following UAS-Dlar constructs expressed with *24B-Gal4*; Dlar$^{KGD→AAA}$, Dlar^{C1638A}, and Dlar ΔFN4-6 rescued sarcomeric actin defects at or better than the UAS-Dlar WT in a Dlar mutant background. Importantly, UAS-Dlar ΔPTPD2 is lethal before the L3 stage indicating an important function in muscle tissue. Additionally, expression of UAS-Trio rescues the Dlar actin phenotype in a Dlar mutant background indicating Dlar and Trio likely function in the same signaling pathway in L3 muscle.

CHAPTER 4

STRUCTURAL ANALYSIS OF RPTP TYPE IIA FN DOMAINS 4-6

Overview

In the *Drosophila* follicular epithelia, the genetic interaction between *Dlar* and *mys* modulates the polarity of actin filaments [98]. The Dlar fragments sufficient for rescue of the aberrant actin polarity phenotype in a *Dlar*-null background were narrowed to the FN4-6 domains [122]. Given our finding that Dlar depletion in larval muscle results in integrin mislocalization and actin hypercontraction, our investigation focused on this region. Sequence analysis uncovered a tripeptide, Lys-Gly-Asp (KGD), in the Dlar FN5 domain that is conserved in the Lar-RPTP homologs across species (Fig.19C). We hypothesized that the FN5 domain of Dlar and integrins may directly interact via the KGD tripeptide. Herein, we report our X-ray crystallographic findings of the KGD in Lar-RPTPs for structural comparison to the RGD containing tenth FNIII repeat of human fibronectin (HFN10).

The crystal structure of Dlar FN5

The adhesive function of the RGD tripeptide to the cell surface was first discovered in the ECM protein, human fibronectin (HFN) [125,126]. HFN is a large glycoprotein that interacts with cell surface receptors and other ECM protein such as integrin, collagen and heparin sulfate proteoglycans (HSPGs). HFN consists of three types of domains, type I (FNI), II (FNII), or III (FNIII) which differ by size, structure and the presence of disulfides [127]. HFN is a dimer, each subunit is composed of 12 FNI,

2 FNII, and 15 to 17 FNIII modules, with the RGD tripeptide located within the tenth FNIII (FN10) domain [125]. FNIII are the largest of the three repeats found in fibronectin and include typically 90-100 amino acid residues forming a beta sandwich (Fig. 19A). This motif is widely spread in animals particularly in extracellular proteins and also in yeast and bacteria [128]. The Dlar FN5 domain and the HFN10 share 30% conservation (Supplementary Table 1) and sequence alignment reveals that the KGD is near the C-terminus and may lie in a flexible loop similar to HFN10 (Fig. 19C).

Specificity of integrin binding is also determined by the flanking sequences and 3-D presentation. In fibronectin, binding to integrin is further stabilized by interactions in the preceding ninth FNIII (HFN9) domain. HFN9 contains the "synergy" region comprised of residues 1373-1380 with the sequence DRVPHSRN and lies in the C'/E loop. To determine if Dlar possesses the structural characteristics of an integrin ligand, we sought to find a crystallizable region of the ECD encompassing the FN5 domain. The following constructs were over-expressed in *E. coli*; FN4-7, FN4-6, FN4-5, FN5-6 and FN5. The FN4-6, FN4-5 and FN5 were soluble, but only the FN5 yielded diffraction quality crystals. Interestingly, a ~5 molar equivalent of Zn^{2+} was required to crystallize Dlar FN5 (Fig. 20). We used the anomalous signal from bound Zn^{2+} ions to calculate experimental phases and obtain an initial model. The final structure was solved by molecular replacement and refined to a resolution of 1.3 Å (R/Rfree = 18.7%/19.3%). Overall, the Dlar FN5 adopts the prototypical FNIII β-sandwich. Two loop regions could not be modeled presumably because they can adopt multiple conformations (dashed lines, Fig. 20). Two Zn^{2+} were found in the crystal structure

labeled "1" and "2" in the figure. The first Zn^{2+} is bound by His-745 in strand C and Asp-766 in strand C' at a crystal contact and may be an artifact of crystallization. The second is coordinated by residues within a single FN5 domain, including the Asp-796 from the KGD motif and two histidine residues, His-745 and His-747, from strand C. Although the KGD lies in the F/G loop, the side chains are not accessible for binding with the Asp-796 positioned downward against the β-strand and the Lys-794 pointing back toward the molecule instead of out in the solvent in contrast to the Arg-1493 and Asp-1495 side chains of HFN10. In addition, the KGD is not in the apex of the loop as seen in fibronectin (Fig. 19A,B) but shifted further C-terminally toward strand G. However, the atypical integrin binding proteins; lamininE, tiggrin and thombrospondin, (TSP), can still interact with integrins by RGD/KDG-independent mechanisms. The human TSP-1 crystal structure revealed a mechanism for integrin binding that utilizes calcium to regulate the availability of the RGD motif for binding [129].

Structural determination of the mammalian orthologs

We sought to increase our understanding of the KGD motif in Lar-RPTPs by assessing the conservation of zinc binding in the mammalian orthologs. Zinc coordination in PTPRD and PTPRS is possible with His at position 747 and replacement with Gln at position 745, which is a weak and less common zinc coordinating residue [130]. Zinc coordination in Lar is abolished by Gln replacing His at position 745 and Val/Thr at 747. Only two fragments were crystallizable, mouse Lar FN5 (Mlar FN5) and human PTPRD FN4-6 (HPTPRD FN4-6). The Mlar FN5 crystal structure was solved by molecular replacement using Dlar FN5 as the model and

refined to a resolution of 1.7 Å (R/Rfree = 19.5%/22.5%) (Fig. 21). Mlar FN5 crystallized in the absence of zinc, but sorbitol from the cryoprotectant is found between the C/C' and E/F loops. Overall, the Mlar FN5 adopts the FNIII β-sandwich and the KGD motif is found in the F/G loop. The KGD is shifted C-terminally toward strand G, with Asp-747 pointed downward even in the absence of Zn^{2+}. The loop is short and the KGD is not available for binding.

HPTPRD FN4-6 crystals were obtained in the absence of zinc. The structure was solved by molecular replacement with Dlar FN5 as the model and partially refined to a resolution of 1.87 Å (R/Rfree = 24.0%/28.6%) (Fig. 22 is the partially refined structure). The overall structure is an extended conformation. The KGD conformation is very similar to the Mlar FN5 KGD motif conformation with the side chains orientated in the same directions and not available for binding. Comparison to the crystal structure of HFN9-10 shows that the HFN9/10 interface has a small degree of rotation and exposed surface area with the G-F-C-C' beta-strand face of HFN9 and HFN10 aligned (Fig. 23) [131]. In contrast, the HPTPRD FN4 is rotated compared to FN5. This causes a shift in the location of the interdomain chain of amino acid residues to be located near the F/G loop instead of away (Fig. 23). The negative Lys of the KGD is now stabilized by the positive Glu in the interdomain linker. In addition, the interactions between the interdomain loops are flip-flopped. The A/B loop region of FN4 is SPSST stabilizing the front region near the interdomain linker and F/G loop. The FN4 E/F loop is LEKWT in the middle. The C/C' loop of FN4 is on the backside. The HFN9/10 interface is different with the RGD extended outward and not contacting any residues in either

domain 9 or 10; it is noted that the RDG motif contacts symmetry units. Stabilization of the 2 domains resides in the E/F loop of HFN9 and A/B loop and the G tail leading into HFN10 domain. This might account for the difference in the E/F loop sequence conservation. As loops can be highly variable in length and sequence, the HFN10 E/F is SGLKPG with PG highly conserved in the E/F loop of the FNIII repeats of fibronectin. The Dlar FN5 sequence for E/F loop is TGLQPD, with the L being most highly conserved followed by the P and then D/E in the orthologs. The rotation of FN4 in comparison to the FN5 domain is also significant in the location of the synergy site which lies in the C'/E loop which resides at the top of HFN9 on the same side as the RGD in HFN10, whereas the C'/E loop of FN4 is now on the opposite side of the KGD in FN5.

Conclusions

In this chapter we analyzed the sequences and crystal structures of the FN5 domains of three orthologs representing the spectrum of the type IIa Lar-RPTPs. FNIII domains are ubiquitous and have low sequence homology; however, the same FNIII domain across species has much higher homology indicating some sequence specific functions between different FNIIIs [132]. Mammalian Lar FN5 binds laminin-nidogen *in vitro,* and Dlar FN4-6 is implicated in epithelial polarity in concert with integrin in the *Drosophila* oocyte. We have uncovered that the FN5 domain of the nine FNIII repeats has a conserved KGD motif in the F/G loop reminiscent of HFN10, the prototypical integrin ligand. However, we show that the KGD motif in the FN5 domains do not display the three-dimensional presentation required for integrin binding. This was later

confirmed by genetic rescue experiments in *Drosophila* where the KGD→AAA amino acid substation as well as deletion of the entire FN4-6 region were able to rescue the aberrant actin phenotype almost as well as full-length Dlar (Chapter 3).

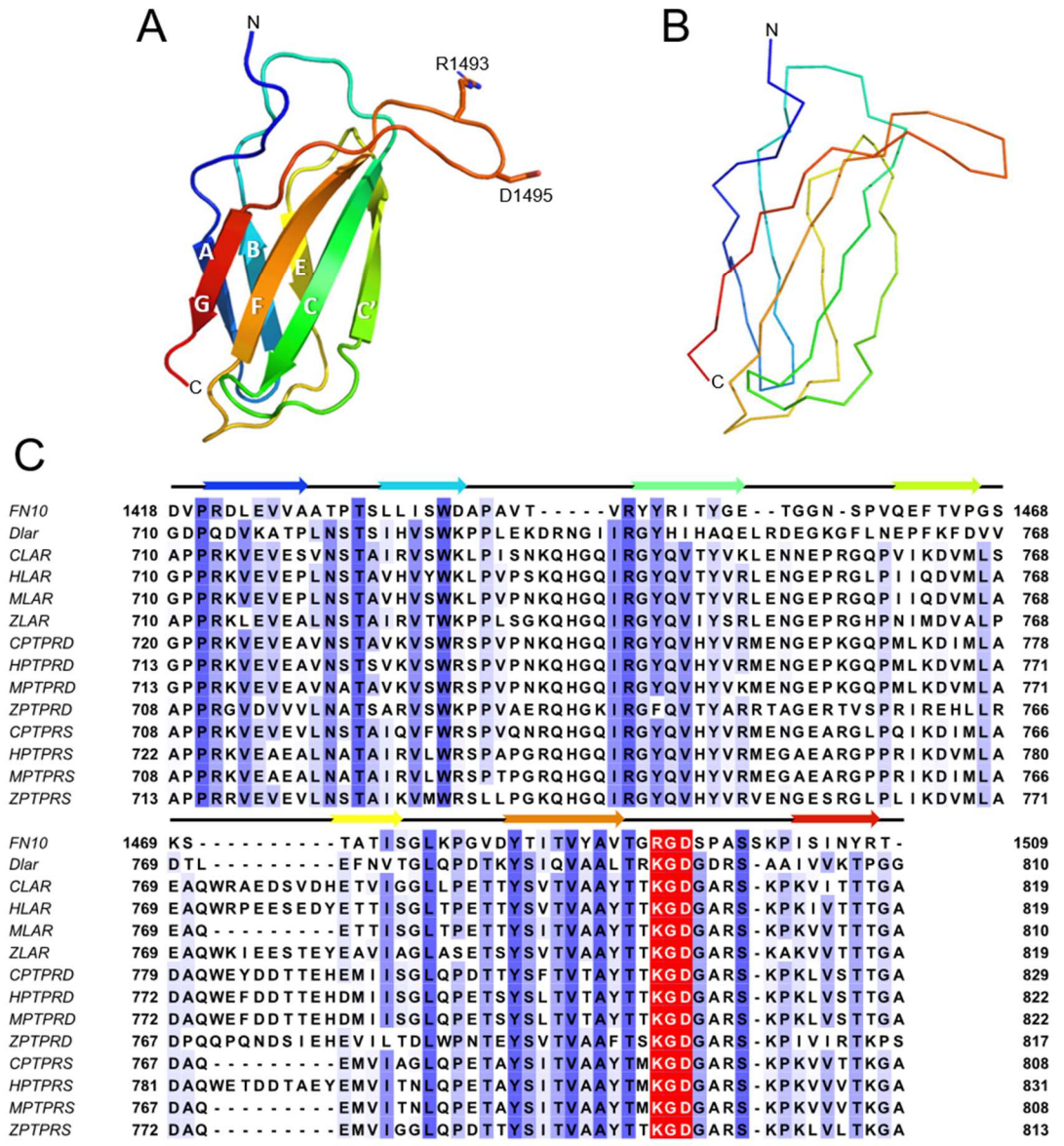

Figure 19. The RGD tripeptide lies in a flexible loop region. (A) Ribbon diagram of FN10 (PDB ID: 1FNF) with labeled strands, A-B-E behind and G-F-C-C' in front. The RGD is in a flexible loop [131]. (B) Stereodiagram of Cα trace of FN10 depicting accessibility of RGD loop [131]. (C) Sequence alignment showing conserved residues in blue and the RGD/KGD in red. Secondary structure based on FN10 structure.

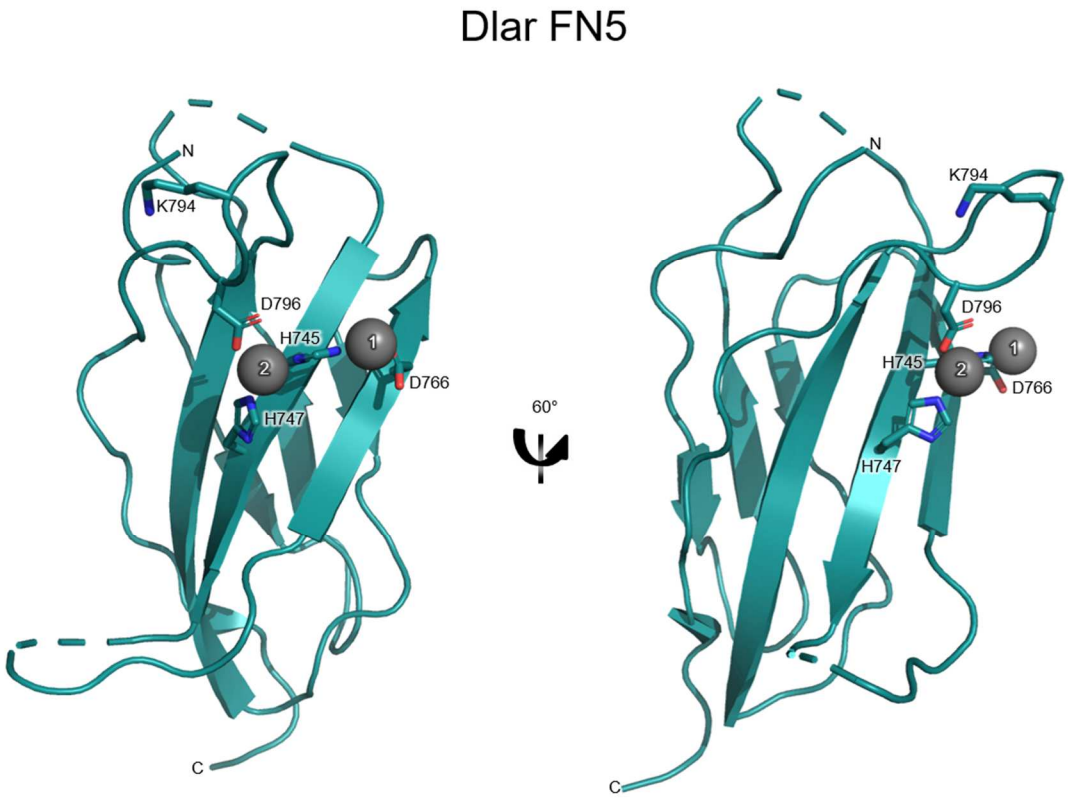

Figure 20. Dlar FN5 crystal structure. Ribbon diagram of Dlar FN5 depicting the KGD and Zn^{2+} (gray spheres) coordinating residues. D796 coordinates a Zn^{2+} (labeled 2) with residues, H745 and H747. Another Zn^{2+} (labeled 1) is coordinated between H745 and D766 at a crystal contact.

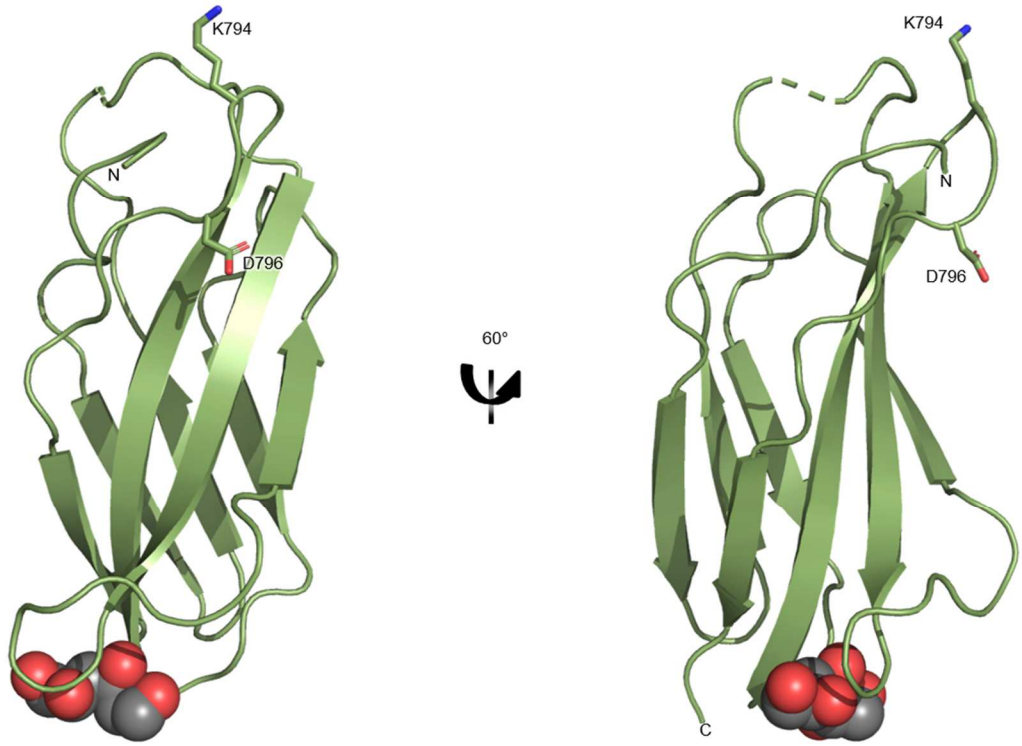

Figure 21. Mlar FN5 crystal structure. Ribbon diagram of Mlar FN5 depicting the KGD and sorbitol molecule from the cryoprotectant.

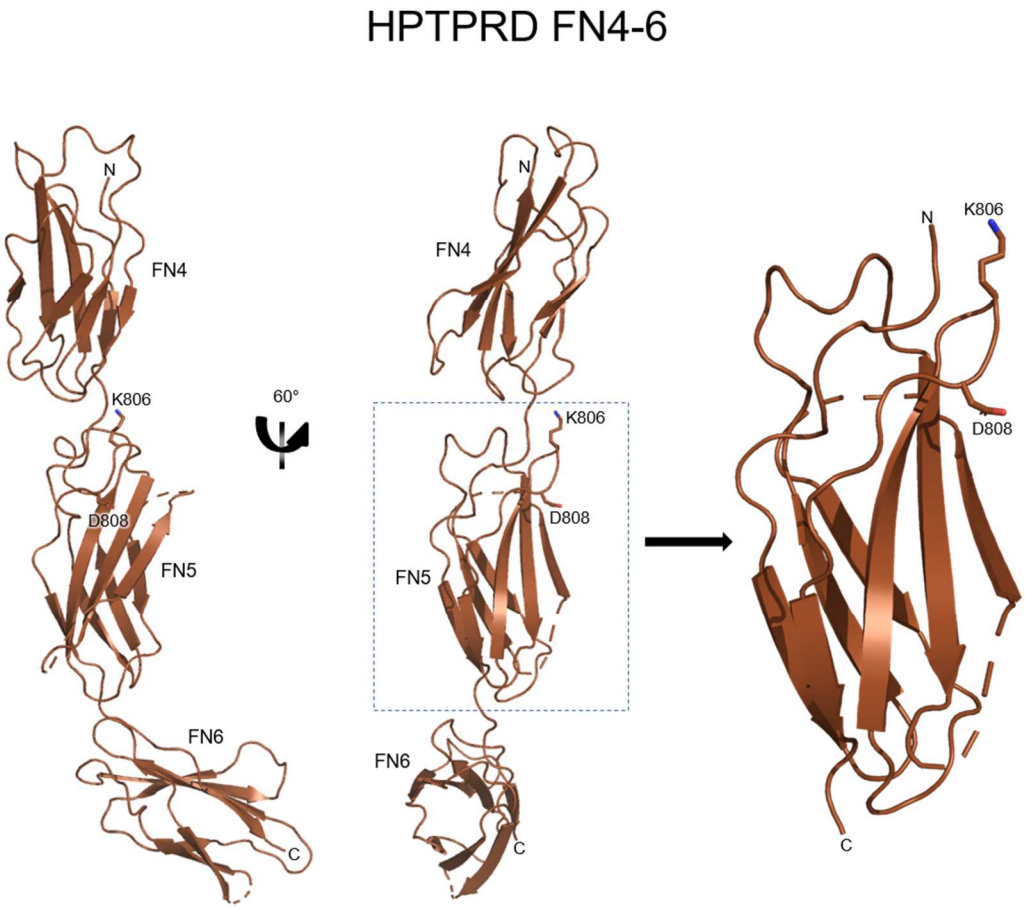

Figure 22. Partially refined HPTPRD FN4-6 crystal structure. Ribbon diagram of partially refined HPTPRD FN4-6 depicting the FN5 domain in context to the flanking domains.

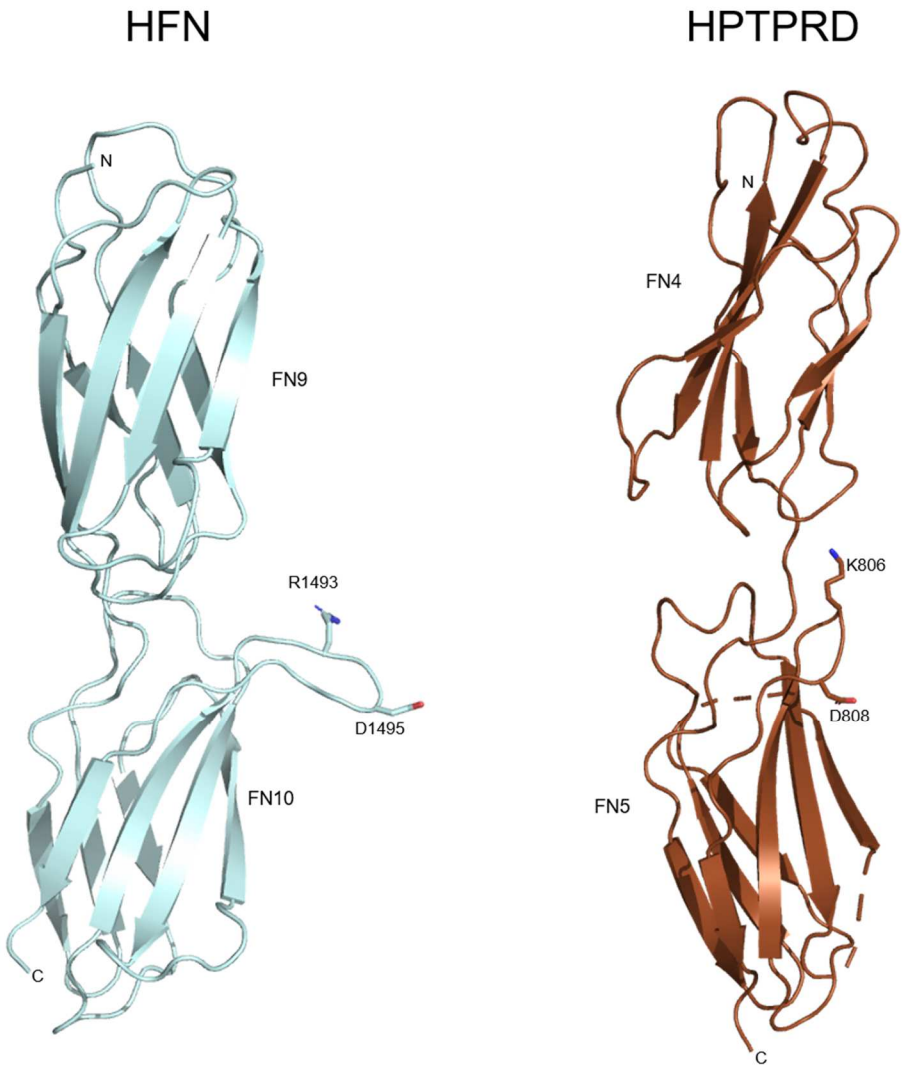

Figure 23. Comparison of interdomain interfaces. Ribbon diagrams of HFN9-10 (light cyan) [131] and HPTPRD FN4-5 (brown) show extensive contacts between the 9/10 interface compared to the 4/5 interface.

TABLE 5

DATA COLLECTION AND REFINEMENT STATISTICS FOR DLAR FN5, MLAR FN5, AND HPTPRD FN4-6 CRYSTAL STRUCTURES

	Dlar FN5	**HPTPRD FN4-6**	**Mlar FN5**
Data collection			
Beamline	APS 22-ID	APS 22-	APS 22-ID
Wavelength (Å)	1	1	1
Unique reflections	22,118	29,323	13,899
Resolution (Å)	50 – 1.3	100 – 1.9	50 – 1.7
Space group	$P2_12_12_1$	$C1_21$	$P3_22_1$
Unit cell			
a, b, c (Å)	40.58, 42.66, 51.35	144.730, 34.64, 95.10	86.11, 86.11, 29.34
α, β, γ (°)	90.0, 90.0, 90.0	90.00, 130.92, 90.0	90.0, 90.0, 120.0
R_{sym}[a]	0.115 (0.290)	0.065 (0.531)	0.119 (0.412)
Completeness[b] (%)	98.0 (94.1)	97.5 (90.8)	98.5 (92.3)
Redundancy	13.0 (9.4)	7.4 (7.5)	21.3 (15.1)
I/σI	12.7 (6.6)	18.9 (3.6)	27.7 (4.2)
Refinement			
Molecules in the asymmetric Unit	1	1	1
Resolution (Å)	32.81 – 1.3	34.09 – 1.87	27.31 – 1.7
R_{work}[c]/R_{free}	0.186/0.191	0.242/0.285	0.198/0.226

"TABLE 5 – Continued."

DATA COLLECTION AND REFINEMENT STATISTICS FOR DLAR FN5, MLAR FN5, AND HPTPRD FN4-6 CRYSTAL STRUCTURES

	Dlar FN5	**HPTPRD FN4-6**	**Mlar FN5**
Refinement			
Number of atoms	830	2,367	884
Protein	735	2,221	763
Ligand	2	0	12
Water	93	146	109
R.m.s. deviations			
Ideal bonds (Å)	0.011	0.008	0.008
Ideal angles (°)	1.48	1.15	1.46
Average B factors (Å^2)	18.05	32.19	20.96
Protein	16.71	32.08	19.55
Ligand	11.29	0	27.74
Water	28.71	33.81	30.09
Ramachandran statistics			
Favored (%)	97.6	95.3	96.9
Allowed (%)	2.4	3.3	3.1

[a]$R_{sym} = \Sigma_h \Sigma_i |I_i(h) - \langle I(h) \rangle| / \Sigma_h \Sigma_i I_i(h)$, where $I_i(h)$ is the *i*th measurement of reflection h and $\langle I(h) \rangle$ is a weighted mean of all measurements of h.
[b]Values in parentheses apply to the high-resolution shell.
[c]$R = \Sigma_h |F_{obs}(h) - F_{calc}(h)| / \Sigma_h |F_{obs}|$. R_{work} and R_{free} were calculated from the working and test reflection sets, respectively. The test set constituted 5% of the total reflections not used in refinement.

CHAPTER 5

DETECTING PHYSICAL INTERACTIONS OF LAR-RPTPS

Overview

Identification of a conserved KGD in the fifth FN III domain of Dlar led us to speculate that Dlar and integrins may physically interact. However, genetic rescue experiments in the *Drosophila* musculature and structural analysis of the motif has shown that the KGD does not have the three-dimensional presentation of an integrin ligand. Despite this, there are distinct regions capable of participating in protein-protein interactions. The mammalian orthologs have binding sites in the Ig1-2, Ig1-3, FN1-2, FN5 and some interactions require both the Ig and FNIII domains. Additionally, the Dlar FN4-6 and the Dlar FN7-9 domains have been implicated in epithelial polarity and R-cell targeting in the brain [122]; however, only ligands to the Ig1-2 have been identified. Hence, we have undertaken a comprehensive effort to identify Dlar-binding partners.

Dlar binding partners in L3 stage

Transient extracellular interactions are hard to capture. They have low affinity and post-translational modifications are important for binding. For this reason, yeast-two-hybrid assays which take place in a yeast nucleus are not adapted for extracellular protein modifications. To detect potential binding partners of Lar-RPTPs, we performed a series of immunoprecitation (IP) and affinity isolation experiments followed by protein identification via mass spectrometry (MS). The initial set of IP experiments are indexed in Table 6. First, mouse monoclonal antibodies against Dlar,

αPS2, and βPS from Developmental Studies Hybridoma Bank (DSHB) were incubated in lysates made from L3 *WT* larvae (see materials and methods). Low yield required visualization by silver stain which rendered many bands beyond the limit of detection of the spectrometer (Thermo Finnigan Linear Ion trap LTQ) via LC-tandem mass spectroscopy (LCMS). Integrin heterodimers were detected by the presence of βPS in the anti-αPS2 IP and both αPS2 and αPS3 in the βPS IP and were utilized as a control to indicate that the lysis conditions had not disrupted complexes. Analysis by western blot and MS indicates that Dlar runs at the same molecular weight as Myosin Heavy Chain (MHC) (Fig. 24). Additional pre-clearing steps were added to remove excessive amounts of MHC, but this did not result in Dlar identification by MS. Switching to polyclonal anti-Dlar Ig12 (Rabbit 29295) and anti-Dlar FN5 (Rabbit 29293) allowed detection of Dlar (4-6% coverage) in the anti-Dlar Ig12 IP, and MHC as the only other identification. For this reason, these initial experiments were not comprehensive and only reflect bands unique from the control, anti-myc and anti-MPTPRG, lanes. Experiment S7-173 (Table 6), resulted in identification of αPS2, αPS3 and a BM protein, Glutactin (Glt), in the Dlar and integrin IPs, supporting continued work on the project.

The mouse monoclonal IPs were repeated and analyzed by LC-MS/MS on an LTQ Orbitrap LX mass spectrometer (Thermo Scientific) for greater sensitivity (Table 7), resulting in a 1-2% Dlar coverage. Optimization of the protocol was achieved through attachment of the rabbit polyclonal antibody against the Dlar Ig12 to NHS-activated sepharose. The SDS-PAGE step becomes unnecessary because the heavy and

light IgG chains remain on the resin during elution allowing for analysis of total protein, resulting in an increase to ~20% coverage for Dlar. All groups represent three technical replicates, raw data is processed through a peptide searching database, Mascot v2.2.04 (Matrix Science). Quantitative analysis of anti-Dlar, anti-αPS2, anti-βPS or NHS-anti-DlarIg12 compared to control (anti-myc or NHS-Rabbit IgG) was verified in Scaffold4 v4.8.7 (Proteome Software) by selecting the following parameters: T-test (Benjamini-Hochberg $p < 0.05$), fold change by category, normalization (minimum value: 0.5), and protein/peptide FDRs to 1%. Analysis of experiment 1353 utilizing stringent pre-clearing with Rat IgG, anti-MHC and protein A/G agarose results show that Dlar peptides are not statistically significant. Accordingly, experiments 1390 and 1412 utilized protein A//G agarose or NHS-resin for pre-clearing and results in Dlar identification that is statistically significant (Fig. 25). However, no known Dlar-binding proteins were identified nor were hits replicated between the two experiments. In contrast, integrin dimers are detected in the 1353, 1390 and 1412 integrin IPs (not shown).

The final series of experiments from fly lysates are indexed in Table 8, LC-MS/MS was carried out on an Orbitrap Fusion Tribrid Mass Spectrometer (Thermo Scientific). The NHS-anti-Dlar Ig12 IPs were repeated with the incorporation of zinc into the lysis buffer based on the Dlar FN5 crystal structure. In addition to the IPs, pull-down experiments were carried out with purified proteins attached to NHS-activated sepharose; these included Dlar FN45, Dlar Ig12, the Dlar ECD (sDlar – for soluble) and the FN1-FN3 domains of the mouse CAM, contactin 4 (CNTN4), as a control. Pull-

down experiments utilizing capture by protein A agarose were carried out with purified sDlar and Glt Fc-fusion proteins from large scale transfections of HEK293 cells. The sDlar/Glt series included +/- EDTA/EGTA versus +/- divalent cations as Glt has multiple metal binding sites [118]. NHS- experiments utilized in-solution digestion from resin and protein A agarose required in-gel digestion to remove the excess bait. Each sample was run in three replicates. The raw data was processed with MaxQuant v1.5.3.8 [133], while the statistical analysis was carried out in Perseus 1.2.0.16 (Max Planck Institute of Biochemistry). Both normal intensities and label-free quantification (LFQ) intensities were analyzed in Perseus because the experiments were carried out over a long period and there may have been differences in handling. The LFQ intensities are normalized before statistical analysis and was designed to handle large datasets that have orders of magnitude differences in protein abundance [134]. Statistical threshold was determined on normalized data by T-test (Benjamini-Hochberg FDR $p < 0.05$), replicates were averaged and log2-transformed. Protein hits that were enriched at least 10-fold compared to control were considered statistically significance (Supplementary Table 2).

The results of the Glt-Fc pull-downs show enrichment of just four proteins. Two of these proteins are alpha subunits of the basement membrane (BM) protein Collagen IV (Col IV): Collagen type IV α1 (Col4a1) and Viking (Vkg) [135]. Col IV is the most abundant component of the BM, but Col IV enrichment is restricted to the Glt pull-downs. Col4a1 is an integrin ligand and mutations in the integrin binding site are implicated in muscular dystrophies in mice [136]. A Glt/Col IV physical interaction could

account for the intergrin and actin phenotypes observed in *Glt*-depleted muscle. Additionally, Dlar is highly enriched in the Glt-Fc; however, all peptides belong to the ECD only and may represent contamination from the sDlar-Fc run on the spectrometer. To support this conclusion, Glt peptides are not statistically significant in Dlar IPs and pull-downs. This leads to speculation that disruption of the BM surrounding muscle may result in integrin/actin phenotypes in the absence of a specific physical interaction. More specifically, Dlar may interact with BM proteins and the integrin phenotype observed in *Dlar*-depleted muscle is the result of disruption to the BM.

The improved protocol and instrumentation results in robust protein identification in the Dlar IPs and pull-downs (Supplementary Table 2). Dlar Ig12 pull-downs identify three HSPGs, known Lar-RPTP ligands (Table 1). First, an *in vivo* Dlar ligand called Syndecan (Sdc), a membrane-bound HSPG which associates with Dlar during the formation of the NMJ [24,25]. The next HSPG is a member of the glypican family called Division abnormally delayed (Dally). There are only two glypicans in flies and the other, Dallylike (dlp), is another *in vivo* Dlar ligand and has been implicated in NMJ formation with Sdc [25]. Last, a secreted HSPG that is incorporated into BMs, terribly reduced optic lobes (Trol), is the homolog to the mammalian proteoglycan Perlecan (Pcan). Trol and Wnt/Wingless (Wg) are implicated in bidirectional regulation of NMJ maturation [137]. Pcan binding partners include Laminin, Fibronectin, integrins and Dytroglycan (Dg), again supporting the hypothesis that Dlar binds to BM proteins in muscle. An additional link to Wnt/Wg signaling is through a

non-HSPG protein identified in the DlarIg12 pull-down called Secreted Wg-interacting molecule (Swim), a secreted lipocalin (Mulligan et al., 2012).

Our use of Dlar fragments from the ECD to make custom antibodies worked well for visualization in tissues but inadvertently may compete for important binding partners during co-IP. For example, the high affinity of Rabbit anti-Dlar Ig12 and anti-Dlar FN5 for sDlar, used as a control in alpha assays (discussed below), shows an increase of 500-fold and 90-fold over background; respectively. In this case, the recognition of the epitope by antibody could dislodge physiological binding partners accounting for the lack of statistically significant HSPG peptides in the anti-DlarIg12 IPs leaving the protocol without a real positive control. However, identification of one protein from both the NHS-sDlar pull-down and anti-DlarIg12 IP warrants examination. Cd98Hc is a subunit of a conserved amino acid transporter which also functions in cell fusion and cell adhesion [138]. Cd98 is a transmembrane glycoprotein that can regulate integrin activation by binding to βPS tails through the Cd98Hc subunit possibly providing the physical link between integrins and Dlar through a tripartite complex or integrin signaling pathway [139,140].

Validation of MS hits from L3 stage

To validate protein-protein interactions identified by IP or pull-down, we utilized three approaches: 1) Fc fusion pull-downs, 2) AlphaAssay and 3) cell surface binding assays. Fc-fusion pull-downs were utilized to investigate the Dlar/Glt interaction by expressing the sDlar, Dlar FN4-6 and full-length Glt as both Fc- and Hgh-fusion proteins. We find the Dlar and Glt bind in the presence of divalent cations,

but the binding is completely abolished with very low amounts of detergent indicating a non-specific interaction and confirming the Dlar IP and pull-down results (Fig. 26). However, membrane receptor/ligand interactions can be low affinity (Kd ~ 1-100uM), resulting in disruption of biologically significant interactions from wash steps [141]. Therefore, a no wash binding assay called Amplified Luminescent Proximity Homogeneous Assay (Alpha) technology (Perkin Elmer) was utilized for further validation of Dlar binding partners.

The AlphaScreen utilizes coated beads to increase avidity by binding multiple tagged-proteins. Further, the proteins are expressed as Fc and FcYTS fusion proteins in HEK293 cells, resulting in divalent proteins which further increase the avidity when bound to protein A coated donor beads and streptactin coated acceptor beads; respectively (Fanslow et al., 1992). FcYTS is the Fc region of an IgY, this allows dimer formation but does not recognize protein A. The Twin-Strep-tag® (TS) portion binds the homotetramer, streptactin. In addition to sDlar and Dlar FN4-6 from the Dlar/Glt Fc pull-downs, we utilized Dlar FN5 and Dlar Ig12 expressed in HEK293 cells. Glt has three distinct regions and the following Glt truncates were created: Gltn1 is the N-terminal carboxylesterase domain (aa18-603), Gltn2 is the carboxylesterase domain and Thr-rich middle region (aa18-617) and Gltc3 is the Thr-rich middle region and c-terminal Gln/Glu-rich regions (aa601-1026). Finally, we began verification of the other IP and pull-down hits from larval lysates beginning with Cd98HC, Swim and Dally.

AlphaAssay detection is through laser excitation at 680 nm of Donor bead and Acceptor bead emission at 520 – 620 nm (Fig. 27). FcYTS fusion proteins are incubated

with Fc only protein to obtain background luminescence which is subtracted from the emission of the FcYTS/FC fusion protein reactions. Interactions are considered significant when emission is ≥ 2 times over background. For positive controls we utilized anti-Dlar Ig12 which binds sDlar and Dlar Ig12. In addition, anti-Dlar FN5 binds to sDlar, Dlar FN4-6 and Dlar FN5. This conveniently confirms the specificity of our antibodies. The assays included +/- Zn^{2+} and +/- heparin (as a surrogate for HS) to determine binding is zinc- or HS-dependent.

Thus far, the AlphaAssays have not validated the MS hits. The yield of Dlar from initial mouse monoclonal antibody IPs was too low to accurately interpret binding partners over background contamination and the Glt/Dlar interaction should not have been investigated without identification in subsequent experiments. The expression of Swim from HEK293 cells was barely detectable by western blot against the Fc or TS epitopes and should be repeated with higher concentration. CD98Hc and Dally expression was confirmed by western blot, but both result in emission < 2. However, over-expression of UAS-Dally at the *Drosophila* NMJ results in Dlar-AP binding indicating that a physiologically relevant positive control is needed to validate the assay parameters [25].

The low affinity and transient protein-protein interactions at the cell surface are thought to be stabilized by clustering in the membrane. The last validation experiments utilize expression of membrane proteins at the cell surface by expressing a Dlar construct consisting of the Dlar ECD, a transmembrane region and an intracellular emerald. To detect binding at the plasma membrane, Fc-fusion proteins are incubated

with anti-human Fc conjugated to AlexaFluor 568 to form a tetramer. The tetramer is incubated with the Dlar-emerald expressing cells, washed and then fixed. Controls are Dlar-emerald alone and anti-Dlar Ig12 incubated with anti-rabbit IgG conjugated to AlexaFluor 568. The following Fc-fusion proteins were assayed for cell surface binding in the presence of heparin: sDlar, APLP, Dally, Glt, Nrg and Vap33. Confocal microscopy confirms the expression of Dlar-emerald and co-localization of Dlar-emerald with anti-DlarIg12, but no Fc-fusion proteins have been confirmed.

Lar-RPTP binding partners in mammalian cell lines

To identify a possible conserved ligand for the FN4-6 domains, pull-down experiments were carried out from the following mammalian cell line lysates: B35 (rat neuroblastoma), C2C12 (mouse myoblast), C6 (rat glioblastoma), HEK293 (human embryonic kidney), and Neuro2a (mouse neuroblastoma). Lysates were incubated with the following purified proteins attached to NHS-resin: the FN4-FN7 domains of mouse LAR (MLar FN4-7) and mouse PTPRD (MPTPRD FN4-7) for bait and the FN1-FN3 domains of mouse CNTN1 (MCNTN1 FN1-3) or mouse CNTN6 (MCNTN6 FN1-3) as negative controls. The raw data was processed in MaxQuant and analyzed in Perseus as described above except only LFQ intensities were analyzed because all the samples were processed the same way around the same time frame (Supplementary Table 3).

The most conspicuous results include in two basement membrane proteins, collagen α1 chain (Col1a1) from Lar/C2C12 and Perlecan (hspg2) from Lar/C2C12, PTPRD/C2C12 and Lar/Neuro2a. Another is the non-integrin transmembrane receptor of the costamere, Dystroglycan (Dg), from both Lar and PTPRD/C6 cells. Dg is

implicated in muscular dystrophies and has roles in neural development as well. Pcan is not the only conserved hit between flies and mammals, Lactadherin from the Lar and PTPRD/C6 pull-downs is the homolog to hemolectin from the NHS-sDlar and NHS-anti-DlarIg12 experiments. Both proteins have roles in immune response and additional proteins from both mammals and flies function in immune response including: Plexin B2, Alpha-1-macroglobulin, complement c3 and Inter-alpha trypsin inhibitor, heavy chain 1 in mammals; and [142–144] C-type lectin 27kD and serine proteases (Jon25Bi, 25Bii, 25Biii, 65Ai, 65Aii, 66Ci, 99Ciii, 99Fi, 99Fii) in flies [145,146]. Validation has not been undertaken for MS identifications from the mammalian cell line pull-downs.

Conclusion

In this chapter, we have presented optimization of an IP protocol to recover statistically significant peptide hits for Dlar from larval lysates. Results from both Glt and Dlar proteome experiments confirm that Dlar and Glt do not physically interact despite a similar phenotype in the L3 musculature resulting in hypercontraction and integrin mislocalization. Both Dlar and Glt interact with BM proteins and it is conceivable that disruption of the BM can account for the muscle phenotypes. However, lack of validation of any Dlar MS/MS hits is a problem. We cannot assess the experimental design without a true positive control. To this end, we have cloned Dlp for expression in HEK293 cells as an Fc- and FcYTS fusion protein. Dlp is an *in vivo* ligand and Dlar/Dlp binding could confirm the validity of the AlphaAssay or cell surface binding assays. HEK293 protein expression may not represent the native post-translational modifications of *Drosophila* receptor and BM proteins. Alternatively,

expression could be carried out in Sf9 or S2 cells. Validation of mammalian cell complexes is conceptually straight forward. The cell lysates should not have the abundance of proteins found in a larval lysate. Further, HEK293 expression of mammalian proteins should more closely represent the native proteins.

TABLE 6

LCMS EXPERIMENTAL INDEX

Experiment	Pre-clear	Control	Bait	Bait	Bait	Buffer
S7-169	protein A/G agarose	anti-myc	anti-Dlar	anti-αPS2/anti-βPS		50mM Tris 7.5, 150mM NaCl, 10% (v/v) glycerol, 0.5% (w/v) Na deoxycholate, 0.5% (v/v) TritonX-100, 0.5mM $CaCl_2$, 0.5mM $MgCl_2$
S7-173	Rat IgG, anti-MHC, protein A/G agarose	anti-myc	anti-Dlar	anti-αPS2	anti-βPS	50mM Tris 7.5, 150mM NaCl, 10% (v/v) glycerol, 0.1% (w/v) Na deoxycholate, 0.1% (v/v) TritonX-100, 0.5mM $CaCl_2$, 0.5mM $MgCl_2$
S7-181(1)	Rat IgG, anti-MHC, protein A/G agarose	anti-myc	anti-Dlar	anti-αPS2	anti-βPS	50mM Tris 7.5, 150mM NaCl, 10% (v/v) glycerol, 0.1% (w/v) Na deoxycholate, 0.1% (v/v) TritonX-100, 0.5mM $CaCl_2$, 0.5mM $MgCl_2$
S7-181(2)	Rat IgG, anti-MHC, protein A/G agarose	anti-MPTPRG	anti-Dlar Ig12	anti-Dlar FN5		50mM Tris 7.5, 150mM NaCl, 10% (v/v) glycerol, 0.1% (w/v) Na deoxycholate, 0.1% (v/v) TritonX-100, 0.5mM $CaCl_2$, 0.5mM $MgCl_2$

LCMS experiments were carried out at the UMKC Core Facility (see materials and methods). Lysates were prepared from *WT* L3 larvae and homogenized in the buffer indicated above plus protease inhibitors. Anti-myc, anti-Dlar (DSHB), anti-αPS2 (DSHB) and anti-βPS (DSHB) are mouse monoclonal antibodies. Anti-MPTPRG, Rb 29295 anti-Dlar Ig12 and Rb 29293 anti-Dlar FN5 are polyclonal custom antibodies, affinity purified from exsanguination. Capture was carried out with protein A/G agarose (Pierce). Protein was eluted from agarose with 4x SDS loading buffer, run on SDS-PAGE and visualized with silver stain.

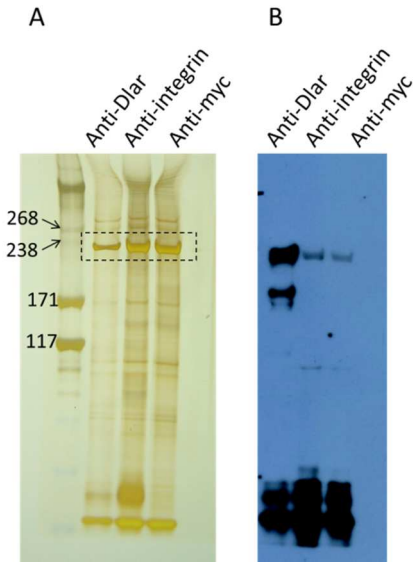

Figure 24. MHC is a high molecular weight contaminant. (A-B) Dlar and integrin IP experiment. After capture with protein A/G agarose, proteins were eluted with 4x SDS loading buffer. Elution fractions were loaded onto a gel in duplicate and run on SDS-PAGE. Gel was cut in half for silver stain (A) and analysis by LCMS. Remaining half of gel was transferred to PVDF for western blotting (B). (A) Silver stain gel for LCMS (experiment S7-169 in Table 6) leads to identification of MHC (dashed box) which is a 225 kDa protein. (B) Western blot with anti-Dlar Ig12 shows Dlar protein in anti-Dlar, anti-integrin and anti-myc IPs.

TABLE 7

LTQ ORBITRAP LX EXPERIMENTAL INDEX

Experiment	Pre-clear	Control	Bait	Bait	Bait	Buffer
1353	Rat IgG, anti-MHC, protein A/G agarose	anti-myc	anti-Dlar	anti-αPS2	anti-βPS	50mM Tris 7.5, 150mM NaCl, 10% (v/v) glycerol, 0.1% (w/v) Na deoxycholate, 0.2% (v/v) TritonX-100, 0.5mM $CaCl_2$, 0.5mM $MgCl_2$
1390	Protein A/G agarose	anti-myc	anti-Dlar	anti-αPS2	anti-βPS	50mM Tris 7.5, 150mM NaCl, 10% (v/v) glycerol, 0.1% (w/v) Na deoxycholate, 0.2% (v/v) TritonX-100, 0.5mM $CaCl_2$, 0.5mM $MgCl_2$
1412	NHS-Rat IgG	NHS-Rb IgG	NHS-anti-Dlar Ig12			50mM Tris 7.5, 150mM NaCl, 10% (v/v) glycerol, 0.1% (w/v) Na deoxycholate, 0.2% (v/v) TritonX-100, 0.5mM $CaCl_2$, 0.5mM $MgCl_2$

LTQ Oribtrap XL LC-MS/MS experiments were carried out at the OSU Core Facility (see materials and methods). Lysates were prepared from *WT* L3 larvae and homogenized in the buffer indicated above plus protease inhibitors. Anti-myc, anti-Dlar (DSHB), anti-αPS2 (DSHB) and anti-βPS (DSHB) are mouse monoclonal antibodies. Capture was carried out with protein A/G agarose (Pierce). Protein was eluted from agarose with 4x SDS loading buffer, run on SDS-PAGE and visualized with coomassie stain. NHS-anti-Dlar Ig12 (Rabbit 29295) is a custom polyclonal affinity purified antibody attached to NHS-activated agarose.

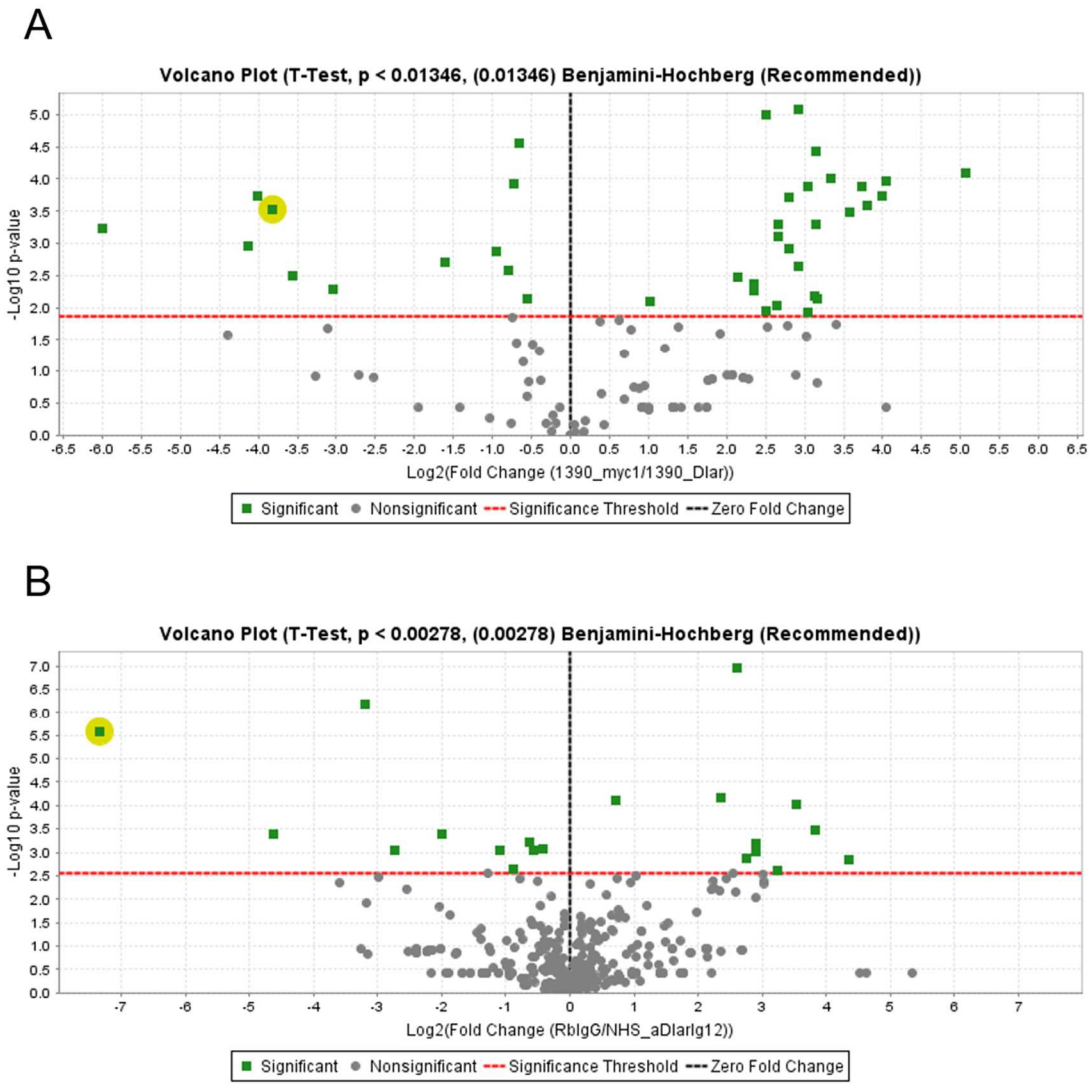

Figure 25. Volcano Plot. Comparison of Dlar IPs with monoclonal mouse anti-Dlar (A) and NHS-Rabbit anti-DlarIg12 (B). Highlighted green squares represent Dlar. Dlar in (B) has larger magnitude fold change (x-axis) and higher statistical significance (y-axis).

TABLE 8

ORBITRAP FUSION TRIBRID EXPERIMENTAL INDEX

Experiment	Pre-clear	Control	Bait	Bait	Buffer
1431	NHS-Rat IgG	NHS-Rb IgG	NHS-anti-Dlar Ig12		50mM Tris 7.5, 150mM NaCl, 10% (v/v) glycerol, 0.1% (w/v) Na deoxycholate, 0.1% (v/v) TritonX-100, 0.5mM $CaCl_2$, 0.5mM $MgCl_2$
1491a	NHS-sepharose	NHS-Rb IgG	NHS-anti-Dlar Ig12		50mM Tris 7.5, 150mM NaCl, 10% (v/v) glycerol, 0.1% (w/v) Na deoxycholate, 0.1% (v/v) TritonX-100, 1mM CaCl2, 1mM MgCl2, 100uM $Zn(OAc)_2$
1454a	NHS-sepharose	NHS-Rb IgG	NHS-anti-Dlar Ig12		50mM Tris 7.5, 150mM NaCl, 1% (v/v) TritonX-100, 1mM $CaCl_2$, 1mM $MgCl_2$, 100uM $Zn(OAc)_2$
1454b	NHS-sepharose	NHS-Rb IgG	NHS-anti-Dlar Ig12		50mM Tris 7.5, 150mM NaCl, 1% (v/v) TritonX-100, 1mM $CaCl_2$, 1mM $MgCl_2$, 100uM $Zn(OAc)_2$
1454c	NHS-sepharose	NHS-Rb IgG (from 1454a)	NHS-Dlar Ig12	NHS-Dlar FN45	50mM Tris 7.5, 150mM NaCl, 1% (v/v) TritonX-100, 1mM $CaCl_2$, 1mM $MgCl_2$, 100uM $Zn(OAc)_2$
1491b	NHS-sepharose	NHS-CNTN4 FN1-3	NHS-Dlar FN45		50mM Tris 7.5, 150mM NaCl, 1% (v/v) TritonX-100, 1mM $CaCl_2$, 1mM $MgCl_2$, 100uM $Zn(OAc)_2$
1491c	NHS-sepharose	NHS-CNTN4 Ig1-3	NHS-sDlar		50mM Tris 7.5, 150mM NaCl, 1% (v/v) TritonX-100, 1mM $CaCl_2$, 1mM $MgCl_2$, 100uM $Zn(OAc)_2$

"TABLE 8 – Continued."

ORBITRAP FUSION TRIBRID EXPERIMENTAL INDEX

Experiment	Pre-clear	Control	Bait	Bait	Bait	Buffer
1452	protein A agarose	Fc	sDlar-Fc	Glt-Fc		50mM Tris 7.5, 150mM NaCl, 1% (v/v) TritonX-100, 1mM EDTA, 1mM EGTA
1453	protein A agarose	Fc	sDlar-Fc	Glt-Fc		50mM Tris 7.5, 150mM NaCl, 1% (v/v) TritonX-100
1456	protein A agarose	Fc	sDlar-Fc	Glt-Fc		50mM Tris 7.5, 150mM NaCl, 1% (v/v) TritonX-100, 1mM $CaCl_2$, 1mM $MgCl_2$, 100uM $Zn(OAc)_2$

Oribtrap Fusion Tribrid LC-MS/MS experiments were carried out at the OSU Core Facility (see materials and methods). Lysates were prepared from *WT* L3 larvae and homogenized in the buffer indicated above plus protease inhibitors. NHS-anti-Dlar Ig12 is Rb29295 custom polyclonal antibodies, affinity purified from exsanguination and attached to NHS-activated sepharose (GE Healthcare). NHS-Dlar Ig12 and NHS-Dlar FN45 are overexpressed in *E. coli,* purified, and attached to NHS-activated sepharose (materials and methods). NHS-resins are centrifuged after incubation, washed three times and frozen in liquid nitrogen. sDlar-Fc (refers to the entire Dlar ECD) and Glt-Fc were expressed as Fc fusion proteins in HEK293 cells. Capture was carried out with protein A agarose (Sigma). Protein was eluted from agarose with 4x SDS loading buffer, run on SDS-PAGE and visualized with coomassie stain.

TABLE 9

MAMMALIAN CELL CULTURE EXPERIMENTAL INDEX

Cell culture	Pre-clear	Control	Control	Bait	Bait	Buffer
C6	CNBr-sepharose	CNTN1 Ig1-3	CNTN6 Ig1-3	Mlar FN4-7	MPTPRD FN4-7	50mM Tris 7.5, 150mM NaCl, 1% (v/v) TritonX-100, 1mM $CaCl_2$, 1mM $MgCl_2$
B35	CNBr-sepharose	CNTN1 Ig1-3	CNTN6 Ig1-3	Mlar FN4-7	MPTPRD FN4-7	50mM Tris 7.5, 150mM NaCl, 1% (v/v) TritonX-100, 1mM $CaCl_2$, 1mM $MgCl_2$
C2C12	CNBr-sepharose	CNTN1 Ig1-3	CNTN6 Ig1-3	Mlar FN4-7	MPTPRD FN4-7	50mM Tris 7.5, 150mM NaCl, 1% (v/v) TritonX-100, 1mM $CaCl_2$, 1mM $MgCl_2$
N2A	CNBr-sepharose	CNTN1 Ig1-3	CNTN6 Ig1-3	Mlar FN4-7	MPTPRD FN4-7	50mM Tris 7.5, 150mM NaCl, 1% (v/v) TritonX-100, 1mM $CaCl_2$, 1mM $MgCl_2$
HEK292	CNBr-sepharose	CNTN1 Ig1-3	CNTN6 Ig1-3	Mlar FN4-7	MPTPRD FN4-7	50mM Tris 7.5, 150mM NaCl, 1% (v/v) TritonX-100, 1mM $CaCl_2$, 1mM $MgCl_2$

Oribtrap Fusion Tribrid LC-MS/MS experiments were carried out at the OSU Core Facility (see materials and methods). Control and bait proteins were overexpressed in *E. coli*, purified by standard methods and attached to CNBr-activated sepharose (GE Healthcare). After incubation in cell culture lysates (homogenized in indicated buffer plus protease inhibitors), resin was washed three times and frozen in liquid nitrogen.

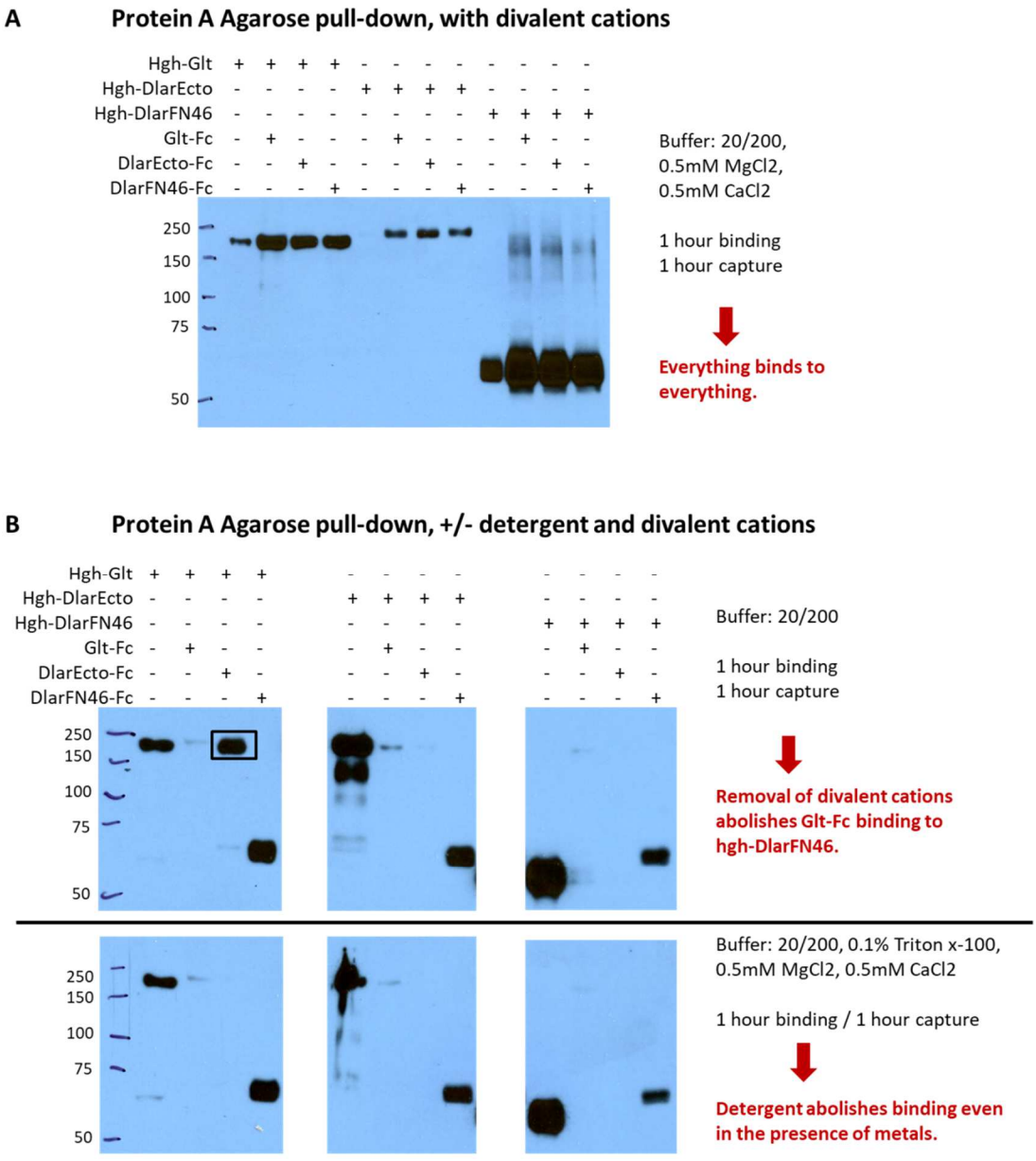

Figure 26. Dlar/Glt binding is abolished in the presence of 0.1% Triton x-100. (A-B) Western blot probed with anti-Hgh antibodies.

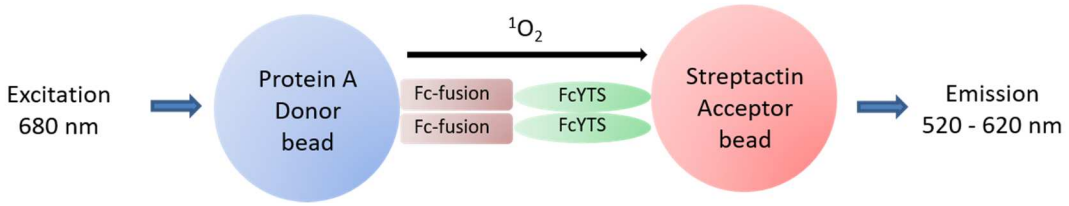

Figure 27. AlphaAssay detection. Upon laser excitation at 680 nm causes a photosensitizer in the Donor beads to convert O_2 to a singlet state. The singlet oxygen molecules react with the chemiluminescer of the Acceptor bead which leads to emission at 520 – 620 nm.

CHAPTER 6

FINAL DISCUSSION

We have found a novel function for Dlar in muscle integrity. Dlar localizes to the larval costamaere. Ablation of Dlar in muscle tissue causes hypercontraction and mislocalization of costameric integrin subunits in L3 stage. Additionally, L3 larvae have reduced crawling speeds compared to *WT*. We find two additional proteins that display the phenotypes of the *Dlar*-null with the expression of RNAi by a muscle driver: the BM protein, Glt, and the Z-disc associated GEF, Trio. However, dystrophic *tn* mutant larvae which display muscle wasting associated with unbundling of myofibers from reduced costamere integrity have characteristics that are missing in the *Dlar*-null phenotype. First, *tn* mutants have a characteristic "thin" pupal phenotype which is characterized by an increased length/width axial ratio due to the inability to complete the muscle contractions necessary for pupation. In contrast, the *Dlar*-null pupae are smaller in both length and width maintaining a length/width ratio similar to *WT* pupae. Both *24B > Glt RNAi* and *24B > trio RNAi* pupae are normal size in both length and width. All *trio* and *Glt RNAi* lines are pupal lethal with the *24B-Gal4* driver. However, only one *Dlar RNAi* line (BL34965) is pupal lethal with the muscle driver. The BL34965 line shows the largest decrease in Dlar by qPCR when compared to the other two RNAi lines (BL40938 and BL47939). Additionally, the *Dlar13.2/Dlar5.5* mutants are pupal lethal. The question is whether the pupal lethality of the *Dlar13.2/Dlar5.5* is solely attributed to defective neural development compared to the muscular expression of the *Dlar RNAi* causing lethality because of off-target effects or

more robust knockdown of Dlar. However, considering that the *trio* and *Glt RNAi* lines are pupal lethal, an examination of the pupae may identify the determinants of lethality. Further, comparison of pupae from *Dlar RNAi* knockdown by both muscle and neural drivers could distinguish between the contribution of each toward pupal lethality.

The next characteristic of *tn* mutants are the disruption of costamere associated proteins including βPS, talin, vinculin and spectrin. Talin localization is normal in Dlar knockdown, but aberrant in Trio knockdown. This can be due to several possibilities 1) Dlar and Trio do not function in the same pathway in muscle tissue, 2) Dlar and Trio function in the same pathway but Trio receives multiple inputs and/or 3) the Dlar RNAi investigated was not the strongest RNAi line and represents incomplete Dlar ablation. The last is the simplest to address, Talin localization in *Dlar13.2/Dlar5.5* mutants should be compared to Talin localization in the Dlar RNAi lines with both muscle and neural drivers. Next, dosage sensitive *Dlar/trio* crosses and double mutants or knockdown could further delineate whether Dlar and Trio genetically interact in muscle tissue. Talin localization in the Glt RNAi lines should be examined as well. The localization of vinculin and spectrin by immunofluorescence would help determine whether the *Dlar*-null represents a disruption of the costamere assembly. Other components of the Z-disc including muscle LIM protein 84B (Mlp84B) and D-titin contribute to muscle integrity [123]. However, *mlp84B* and *Dtitin* mutants exhibit the pupal axial ratio of *tn* mutants indicating that we are probably looking for a different protein association.

The non-integrin component of the costamere is the DPC, the transmembrane receptor of the DPG is dystroglycan (Dg). *Dg* mutants have a hypercontraction phenotype similar to Dlar RNAi. *Dg* mutants display both neural and muscular defects. Knockdown by RNAi with a muscle driver results in hypercontraction and the neural driver does not. However, *Dg*-depleted larvae do not display reduced locomotor function and display some attachment defects, unlike the *Dlar*-null phenotype. Dg staining reveals localization to the sarcomeres, t-tubules and post-synapse; whereas, Dlar localization is more limited. Integrin localization and pupal size were not described for Dg mutants [124]. Both Mlar and HPTPRD pull-down Dg from C6 cell lysates indicating these proteins may interact. A *Dlar/Dg* double mutant could determine a genetic interaction. Also, confirmation of the physical interaction by binding assays.

One of the greatest impediments to the genetic characterization of Dlar in muscle, is the inconsistency of the actin phenotype. Due to this, the rescue experiments are not robust. It is advisable to find a different parameter to measure. The muscular expression of Dlar cannot rescue the lethality of the *Dlar* mutant. For this reason, possibly a locomotor assay would have been a better option, dependent on the results of characterization of the locomotor function of the Dlar RNAi knockdown with a neural driver. Additionally, the rescue of the integrin mislocalization could be an option.

Another complication with the genetic characterization of Dlar in muscle is the proposed interaction with Glt. As with Trio, Glt-depletion results in the characteristics

of Dlar-depletion, however we do not pull-down Glt with Dlar and vice versa in statistically relevant amounts in improved Dlar/Glt proteomics experiments. However, both Dlar and Glt proteins seem to associate with components of BMs, suggesting that the disruption of the BM surrounding the musculature could contribute to the actin and integrin phenotypes observed without specific physical interactions. Validation of the MS hits by binding assays will elucidate these interactions. First, a confirmed *in vivo* binding partner needs to be utilized as a positive control because the Dlar interaction with our anti-Dlar antibodies do not represent the low affinity, transient interactions associated with cell surface binding. AP-fusion proteins were utilized to detect in vivo interactions of Dlar with both Dlp and Sdc at the NMJ. We tried similar experiments at the larval costamere without success but determined that either the endogenous complex was preventing binding or that we had not identified binding partners. Again, a proper positive control could help determine whether this assay could work at the costamere, such as Sdc-AP or Dlp-AP in addition to utilization of over-expression of Dlar in the muscle by *24B-Gal4*.

One result of the rescue experiments is the determination that the FN4-6 and KGD tripeptide are not important for function in muscle tissue. This was confirmed by the x-ray crystallographic structures of Dlar and the mammalian orthologs indicating that Lar-RPTPs are not integrin ligands. Additional rescue experiments utilizing different truncations of the ECD to determine which fragments are important would help identify the type of ligands to search for in the proteomics data. Likewise, the lethality of the ΔPTPD2 domain indicates that this region is important to function in

the muscle. Additional experiments could include identification of Dlar substrates by pull-down with the PTPase domains. Our attempts to express the PTPase domains in *E. coli* were unsuccessful and may require mammalian or S2 cell expression. Future experiments to identify Dlar binding partners could include protein expression in S2 cells to ensure proper post-translational modifications. Further, pull-down experiments with the ECD fragments could be carried out with S2 cell lysates instead of larval lysates which may help maintain the low affinity interactions.

Last, the largest decrease in overall size of Dlar-null flies are seen in the BL34965 line; however, the Dlar mutants are also smaller than *WT* indicating that this aspect of the phenotype is not an off-target effect of RNAi. The size phenotype was not observed in the Trio or Glt knockdowns. Feeding assays could determine if there is nutritional component to the decrease in size. Alternatively, Dlar may function in the insulin signaling pathway in *Drosophila*. It was established in 1992 that Lar can dephosphorylate the insulin receptor kinase *in vitro*, and more recent studies have implicated both PTPRS and PTPRD in insulin signaling [147–149].

Taken together, we propose the following model for Dlar function in muscle tissue. Dlar interacts with the BM which provides support to the underlying tissue. When BMs are defective, the adjacent layers lose integrity. Mutations to integrins and BM proteins result in similar phenotypes. Therefore, BM/Dlar interactions lead to signaling through the GEF Trio. Trio signaling leads to cytoskeletal reorganization through small GTPases. Inside-out integrin signaling causes low affinity integrin conformation and loss of binding to integrin ligands in the BM.

APPENDIX

Supplementary Tables

Supplementary Table 1: Percent Identity Matrix - created by Clustal2.1

Receptor and phosphatase domains

1: sp|P16621|LAR_DROME	100.00	50.35	51.48	50.05
2: sp|P10586|PTPRF_HUMAN	50.35	100.00	70.32	67.77
3: sp|P23468|PTPRD_HUMAN	51.48	70.32	100.00	72.75
4: sp|Q13332|PTPRS_HUMAN	50.05	67.77	72.75	100.00

1: sp|P10586|PTPRF_HUMAN	100.00	70.32	67.77
2: sp|P23468|PTPRD_HUMAN	70.32	100.00	72.75
3: sp|Q13332|PTPRS_HUMAN	67.77	72.75	100.00

Phosphatase domains

1: sp|P16621|LAR_DROME	100.00	75.18	75.18	76.08
2: sp|P10586|PTPRF_HUMAN	75.18	100.00	89.93	90.83
3: sp|Q13332|PTPRS_HUMAN	75.18	89.93	100.00	92.81
4: sp|P23468|PTPRD_HUMAN	76.08	90.83	92.81	100.00

1: sp|P10586|PTPRF_HUMAN	100.00	89.93	90.83
2: sp|Q13332|PTPRS_HUMAN	89.93	100.00	92.81
3: sp|P23468|PTPRD_HUMAN	90.83	92.81	100.00

FN5 domain

1: Dlar	100.00	38.61	37.62	39.60
2: HLAR	38.61	100.00	70.00	64.55
3: HPTPRD	37.62	70.00	100.00	70.91
4: HPTPRS	39.60	64.55	70.91	100.00

1: HLAR	100.00	70.00	64.55
2: HPTPRD	70.00	100.00	70.91
3: HPTPRS	64.55	70.91	100.00

Fibronectin FN10

1: 1TTF_A|PDBID|CHAIN|SEQUENCE	100.00	25.88	30.43	29.35	26.09
2: Dlar/710-810	25.88	100.00	42.42	40.40	43.43
3: HLAR/710-819	30.43	42.42	100.00	70.00	64.55
4: HPTPRD/713-822	29.35	40.40	70.00	100.00	70.91

5: HPTPRS/722-831	26.09	43.43	64.55	70.91	100.00

1: 1TTF_A|PDBID|CHAIN|SEQUENCE	100.00	30.59
2: Dlar/710-810	30.59	100.00

Supplementary Table 2: Statistically significant proteins with signal sequences from Orbitrap Fusion Tribrid LC-MS/MS from fly lysates. Peptide and proteins identifications from MaxQuant and verification and analysis in Perseus.

Enrichment	Sample intensity (log2)	Control Intensity (Log2)	Student's T-test significant	Gene names	Pulled from
3,378	28.15678	20.03162	sDlar_Rb_IgG	Alp1	sDlar vs RbIgG
2,091	28.97246	21.32706	sDlar_Rb_IgG	Alp1	sDlar vs RbIgG LFQ
860	26.78905	20.03162	anti-Dlar_Rb_IgG	Alp1	anti-Dlar vs RbIgG
1,500	28.64031	21.32706	anti-Dlar_Rb_IgG	Alp1	anti-Dlar vs RbIgG LFQ
615	26.22823	19.80595	DlarIg12_RbIgG	Alp1	DlarIg12 vs RbIgG
11,511	26.18573	16.83467	DlarIg12_RbIgG	Alp1	DlarIg12 vs RbIgG LFQ
566	26.14418	19.80595	DlarFN45_RbIgG	Alp1	DlarFN45 vs RbIgG
7,328	25.73412	16.83467	DlarFN45_RbIgG	Alp1	DlarFN45 vs RbIgG LFQ
21	21.46219	18.43224	anti-Dlar_Rb_IgG	alpha-Est2	anti-Dlar vs RbIgG
12	21.04434	18.52814	anti-Dlar_Rb_IgG	alpha-Est4	anti-Dlar vs RbIgG
24	21.74526	18.55659	sDlar_Rb_IgG	Caix	sDlar vs RbIgG
19	19.23932	16.27402	Glt-Fc_Fc	Caix	Glt-Fc vs Fc
23	22.18997	19.05711	sDlar_Rb_IgG	CD98hc	sDlar vs RbIgG
47	22.91561	19.05711	anti-Dlar_Rb_IgG	CD98hc	anti-Dlar vs RbIgG
339	24.50996	18.68266	sDlar_Rb_IgG	cg10211	sDlar vs RbIgG
60	25.63362	21.54656	sDlar_Rb_IgG	cg10211	sDlar vs RbIgG LFQ
302	24.39316	18.68266	anti-Dlar_Rb_IgG	cg10211	anti-Dlar vs RbIgG
70	25.80154	21.54656	anti-Dlar_Rb_IgG	cg10211	anti-Dlar vs RbIgG LFQ
86	21.13333	16.67632	Dlar-Fc_Fc	CG13492	sDlar-Fc vs Fc
17	20.9239	18.08106	sDlar_Rb_IgG	CG1371	sDlar vs RbIgG
101	26.37013	21.75397	sDlar_Rb_IgG	CG2233	sDlar vs RbIgG
19	27.27293	24.32065	sDlar_Rb_IgG	CG2233	sDlar vs RbIgG LFQ

38	25.3981	21.75397	anti-Dlar_Rb_IgG	CG2233	anti-Dlar vs RbIgG
69	25.00599	20.77828	DlarIg12_RbIgG	CG2233	DlarIg12 vs RbIgG
85	25.07545	20.6344	DlarIg12_RbIgG	CG2233	DlarIg12 vs RbIgG LFQ
36	24.34881	20.77828	DlarFN45_RbIgG	CG2233	DlarFN45 vs RbIgG
13	23.23427	20.6344	DlarFN45_RbIgG	CG2233	DlarFN45 vs RbIgG LFQ
15	27.02179	24.32065	anti-Dlar_Rb_IgG	CG2233	anti-Dlar vs RbIgG LFQ
191	21.93557	16.68377	Glt-Fc_Fc	Cg25C	Glt-Fc vs Fc
38	24.1047	20.45928	Glt-Fc_Fc	Cg25C	Glt-Fc vs Fc LFQ
187	22.72542	17.49358	DlarFN45_RbIgG	CG32302	DlarFN45 vs RbIgG
37	22.42609	18.80447	DlarFN45_RbIgG	CG32302	DlarFN45 vs RbIgG LFQ
21	23.51485	20.4807	sDlar_Rb_IgG	CG32521-RB;CG32521-RC	sDlar vs RbIgG
62	25.3435	21.21833	DlarFN45_RbIgG	CG4115	DlarFN45 vs RbIgG
74	25.06595	20.76782	DlarFN45_RbIgG	CG4115	DlarFN45 vs RbIgG LFQ
17	24.76309	21.9512	sDlar_Rb_IgG	CG42486-RA	sDlar vs RbIgG
36	21.88606	18.31079	sDlar_Rb_IgG	CG5080	sDlar vs RbIgG
16	20.26385	17.47684	DlarIg12_RbIgG	CG6933-RA;CG6933-RC	DlarIg12 vs RbIgG
22	20.30575	17.19364	Dlar-Fc_Fc	CG7300	sDlar-Fc vs Fc
24	21.12288	17.94264	sDlar_Rb_IgG	cg7953	sDlar vs RbIgG
31	21.33342	17.9096	sDlar_Rb_IgG	CG8563-RA	sDlar vs RbIgG
45	22.63823	18.82978	sDlar_Rb_IgG	CG9572-RB;CG9572-RA	sDlar vs RbIgG
29	21.72205	18.34757	sDlar_Rb_IgG	Cht5	sDlar vs RbIgG
14	20.99438	18.34757	anti-Dlar_Rb_IgG	Cht5	anti-Dlar vs RbIgG
12	27.86331	25.37262	sDlar_Rb_IgG	Clect27	sDlar vs RbIgG
36	26.78407	23.21021	DlarFN45_RbIgG	Clect27	DlarFN45 vs RbIgG
17	26.19935	23.38929	DlarFN45_RbIgG	Clect27	DlarFN45 vs RbIgG LFQ

13	20.05828	17.46348	antiDlar(Ig12)_RbIgG	Cpr64Ad	anti-Dlar(Ig12) vs RbIgG a
18	26.68016	23.80902	sDlar_Rb_IgG	CtsB1	sDlar vs RbIgG
11	21.12912	18.69379	DlarIg12_RbIgG	Dally	DlarIg12 vs RbIgG LFQ
294,537	33.28099	20.68782	Glt-Fc_Fc	Glt	Glt-Fc vs Fc
84,203,749	36.09203	17.84328	Glt-Fc_Fc	Glt	Glt-Fc vs Fc LFQ
11	21.29709	18.88894	sDlar_Rb_IgG	Hml	sDlar vs RbIgG
27	22.19874	18.88894	anti-Dlar_Rb_IgG	Hml	anti-Dlar vs RbIgG
81	21.57778	17.17867	DlarIg12_RbIgG	Jon25Bi	DlarIg12 vs RbIgG
12	21.48075	19.01214	DlarIg12_RbIgG	Jon25Bi	DlarIg12 vs RbIgG LFQ
154	22.2149	17.17867	DlarFN45_RbIgG	Jon25Bi	DlarFN45 vs RbIgG
15	21.71079	19.01214	DlarFN45_RbIgG	Jon25Bi	DlarFN45 vs RbIgG LFQ
15	20.78237	18.05059	DlarIg12_RbIgG	Jon25Bii	DlarIg12 vs RbIgG
16	20.96564	18.20141	DlarIg12_RbIgG	Jon25Bii	DlarIg12 vs RbIgG LFQ
72	22.32674	18.05059	DlarFN45_RbIgG	Jon25Bii	DlarFN45 vs RbIgG
50	22.10348	18.20141	DlarFN45_RbIgG	Jon25Bii	DlarFN45 vs RbIgG LFQ
84	26.37494	21.94646	sDlar_Rb_IgG	Jon25Biii	sDlar vs RbIgG
39	25.03456	21.37836	DlarIg12_RbIgG	Jon25Biii	DlarIg12 vs RbIgG
44	24.85253	21.07326	DlarIg12_RbIgG	Jon25Biii	DlarIg12 vs RbIgG LFQ
48	25.24198	21.37836	DlarFN45_RbIgG	Jon25Biii	DlarFN45 vs RbIgG
43	24.83904	21.07326	DlarFN45_RbIgG	Jon25Biii	DlarFN45 vs RbIgG LFQ
28	21.87609	18.53061	sDlar_Rb_IgG	Jon65Ai	sDlar vs RbIgG
23	21.80629	18.68608	DlarFN45_RbIgG	Jon66Ci	DlarFN45 vs RbIgG
75	24.24133	19.92638	DlarIg12_RbIgG	Jon99Ciii;Jon65Aii	DlarIg12 vs RbIgG
61	24.04143	19.92713	DlarIg12_RbIgG	Jon99Ciii;Jon65Aii	DlarIg12 vs RbIgG LFQ
99	24.51875	19.92638	DlarFN45_RbIgG	Jon99Ciii;Jon65Aii	DlarFN45 vs RbIgG
48	23.80449	19.92713	DlarFN45_RbIgG	Jon99Ciii;Jon65Aii	DlarFN45 vs RbIgG LFQ

42	21.5871	17.85711	sDlar_Rb_IgG	Jon99Fii;Jon99Fi	sDlar vs RbIgG
34	21.39263	17.85711	anti-Dlar_Rb_IgG	Jon99Fii;Jon99Fi	anti-Dlar vs RbIgG
79	21.904	17.53839	DlarIg12_RbIgG	Jon99Fii;Jon99Fi;Jon44E	DlarIg12 vs RbIgG
14	21.857	19.19548	DlarIg12_RbIgG	Jon99Fii;Jon99Fi;Jon44E	DlarIg12 vs RbIgG LFQ
67	21.74743	17.53839	DlarFN45_RbIgG	Jon99Fii;Jon99Fi;Jon44E	DlarFN45 vs RbIgG
3,803,606	37.27396	22.12249	sDlar_Rb_IgG	Lar	sDlar vs RbIgG LFQ
67,091	32.01704	20.90323	anti-Dlar_Rb_IgG	Lar	anti-Dlar vs RbIgG
21,871	32.11539	22.12249	anti-Dlar_Rb_IgG	Lar	anti-Dlar vs RbIgG LFQ
15,509	26.5796	16.9304	anti-DlarIg12_RbIgG	Lar	anti-Dlar(Ig12) vs RbIgG
805	25.30069	18.61043	anti-Ig12_RbIgG	Lar	anti-Dlar(Ig12) vs RbIgG LFQ
25,693	38.18935	28.03538	DlarFN46_CNTN4FN13	Lar	DlarFN46 vs CNTN4FN13
351,509	39.91277	27.14277	DlarFN46_CNTN4FN13	Lar	DlarFN46 vs CNTN4FN13 LFQ
4,030,657	35.01633	19.80689	Dlar-Fc_Fc	Lar	sDlar-Fc vs Fc
1,612,329	35.54472	21.25153	Dlar-Fc_Fc	Lar	sDlar-Fc vs Fc LFQ
12,513	29.24141	19.80689	Glt-Fc_Fc	Lar	Glt-Fc vs Fc
8,533	30.30324	21.25153	Glt-Fc_Fc	Lar	Glt-Fc vs Fc LFQ
10,472	27.35624	18.0998	antiDlar(Ig12)_RbIgG	Lar	anti-Dlar(Ig12) vs RbIgG a
3,389	25.44746	17.31921	anti-Dlar(Ig12)_RbIgG	Lar	anti-Dlar(Ig12) vs RbIgG LFQ a
462,069	31.14327	18.0998	DlarIg12_RbIgG	Lar	DlarIg12 vs RbIgG
55,112	28.5229	17.60577	DlarIg12_RbIgG	Lar	DlarIg12 vs RbIgG LFQ
586,695	31.38206	18.0998	DlarFN45_RbIgG	Lar	DlarFN45 vs RbIgG
1,582,110	31.88004	17.60577	DlarFN45_RbIgG	Lar	DlarFN45 vs RbIgG LFQ
11	20.78485	18.39534	sDlar_Rb_IgG	Loh	sDlar vs RbIgG
13	23.81763	21.27333	DlarIg12_RbIgG	Lsp1alpha	DlarIg12 vs RbIgG

13	23.70957	21.11	DlarIg12_RbIgG	Lsp1alpha	DlarIg12 vs RbIgG LFQ
30	24.66221	21.27333	DlarFN45_RbIgG	Lsp1alpha	DlarFN45 vs RbIgG
22	24.19746	21.11	DlarFN45_RbIgG	Lsp1alpha	DlarFN45 vs RbIgG LFQ
14	30.30062	27.68224	sDlar_Rb_IgG	Lsp1gamma	sDlar vs RbIgG
13	21.53274	18.95229	DlarIg12_RbIgG	Muc55B	DlarIg12 vs RbIgG
18	21.53787	18.66364	DlarIg12_RbIgG	Muc55B	DlarIg12 vs RbIgG LFQ
31	21.43781	18.0193	sDlar_Rb_IgG	Muc68Ca	sDlar vs RbIgG
11	20.74222	18.32239	DlarIg12_RbIgG	NimC1	DlarIg12 vs RbIgG LFQ
13	20.8637	18.32239	DlarFN45_RbIgG	NimC1	DlarFN45 vs RbIgG LFQ
58	27.8649	23.79759	sDlar_Rb_IgG	Nw	sDlar vs RbIgG
37	28.7631	25.14802	sDlar_Rb_IgG	Nw	sDlar vs RbIgG LFQ
20	28.13531	25.14802	anti-Dlar_Rb_IgG	Nw	anti-Dlar vs RbIgG LFQ
12	20.47853	18.03159	DlarIg12_RbIgG	PGRP-SB1	DlarIg12 vs RbIgG
20	21.04634	18.03159	DlarFN45_RbIgG	PGRP-SB1	DlarFN45 vs RbIgG
83	25.91666	21.49882	sDlar_Rb_IgG	Ppn	sDlar vs RbIgG
22	26.46145	23.38824	sDlar_Rb_IgG	Ppn	sDlar vs RbIgG LFQ
25	24.70978	21.49882	anti-Dlar_Rb_IgG	Ppn	anti-Dlar vs RbIgG
18	26.26465	23.38824	anti-Dlar_Rb_IgG	Ppn	anti-Dlar vs RbIgG LFQ
104	23.37915	18.73437	DlarIg12_RbIgG	Ppn	DlarIg12 vs RbIgG
89	23.15657	18.66605	DlarIg12_RbIgG	Ppn	DlarIg12 vs RbIgG LFQ
353	24.59963	18.73437	DlarFN45_RbIgG	Ppn	DlarFN45 vs RbIgG
315	24.41931	18.66605	DlarFN45_RbIgG	Ppn	DlarFN45 vs RbIgG LFQ
43	22.03869	18.28534	DlarIg12_RbIgG	Sdc	DlarIg12 vs RbIgG LFQ
141	22.42936	17.48385	DlarIg12_RbIgG	sp151	DlarIg12 vs RbIgG
84	22.38459	17.95657	DlarIg12_RbIgG	sp151	DlarIg12 vs RbIgG LFQ
162	22.57247	17.48385	DlarFN45_RbIgG	sp151	DlarFN45 vs RbIgG

69	22.18483	17.95657	DlarFN45_RbIgG	sp151	DlarFN45 vs RbIgG LFQ
289	24.80302	19.13796	DlarIg12_RbIgG	Swim	DlarIg12 vs RbIgG
1,263	24.84953	17.70813	DlarIg12_RbIgG	Swim	DlarIg12 vs RbIgG LFQ
29	22.07463	18.70361	DlarIg12_RbIgG	Troll	DlarIg12 vs RbIgG LFQ
11	20.10482	17.70745	DlarFN45_RbIgG	Vago	DlarFN45 vs RbIgG
81	20.78732	16.39874	Glt-Fc_Fc	Vkg	Glt-Fc vs Fc

Supplementary Table 3: Statistically significant proteins with signal sequences from Orbitrap Fusion Tribrid LC-MS/MS from mammalian cell line lysates. Peptide and proteins identifications from MaxQuant and verification and analysis in Perseus

Enrichment	Sample intensity (log2)	Control Intensity (Log2)	Student's T-test significant	Gene Name	Protein - Cell line	Fly homolog
59	*27.99016*	*23.91841*	*PTPRD_CNTN1+6*	*A1m*	*PTPRD - C6*	*tep2, tep4?*
1,261	30.84461	23.7051	PTPRD_CNTN1+6	Adgrg1	PTPRD - B35	cg11318, cirl?
617	29.19213	22.76675	PTPRD_CNTN1+6	Angptl2	PTPRD - C2C12	cg41520, 30281, 30280
75,160	33.38998	22.16261	PTPRD_CNTN1+6	Apod	PTPRD - B35	nlaz
13	*25.77442*	*23.20596*	*PTPRD_CNTN1+6*	*Bsg*	*PTPRD - C6*	*bsg*
18	*29.24459*	*26.37393*	*LAR_CNTN1+6*	*Bsg*	*LAR - C6*	*bsg*
821	28.29807	21.58786	PTPRD_CNTN1+6	C3	PTPRD - C2C12	tep2, tep1, tep4?
164	27.65492	22.5549	LAR_CNTN1+6	Cd99	LAR - C6	no significant hit
47	29.88983	26.04015	PTPRD_CNTN1+6	Chrdl1	PTPRD - C6	sog
50	22.87581	18.97136	LAR_CNTN1+6	Col1a1	LAR - C2C12	Col4a1 / vkg
13	*24.89712*	*22.35587*	*PTPRD_CNTN1+6*	*Ctsb*	*PTPRD - C6*	*ctsb1*
18	*27.36611*	*24.4576*	*LAR_CNTN1+6*	*Ctsb*	*LAR - C6*	*ctsb1*
32	*25.97482*	*22.49776*	*PTPRD_CNTN1+6*	*Ctsd*	*PTPRD - C6*	*cathD, cg10104, 17134*
25,506	*31.89558*	*21.74891*	*PTPRD_CNTN1+6*	*Ctsf*	*PTPRD - B35*	*cg12163*
26	*25.35642*	*22.08314*	*LAR_CNTN1+6*	*Ctsf*	*LAR - C6*	*cg12163*
36	22.77983	19.18565	PTPRD_CNTN1+6	Dag1	PTPRD - C6	dg
241	27.68432	22.20015	LAR_CNTN1+6	Dag1	LAR - C6	dg
96,839	34.46069	22.97988	PTPRD_CNTN1+6	Dhh	PTPRD - B35	hh
10	27.90518	25.55421	PTPRD_CNTN1+6	Emb	PTPRD - Neuro2a	dip-eta

13	25.01954	22.44803	LAR_CNTN1+6	Emb	LAR - Neuro2a	dip-eta
31	*29.73688*	*26.30634*	*LAR_CNTN1+6*	*Grn*	*LAR - C6*	*no significant hit*
494	28.59249	22.3892	PTPRD_CNTN1+6	Hspg2	PTPRD - C2C12	trol
309	24.87061	19.13603	LAR_CNTN1+6	Hspg2	LAR - C2C12	trol
13	24.52546	21.92719	LAR_CNTN1+6	Hspg2	LAR - Neuro2a	trol
18	*25.27803*	*22.38131*	*PTPRD_CNTN1+6*	*Igf2r*	*PTPRD - C6*	*lerp*
33	*25.57039*	*22.06979*	*PTPRD_CNTN1+6*	*Il1rap*	*PTPRD - C6*	*tollo*
12	33.09388	30.5823	PTPRD_CNTN1+6	Itga1	PTPRD - C6	mew
17	25.32334	22.50592	PTPRD_CNTN1+6	Itga5	PTPRD - C6	if
42	*23.174*	*19.43974*	*PTPRD_CNTN1+6*	*Itga6*	*PTPRD - C6*	*mew*
18	*26.85043*	*23.95673*	*LAR_CNTN1+6*	*Itga6*	*LAR - C6*	*mew*
24	25.85816	22.69468	PTPRD_CNTN1+6	Itga7	PTPRD - C6	mew
14	*28.54004*	*25.91737*	*PTPRD_CNTN1+6*	*Itgb1*	*PTPRD - C6*	*mys*
11	*27.91974*	*25.49579*	*LAR_CNTN1+6*	*Itgb1*	*LAR - C6*	*mys*
111	27.82469	23.11092	PTPRD_CNTN1+6	Itih1	PTPRD - C6	stj?
1,119	28.59783	21.57727	LAR_CNTN1+6	Itih1	LAR - C6	stj?
16	*24.82886*	*22.08617*	*PTPRD_CNTN1+6*	*Lgals1*	*PTPRD - C6*	*galectin*
13	*33.10878*	*30.5823*	*LAR_CNTN1+6*	*Lgals1*	*LAR - C6*	*galectin*
28	*25.53668*	*22.21152*	*LAR_CNTN1+6*	*Lgmn*	*LAR - C6*	*PIG-K*
19	*29.24923*	*26.31835*	*LAR_CNTN1+6*	*Lrpap1*	*LAR - C6*	*CG8507*
49	*26.92298*	*23.03936*	*PTPRD_CNTN1+6*	*Ltbp3*	*PTPRD - C6*	*frac, dpy*
145	*27.36595*	*22.39017*	*LAR_CNTN1+6*	*Ltbp3*	*LAR - C6*	*frac, dpy*
17	*25.3963*	*22.56957*	*PTPRD_CNTN1+6*	*M6pr*	*PTPRD - C6*	*no significant hit*
98	26.83846	22.24983	PTPRD_CNTN1+6	Mfge8	PTPRD - C6	hml
306	27.89954	22.17464	LAR_CNTN1+6	Mfge8	LAR - C6	hml
17	25.08257	22.23932	LAR_CNTN1+6	Mgp	LAR - C6	no significant hit

12	*24.98802*	*22.46601*	*PTPRD_CNTN1+6*	*Mlec*	*PTPRD - C6*	*cg9257*
14	*32.98019*	*30.31883*	*LAR_CNTN1+6*	*Mlec*	*LAR - C6*	*cg9257*
63	*28.1032*	*23.95673*	*PTPRD_CNTN1+6*	*Mrc2*	*PTPRD - C6*	*tfc, fw, cg12111?*
161	*27.52753*	*22.446*	*LAR_CNTN1+6*	*Mrc2*	*LAR - C6*	*tfc, fw, cg12111?*
425	27.62742	21.57571	PTPRD_CNTN1+6	Mxra7	PTPRD - C2C12	cg7407?
3,090	27.1048	19.06883	PTPRD_CNTN1+6	Oaf	PTPRD - B35	oaf
48	26.73518	22.85765	PTPRD_CNTN1+6	Oaf	PTPRD - C6	oaf
47	26.72806	22.87926	PTPRD_CNTN1+6	Plxnb2	PTPRD - C6	plexa, plexb
49	26.55009	22.66676	LAR_CNTN1+6	Plxnb2	LAR - C6	plexa, plexb
11	*32.6785*	*30.31883*	*PTPRD_CNTN1+6*	*Psap*	*PTPRD - Neuro2a*	*sap-r*
11	*28.9749*	*26.56358*	*LAR_CNTN1+6*	*Psap*	*LAR - C6*	*sap-r*
784,844	35.27284	21.6996	PTPRD_CNTN1+6	Ptprd	PTPRD - B35	
839	29.19387	22.46202	PTPRD_CNTN1+6	Ptprd	PTPRD - C2C12	
282	27.86591	22.2226	PTPRD_CNTN1+6	Ptprd	PTPRD - C6	
12	27.9741	25.49579	PTPRD_CNTN1+6	PTPRD	PTPRD - HEK293	
11	26.88309	24.4576	PTPRD_CNTN1+6	Ptprd	PTPRD - Neuro2a	
59	26.6569	22.58327	LAR_CNTN1+6	Ptprd	LAR - C6	
194,025	34.306	22.13026	LAR_CNTN1+6	Ptprf	LAR - B35	
102,498	33.6345	22.0969	PTPRD_CNTN1+6	Ptprf	PTPRD - B35	
623	28.17455	21.73938	PTPRD_CNTN1+6	Ptprf	PTPRD - C2C12	
245	27.87929	22.37801	PTPRD_CNTN1+6	Ptprf	PTPRD - C6	
12	28.82854	26.37393	PTPRD_CNTN1+6	PTPRF	PTPRD - HEK293	
11	21.59905	19.19614	PTPRD_CNTN1+6	Ptprf	PTPRD - Neuro2a	

27,479	34.13958	23.91841	LAR_CNTN1+6	Ptprf	LAR - C2C12	
598,607	37.06527	23.76291	LAR_CNTN1+6	Ptprf	LAR - C6	
23,097	31.62318	21.57571	LAR_CNTN1+6	PTPRF	LAR - HEK293	
148,840	33.87482	21.96419	LAR_CNTN1+6	Ptprf	LAR - Neuro2a	
24	25.69123	22.52002	PTPRD_CNTN1+6	Serpinc1	PTPRD - C6	spn42Da
29	25.1102	21.7578	LAR_CNTN1+6	Slc1a4	LAR - C6	Eaat1, Eaat2
37	*25.78014*	*22.15934*	*LAR_CNTN1+6*	*Slc1a5*	*LAR - C6*	*Eaat1, Eaat2*
11	26.61246	24.19382	LAR_CNTN1+6	Vps37b	LAR - C6	Vps37b
3,426	31.41986	23.28057	PTPRD_CNTN1+6	Vwa1	PTPRD - B35	no significant hit

REFERENCES

(1) Kaneko, T.; Joshi, R.; Feller, S. M.; Li, S. S. Phosphotyrosine Recognition Domains: The Typical, the Atypical and the Versatile. *Cell Commun. Signal. CCS* **2012**, *10*, 32.

(2) Pawson, T. Specificity in Signal Transduction: From Phosphotyrosine-SH2 Domain Interactions to Complex Cellular Systems. *Cell* **2004**, *116* (2), 191–203.

(3) Miller, W. T. Tyrosine Kinase Signaling and the Emergence of Multicellularity. *Biochim. Biophys. Acta* **2012**, *1823* (6), 1053–1057.

(4) Hendriks, W. J. A. J.; Elson, A.; Harroch, S.; Pulido, R.; Stoker, A.; Hertog, J. den. Protein Tyrosine Phosphatases in Health and Disease. *FEBS J.* **2013**, *280* (2), 708–730.

(5) Collett, M. S.; Purchio, A. F.; Erikson, R. L. Avian Sarcoma Virus-Transforming Protein, Pp60src Shows Protein Kinase Activity Specific for Tyrosine. *Nature* **1980**, *285* (5761), 167–169.

(6) Hunter, T.; Sefton, B. M. Transforming Gene Product of Rous Sarcoma Virus Phosphorylates Tyrosine. *Proc. Natl. Acad. Sci. U. S. A.* **1980**, *77* (3), 1311–1315.

(7) Collett, M. S.; Erikson, E.; Purchio, A. F.; Brugge, J. S.; Erikson, R. L. A Normal Cell Protein Similar in Structure and Function to the Avian Sarcoma Virus Transforming Gene Product. *Proc. Natl. Acad. Sci.* **1979**, *76* (7), 3159–3163.

(8) Shalloway, D.; Zelenetz, A. D.; Cooper, G. M. Molecular Cloning and Characterization of the Chicken Gene Homologous to the Transforming Gene of Rous Sarcoma Virus. *Cell* **1981**, *24* (2), 531–541.

(9) Bjorge, J. D.; Jakymiw, A.; Fujita, D. J. Selected Glimpses into the Activation and Function of Src Kinase. *Oncogene* **2000**, *19* (49), 5620–5635.

(10) Stehelin, D.; Guntaka, R. V.; Varmus, H. E.; Bishop, J. M. Purification of DNA Complementary to Nucleotide Sequences Required for Neoplastic Transformation of Fibroblasts by Avian Sarcoma Viruses. *J. Mol. Biol.* **1976**, *101* (3), 349–365.

(11) Xu, W.; Harrison, S. C.; Eck, M. J. Three-Dimensional Structure of the Tyrosine Kinase c-Src. *Nature* **1997**, *385* (6617), 595–602.

(12) Takeya, T.; Hanafusa, H. Structure and Sequence of the Cellular Gene Homologous to the RSV Src Gene and the Mechanism for Generating the Transforming Virus. *Cell* **1983**, *32* (3), 881–890.

(13) Tabernero, L.; Aricescu, A. R.; Jones, E. Y.; Szedlacsek, S. E. Protein Tyrosine Phosphatases: Structure–Function Relationships. *FEBS J.* **2008**, *275* (5), 867–882.

(14) Pulido, R.; Serra-Pagès, C.; Tang, M.; Streuli, M. The LAR/PTP Delta/PTP Sigma Subfamily of Transmembrane Protein-Tyrosine-Phosphatases: Multiple Human LAR, PTP Delta, and PTP Sigma Isoforms Are Expressed in

a Tissue-Specific Manner and Associate with the LAR-Interacting Protein LIP.1. *Proc. Natl. Acad. Sci. U. S. A.* **1995**, *92* (25), 11686–11690.

(15) Streuli, M.; Krueger, N. X.; Tsai, A. Y.; Saito, H. A Family of Receptor-Linked Protein Tyrosine Phosphatases in Humans and Drosophila. *Proc. Natl. Acad. Sci.* **1989**, *86* (22), 8698–8702.

(16) Streuli, M.; Krueger, N. X.; Ariniello, P. D.; Tang, M.; Munro, J. M.; Blattler, W. A.; Adler, D. A.; Disteche, C. M.; Saito, H. Expression of the Receptor-Linked Protein Tyrosine Phosphatase LAR: Proteolytic Cleavage and Shedding of the CAM-like Extracellular Region. *EMBO J.* **1992**, *11* (3), 897–907.

(17) Serra-Pages, C.; Saito, H.; Streuli, M. Mutational Analysis of Proprotein Processing, Subunit Association, and Shedding of the LAR Transmembrane Protein Tyrosine Phosphatase. *J. Biol. Chem.* **1994**, *269* (38), 23632–23641.

(18) Aicher, B.; Lerch, M.; Müller, T.; Schilling, J. Cellular Redistribution of Protein Tyrosine Phosphatases LAR and PTPσ by Inducible Proteolytic Processing. *J. Cell* **1997**.

(19) Ruhe, J. E.; Streit, S.; Hart, S.; Ullrich, A. EGFR Signaling Leads to Downregulation of PTP-LAR via TACE-Mediated Proteolytic Processing. *Cell. Signal.* **2006**, *18* (9), 1515–1527.

(20) Haapasalo, A.; Kim, D. Y.; Carey, B. W.; Turunen, M. K.; Pettingell, W. H.; Kovacs, D. M. Presenilin/γ-Secretase-Mediated Cleavage Regulates Association of Leukocyte-Common Antigen-Related (LAR) Receptor Tyrosine Phosphatase with β-Catenin. *J. Biol. Chem.* **2007**, *282* (12), 9063–9072.

(21) Biersmith, B. H.; Hammel, M.; Geisbrecht, E. R.; Bouyain, S. The Immunoglobulin-like Domains 1 and 2 of the Protein Tyrosine Phosphatase LAR Adopt an Unusual Horseshoe-like Conformation. *J. Mol. Biol.* **2011**, *408* (4), 616–627.

(22) Coles, C. H.; Shen, Y.; Tenney, A. P.; Siebold, C.; Sutton, G. C.; Lu, W.; Gallagher, J. T.; Jones, E. Y.; Flanagan, J. G.; Aricescu, A. R. Proteoglycan-Specific Molecular Switch for RPTPσ Clustering and Neuronal Extension. *Science* **2011**, *332* (6028), 484–488.

(23) Aricescu, A. R.; McKinnell, I. W.; Halfter, W.; Stoker, A. W. Heparan Sulfate Proteoglycans Are Ligands for Receptor Protein Tyrosine Phosphatase. *Mol. Cell. Biol.* **2002**, *22* (6), 1881–1892.

(24) Fox, A. N.; Zinn, K. The Heparan Sulfate Proteoglycan Syndecan Is an In Vivo Ligand for the Drosophila LAR Receptor Tyrosine Phosphatase. *Curr. Biol.* **2005**, *15* (19), 1701–1711.

(25) Johnson, K. G.; Tenney, A. P.; Ghose, A.; Duckworth, A. M.; Higashi, M. E.; Parfitt, K.; Marcu, O.; Heslip, T. R.; Marsh, J. L.; Schwarz, T. L.; et al. The HSPGs Syndecan and Dallylike Bind the Receptor Phosphatase LAR and Exert Distinct Effects on Synaptic Development. *Neuron* **2006**, *49* (4), 517–531.

(26) Shen, Y.; Tenney, A. P.; Busch, S. A.; Horn, K. P.; Cuascut, F. X.; Liu, K.; He, Z.; Silver, J.; Flanagan, J. G. PTPσ Is a Receptor for Chondroitin Sulfate Proteoglycan, an Inhibitor of Neural Regeneration. *Science* **2009**, *326* (5952), 592–596.

(27) Choi, Y.; Nam, J.; Whitcomb, D. J.; Song, Y. S.; Kim, D.; Jeon, S.; Um, J. W.; Lee, S.-G.; Woo, J.; Kwon, S.-K.; et al. SALM5 Trans-Synaptically Interacts with LAR-RPTPs in a Splicing-Dependent Manner to Regulate Synapse Development. *Sci. Rep.* **2016**, *6*.

(28) Li, Y.; Zhang, P.; Choi, T.-Y.; Park, S. K.; Park, H.; Lee, E.-J.; Lee, D.; Roh, J. D.; Mah, W.; Kim, R.; et al. Splicing-Dependent Trans-Synaptic SALM3–LAR-RPTP Interactions Regulate Excitatory Synapse Development and Locomotion. *Cell Rep.* **2015**, *12* (10), 1618–1630.

(29) Takahashi, H.; Arstikaitis, P.; Prasad, T.; Bartlett, T. E.; Wang, Y. T.; Murphy, T. H.; Craig, A. M. Postsynaptic TrkC and Presynaptic PTPσ Function as a Bidirectional Excitatory Synaptic Organizing Complex. *Neuron* **2011**, *69* (2), 287–303.

(30) Um, J. W.; Kim, K. H.; Park, B. S.; Choi, Y.; Kim, D.; Kim, C. Y.; Kim, S. J.; Kim, M.; Ko, J. S.; Lee, S.-G.; et al. Structural Basis for LAR-RPTP/Slitrk Complex-Mediated Synaptic Adhesion. *Nat. Commun.* **2014**, *5*, 5423.

(31) Yamagata, A.; Sato, Y.; Goto-Ito, S.; Uemura, T.; Maeda, A.; Shiroshima, T.; Yoshida, T.; Fukai, S. Structure of Slitrk2–PTPδ Complex Reveals Mechanisms for Splicing-Dependent Trans-Synaptic Adhesion. *Sci. Rep.* **2015**, *5*.

(32) Yim, Y. S.; Kwon, Y.; Nam, J.; Yoon, H. I.; Lee, K.; Kim, D. G.; Kim, E.; Kim, C. H.; Ko, J. Slitrks Control Excitatory and Inhibitory Synapse Formation with LAR Receptor Protein Tyrosine Phosphatases. *Proc. Natl. Acad. Sci.* **2013**, *110* (10), 4057–4062.

(33) Yoshida, T.; Yasumura, M.; Uemura, T.; Lee, S.-J.; Ra, M.; Taguchi, R.; Iwakura, Y.; Mishina, M. IL-1 Receptor Accessory Protein-Like 1 Associated with Mental Retardation and Autism Mediates Synapse Formation by Trans-Synaptic Interaction with Protein Tyrosine Phosphatase δ. *J. Neurosci.* **2011**, *31* (38), 13485–13499.

(34) Yoshida, T.; Shiroshima, T.; Lee, S.-J.; Yasumura, M.; Uemura, T.; Chen, X.; Iwakura, Y.; Mishina, M. Interleukin-1 Receptor Accessory Protein Organizes Neuronal Synaptogenesis as a Cell Adhesion Molecule. *J. Neurosci.* **2012**, *32* (8), 2588–2600.

(35) Song, Y. S.; Lee, H.-J.; Prosselkov, P.; Itohara, S.; Kim, E. Trans-Induced Cis Interaction in the Tripartite NGL-1, Netrin-G1 and LAR Adhesion Complex Promotes Development of Excitatory Synapses. *J Cell Sci* **2013**, *126* (21), 4926–4938.

(36) O'Grady, P.; Krueger, N. X.; Streuli, M.; Saito, H. Genomic Organization of the Human LAR Protein Tyrosine Phosphatase Gene and Alternative Splicing in the Extracellular Fibronectin Type-III Domains. *J. Biol. Chem.* **1994**, *269* (40), 25193–25199.

(37) Yang, T.; Bernabeu, R.; Xie, Y.; Zhang, J. S.; Massa, S. M.; Rempel, H. C.; Longo, F. M. Leukocyte Antigen-Related Protein Tyrosine Phosphatase Receptor: A Small Ectodomain Isoform Functions as a Homophilic Ligand and Promotes Neurite Outgrowth. *J. Neurosci.* **2003**, *23* (8), 3353–3363.
(38) Wang, J.; Bixby, J. L. Receptor Tyrosine Phosphatase-δ Is a Homophilic, Neurite-Promoting Cell Adhesion Molecule for CNS Neurons. *Mol. Cell. Neurosci.* **1999**, *14* (4), 370–384.
(39) Takahashi, H.; Craig, A. M. Protein Tyrosine Phosphatases PTPδ, PTPσ, and LAR: Presynaptic Hubs for Synapse Organization. *Trends Neurosci.* **2013**, *36* (9), 522–534.
(40) Desai, C. J.; Popova, E.; Zinn, K. A Drosophila Receptor Tyrosine Phosphatase Expressed in the Embryonic CNS and Larval Optic Lobes Is a Member of the Set of Proteins Bearing the "HRP" Carbohydrate Epitope. *J. Neurosci.* **1994**, *14* (12), 7272–7283.
(41) Hariharan, I. K.; Chuang, P. T.; Rubin, G. M. Cloning and Characterization of a Receptor-Class Phosphotyrosine Phosphatase Gene Expressed on Central Nervous System Axons in Drosophila Melanogaster. *Proc. Natl. Acad. Sci. U. S. A.* **1991**, *88* (24), 11266–11270.
(42) Krueger, N. X.; Saito, H. A Human Transmembrane Protein-Tyrosine-Phosphatase, PTP Zeta, Is Expressed in Brain and Has an N-Terminal Receptor Domain Homologous to Carbonic Anhydrases. *Proc. Natl. Acad. Sci. U. S. A.* **1992**, *89* (16), 7417–7421.
(43) Pulido, R.; Krueger, N. X.; Serra-Pagès, C.; Saito, H.; Streuli, M. Molecular Characterization of the Human Transmembrane Protein-Tyrosine Phosphatase δ EVIDENCE FOR TISSUE-SPECIFIC EXPRESSION OF ALTERNATIVE HUMAN TRANSMEMBRANE PROTEIN-TYROSINE PHOSPHATASE δ ISOFORMS. *J. Biol. Chem.* **1995**, *270* (12), 6722–6728.
(44) Tian, S.-S.; Tsoulfas, P.; Zinn, K. Three Receptor-Linked Protein-Tyrosine Phosphatases Are Selectively Expressed on Central Nervous System Axons in the Drosophila Embryo. *Cell* **1991**, *67* (4), 675–685.
(45) Yang, X.; Seow, K. T.; Bahri, S. M.; Oon, S. H.; Chia, W. Two Drosophila Receptor-like Tyrosine Phosphatase Genes Are Expressed in a Subset of Developing Axons and Pioneer Neurons in the Embryonic CNS. *Cell* **1991**, *67* (4), 661–673.
(46) Hatzihristidis, T.; Desai, N.; Hutchins, A. P.; Meng, T.-C.; Tremblay, M. L.; Miranda-Saavedra, D. A Drosophila-Centric View of Protein Tyrosine Phosphatases. *FEBS Lett.* **2015**, *589* (9), 951–966.
(47) Schindelholz, B.; Knirr, M.; Warrior, R.; Zinn, K. Regulation of CNS and Motor Axon Guidance in Drosophila by the Receptor Tyrosine Phosphatase DPTP52F. *Development* **2001**, *128* (21), 4371–4382.
(48) Desai, C. J.; Gindhart, J. G.; Goldstein, L. S. B.; Zinn, K. Receptor Tyrosine Phosphatases Are Required for Motor Axon Guidance in the Drosophila Embryo. *Cell* **1996**, *84* (4), 599–609.

(49) Krueger, N. X.; Vactor, D. V.; Wan, H. I.; Gelbart, W. M.; Goodman, C. S.; Saito, H. The Transmembrane Tyrosine Phosphatase DLAR Controls Motor Axon Guidance in Drosophila. *Cell* **1996**, *84* (4), 611–622.
(50) Desai, C. J.; Krueger, N. X.; Saito, H.; Zinn, K. Competition and Cooperation among Receptor Tyrosine Phosphatases Control Motoneuron Growth Cone Guidance in Drosophila. *Development* **1997**, *124* (10), 1941–1952.
(51) Sun, Q.; Bahri, S.; Schmid, A.; Chia, W.; Zinn, K. Receptor Tyrosine Phosphatases Regulate Axon Guidance across the Midline of the Drosophila Embryo. *Development* **2000**, *127* (4), 801–812.
(52) Sun, Q.; Schindelholz, B.; Knirr, M.; Schmid, A.; Zinn, K. Complex Genetic Interactions among Four Receptor Tyrosine Phosphatases Regulate Axon Guidance in Drosophila. *Mol. Cell. Neurosci.* **2001**, *17* (2), 274–291.
(53) Omotade, O. F.; Pollitt, S. L.; Zheng, J. Q. Actin-Based Growth Cone Motility and Guidance. *Mol. Cell. Neurosci.* **2017**, *84*, 4–10.
(54) Wills, Z.; Bateman, J.; Korey, C. A.; Comer, A.; Vactor, D. V. The Tyrosine Kinase Abl and Its Substrate Enabled Collaborate with the Receptor Phosphatase Dlar to Control Motor Axon Guidance. *Neuron* **1999**, *22* (2), 301–312.
(55) Ahern-Djamali, S. M.; Bachmann, C.; Hua, P.; Reddy, S. K.; Kastenmeier, A. S.; Walter, U.; Hoffmann, F. M. Identification of Profilin and Src Homology 3 Domains as Binding Partners for Drosophila Enabled. *Proc. Natl. Acad. Sci. U. S. A.* **1999**, *96* (9), 4977–4982.
(56) Wills, Z.; Marr, L.; Zinn, K.; Goodman, C. S.; Vactor, D. V. Profilin and the Abl Tyrosine Kinase Are Required for Motor Axon Outgrowth in the Drosophila Embryo. *Neuron* **1999**, *22* (2), 291–299.
(57) Bateman, J.; Shu, H.; Vactor, D. V. The Guanine Nucleotide Exchange Factor Trio Mediates Axonal Development in the Drosophila Embryo. *Neuron* **2000**, *26* (1), 93–106.
(58) Liebl, E. C.; Forsthoefel, D. J.; Franco, L. S.; Sample, S. H.; Hess, J. E.; Cowger, J. A.; Chandler, M. P.; Shupert, A. M.; Seeger, M. A. Dosage-Sensitive, Reciprocal Genetic Interactions between the Abl Tyrosine Kinase and the Putative GEF Trio Reveal Trio's Role in Axon Pathfinding. *Neuron* **2000**, *26* (1), 107–118.
(59) Maurel-Zaffran, C.; Suzuki, T.; Gahmon, G.; Treisman, J. E.; Dickson, B. J. Cell-Autonomous and -Nonautonomous Functions of LAR in R7 Photoreceptor Axon Targeting. *Neuron* **2001**, *32* (2), 225–235.
(60) Clandinin, T. R.; Lee, C.-H.; Herman, T.; Lee, R. C.; Yang, A. Y.; Ovasapyan, S.; Zipursky, S. L. Drosophila LAR Regulates R1-R6 and R7 Target Specificity in the Visual System. *Neuron* **2001**, *32* (2), 237–248.
(61) Prakash, S.; Maclendon, H.; Dubreuil, C. I.; Ghose, A.; Hwa, J.; Dennehy, K. A.; Tomalty, K. M. H.; Clark, K.; Van Vactor, D.; Clandinin, T. R. Complex Interactions amongst N-Cadherin, DLAR, and Liprin-α Regulate Drosophila Photoreceptor Axon Targeting. *Dev. Biol.* **2009**, *336* (1), 10–19.

(62) Serra-Pagès, C.; Kedersha, N. L.; Fazikas, L.; Medley, Q.; Debant, A.; Streuli, M. The LAR Transmembrane Protein Tyrosine Phosphatase and a Coiled-Coil LAR-Interacting Protein Co-Localize at Focal Adhesions. *EMBO J.* **1995**, *14* (12), 2827–2838.
(63) Kaufmann, N.; DeProto, J.; Ranjan, R.; Wan, H.; Vactor, D. V. Drosophila Liprin-α and the Receptor Phosphatase Dlar Control Synapse Morphogenesis. *Neuron* **2002**, *34* (1), 27–38.
(64) Uetani, N.; Chagnon, M. J.; Kennedy, T. E.; Iwakura, Y.; Tremblay, M. L. Mammalian Motoneuron Axon Targeting Requires Receptor Protein Tyrosine Phosphatases σ and δ. *J. Neurosci.* **2006**, *26* (22), 5872–5880.
(65) Schaapveld, R. Q. J.; Schepens, J. T. G.; Bächner, D.; Attema, J.; Wieringa, B.; Jap, P. H. K.; Hendriks, W. J. A. J. Developmental Expression of the Cell Adhesion Molecule-like Protein Tyrosine Phosphatases LAR, RPTPδ and RPTPσ in the Mouse. *Mech. Dev.* **1998**, *77* (1), 59–62.
(66) Brand, A. H.; Perrimon, N. Targeted Gene Expression as a Means of Altering Cell Fates and Generating Dominant Phenotypes. *Development* **1993**, *118* (2), 401–415.
(67) Ervasti, J. M. Costameres: The Achilles' Heel of Herculean Muscle. *J. Biol. Chem.* **2003**, *278* (16), 13591–13594.
(68) Barresi, R.; Campbell, K. P. Dystroglycan: From Biosynthesis to Pathogenesis of Human Disease. *J. Cell Sci.* **2006**, *119* (2), 199–207.
(69) Häuselmann, S. P.; Rosc-Schlüter, B. I.; Lorenz, V.; Plaisance, I.; Brink, M.; Pfister, O.; Kuster, G. M. B1-Integrin Is up-Regulated via Rac1-Dependent Reactive Oxygen Species as Part of the Hypertrophic Cardiomyocyte Response. *Free Radic. Biol. Med.* **2011**, *51* (3), 609–618.
(70) Hynes, R. O. Integrins: Bidirectional, Allosteric Signaling Machines. *Cell* **2002**, *110* (6), 673–687.
(71) Maartens, A. P.; Brown, N. H. Chapter Seven - Anchors and Signals: The Diverse Roles of Integrins in Development. In *Current Topics in Developmental Biology*; Yap, A. S., Ed.; Cellular Adhesion in Development and Disease; Academic Press, 2015; Vol. 112, pp 233–272.
(72) Kapp, T. G.; Rechenmacher, F.; Neubauer, S.; Maltsev, O. V.; Cavalcanti-Adam, E. A.; Zarka, R.; Reuning, U.; Notni, J.; Wester, H.-J.; Mas-Moruno, C.; et al. A Comprehensive Evaluation of the Activity and Selectivity Profile of Ligands for RGD-Binding Integrins. *Sci. Rep.* **2017**, *7*, 39805.
(73) Narasimha, M.; Brown, N. H. *Integrins and Associated Proteins in Drosophila Development*; Landes Bioscience, 2013.
(74) Schöck, F.; Perrimon, N. Retraction of the Drosophila Germ Band Requires Cell–Matrix Interaction. *Genes Dev.* **2003**, *17* (5), 597–602.
(75) Gotwals, P. J.; Fessler, L. I.; Wehrli, M.; Hynes, R. O. Drosophila PS1 Integrin Is a Laminin Receptor and Differs in Ligand Specificity from PS2. *Proc. Natl. Acad. Sci. U. S. A.* **1994**, *91* (24), 11447–11451.

(76) Subramanian, A.; Wayburn, B.; Bunch, T.; Volk, T. Thrombospondin-Mediated Adhesion Is Essential for the Formation of the Myotendinous Junction in Drosophila. *Development* **2007**, *134* (7), 1269–1278.
(77) Frantz, C.; Stewart, K. M.; Weaver, V. M. The Extracellular Matrix at a Glance. *J. Cell Sci.* **2010**, *123* (24), 4195–4200.
(78) Takada, Y.; Ye, X.; Simon, S. The Integrins. *Genome Biol.* **2007**, *8* (5), 215.
(79) Campbell, I. D.; Humphries, M. J. Integrin Structure, Activation, and Interactions. *Cold Spring Harb. Perspect. Biol.* **2011**, *3* (3), a004994.
(80) Takagi, J.; Petre, B. M.; Walz, T.; Springer, T. A. Global Conformational Rearrangements in Integrin Extracellular Domains in Outside-In and Inside-Out Signaling. *Cell* **2002**, *110* (5), 599–611.
(81) Bulgakova, N. A.; Klapholz, B.; Brown, N. H. Cell Adhesion in Drosophila: Versatility of Cadherin and Integrin Complexes during Development. *Curr. Opin. Cell Biol.* **2012**, *24* (5).
(82) Schoenwaelder, S. M.; Burridge, K. Bidirectional Signaling between the Cytoskeleton and Integrins. *Curr. Opin. Cell Biol.* **1999**, *11* (2), 274–286.
(83) Bogaert, T.; Brown, N.; Wilcox, M. The Drosophila PS2 Antigen Is an Invertebrate Integrin That, like the Fibronectin Receptor, Becomes Localized to Muscle Attachments. *Cell* **1987**.
(84) Leptin, M.; Lehmann, R.; Bogaert, T.; Wilcox, M. The Function of PS Integrins during Drosophila Embryogenesis. *Cell* **1989**.
(85) Volk, T.; Fessler, L. I.; Fessler, J. H. A Role for Integrin in the Formation of Sarcomeric Cytoarchitecture. *Cell* **1990**, *63* (3), 525–536.
(86) Bökel, C.; Brown, N. H. Integrins in Development: Moving on, Responding to, and Sticking to the Extracellular Matrix. *Dev. Cell* **2002**, *3* (3), 311–321.
(87) LaBeau-DiMenna, E. M.; Clark, K. A.; Bauman, K. D.; Parker, D. S.; Cripps, R. M.; Geisbrecht, E. R. Thin, a Trim32 Ortholog, Is Essential for Myofibril Stability and Is Required for the Integrity of the Costamere in Drosophila. *Proc. Natl. Acad. Sci. U. S. A.* **2012**, *109* (44), 17983–17988.
(88) Abmayr, S. M.; Zhuang, S.; Geisbrecht, E. R. Myoblast Fusion in Drosophila. *Methods Mol. Biol. Clifton NJ* **2008**, *475*, 75–97.
(89) Brooks, D. S.; Vishal, K.; Kawakami, J.; Bouyain, S.; Geisbrecht, E. R. Optimization of WrMTrck to Monitor Drosophila Larval Locomotor Activity. *J. Insect Physiol.* **2016**, *93–94*, 11–17.
(90) Perkins, A. D.; Lee, M. J. J.; Tanentzapf, G. The Systematic Identification of Cytoskeletal Genes Required for Drosophila Melanogaster Muscle Maintenance. *Sci. Data* **2014**, *1*.
(91) Bouyain, S.; Watkins, D. J. The Protein Tyrosine Phosphatases PTPRZ and PTPRG Bind to Distinct Members of the Contactin Family of Neural Recognition Molecules. *Proc. Natl. Acad. Sci. U. S. A.* **2010**, *107* (6), 2443–2448.
(92) Schmidt, T. G. M.; Batz, L.; Bonet, L.; Carl, U.; Holzapfel, G.; Kiem, K.; Matulewicz, K.; Niermeier, D.; Schuchardt, I.; Stanar, K. Development of the Twin-Strep-Tag® and Its Application for Purification of Recombinant

Proteins from Cell Culture Supernatants. *Protein Expr. Purif.* **2013**, *92* (1), 54–61.
(93) Otwinowski, Z.; Minor, W. Processing of X-Ray Diffraction Data Collected in Oscillation Mode. *Methods Enzymol.* **1997**, *276*, 307–326.
(94) Adams, P. D.; Afonine, P. V.; Bunkóczi, G.; Chen, V. B.; Davis, I. W.; Echols, N.; Headd, J. J.; Hung, L.-W.; Kapral, G. J.; Grosse-Kunstleve, R. W.; et al. PHENIX: A Comprehensive Python-Based System for Macromolecular Structure Solution. *Acta Crystallogr. D Biol. Crystallogr.* **2010**, *66* (Pt 2), 213–221.
(95) Emsley, P.; Cowtan, K. Coot: Model-Building Tools for Molecular Graphics. *Acta Crystallogr. D Biol. Crystallogr.* **2004**, *60* (Pt 12 Pt 1), 2126–2132.
(96) Bate, M. The Embryonic Development of Larval Muscles in Drosophila. *Development* **1990**, *110* (3), 791–804.
(97) Folker, E. S.; Baylies, M. K. Nuclear Positioning in Muscle Development and Disease. *Front. Physiol.* **2013**, *4*.
(98) Bateman, J.; Reddy, R. S.; Saito, H.; Van Vactor, D. The Receptor Tyrosine Phosphatase Dlar and Integrins Organize Actin Filaments in the Drosophila Follicular Epithelium. *Curr. Biol.* **2001**.
(99) Duffy, J. B.; Harrison, D. A.; Perrimon, N. Identifying Loci Required for Follicular Patterning Using Directed Mosaics. *Development* **1998**, *125* (12), 2263–2271.
(100) Zeidler, M. P.; Tan, C.; Bellaiche, Y.; Cherry, S.; Häder, S.; Gayko, U.; Perrimon, N. Temperature-Sensitive Control of Protein Activity by Conditionally Splicing Inteins. *Nat. Biotechnol.* **2004**, *22* (7), 871–876.
(101) Brown, N. H. Null Mutations in the Alpha PS2 and Beta PS Integrin Subunit Genes Have Distinct Phenotypes. *Development* **1994**, *120* (5), 1221–1231.
(102) Klapholz, B.; Brown, N. H. Talin – the Master of Integrin Adhesions. *J. Cell Sci.* **2017**, *130* (15), 2435–2446.
(103) Rees, D. J. G.; Ades, S. E.; Singer, S. J.; Hynes, R. O. Sequence and Domain Structure of Talin. *Nat. Lond.* **1990**, *347* (6294), 685–689.
(104) Calderwood, D. A.; Yan, B.; Pereda, J. M. de; Alvarez, B. G.; Fujioka, Y.; Liddington, R. C.; Ginsberg, M. H. The Phosphotyrosine Binding-like Domain of Talin Activates Integrins. *J. Biol. Chem.* **2002**, *277* (24), 21749–21758.
(105) Fillingham, I.; Gingras, A. R.; Papagrigoriou, E.; Patel, B.; Emsley, J.; Critchley, D. R.; Roberts, G. C. K.; Barsukov, I. L. A Vinculin Binding Domain from the Talin Rod Unfolds to Form a Complex with the Vinculin Head. *Structure* **2005**, *13* (1), 65–74.
(106) Gingras, A. R.; Bate, N.; Goult, B. T.; Patel, B.; Kopp, P. M.; Emsley, J.; Barsukov, I. L.; Roberts, G. C. K.; Critchley, D. R. Central Region of Talin Has a Unique Fold That Binds Vinculin and Actin. *J. Biol. Chem.* **2010**, *285* (38), 29577–29587.

(107) Yao, M.; Goult, B. T.; Chen, H.; Cong, P.; Sheetz, M. P.; Yan, J. Mechanical Activation of Vinculin Binding to Talin Locks Talin in an Unfolded Conformation. *Sci. Rep.* **2014**, *4*, 4610.
(108) Anthis, N. J.; Haling, J. R.; Oxley, C. L.; Memo, M.; Wegener, K. L.; Lim, C. J.; Ginsberg, M. H.; Campbell, I. D. β Integrin Tyrosine Phosphorylation Is a Conserved Mechanism for Regulating Talin-Induced Integrin Activation. *J. Biol. Chem.* **2009**, *284* (52), 36700–36710.
(109) Oxley, C. L.; Anthis, N. J.; Lowe, E. D.; Vakonakis, I.; Campbell, I. D.; Wegener, L. An Integrin Phosphorylation Switch THE EFFECT OF B3 INTEGRIN TAIL PHOSPHORYLATION ON DOK1 AND TALIN BINDING. *J. Biol. Chem.* **2008**, *283* (9), 5420–5426.
(110) Tadokoro, S.; Shattil, S. J.; Eto, K.; Tai, V.; Liddington, R. C.; de Pereda, J. M.; Ginsberg, M. H.; Calderwood, D. A. Talin Binding to Integrin β Tails: A Final Common Step in Integrin Activation. *Science* **2003**, *302* (5642), 103–106.
(111) Brown, N. H.; Gregory, S. L.; Rickoll, W. L.; Fessler, L. I.; Prout, M.; White, R. A. H.; Fristrom, J. W. Talin Is Essential for Integrin Function in Drosophila. *Dev. Cell* **2002**, *3* (4), 569–579.
(112) Bécam, I. E.; Tanentzapf, G.; Lepesant, J.-A.; Brown, N. H.; Huynh, J.-R. Integrin-Independent Repression of Cadherin Transcription by Talin during Axis Formation in *Drosophila*. *Nat. Cell Biol.* **2005**, *7* (5), 510–516.
(113) Debant, A.; Serra-Pages, C.; Seipel, K.; O'Brien, S.; Tang, M.; Park, S. H.; Streuli, M. The Multidomain Protein Trio Binds the LAR Transmembrane Tyrosine Phosphatase, Contains a Protein Kinase Domain, and Has Separate Rac-Specific and Rho-Specific Guanine Nucleotide Exchange Factor Domains. *Proc. Natl. Acad. Sci.* **1996**, *93* (11), 5466–5471.
(114) Forsthoefel, D. J.; Liebl, E. C.; Kolodziej, P. A.; Seeger, M. A. The Abelson Tyrosine Kinase, the Trio GEF and Enabled Interact with the Netrin Receptor Frazzled in Drosophila. *Development* **2005**, *132* (8), 1983–1994.
(115) O'Brien, S. P.; Seipel, K.; Medley, Q. G.; Bronson, R.; Segal, R.; Streuli, M. Skeletal Muscle Deformity and Neuronal Disorder in Trio Exchange Factor-Deficient Mouse Embryos. *Proc. Natl. Acad. Sci.* **2000**, *97* (22), 12074–12078.
(116) Bateman, J.; Shu, H.; Van, D. V. The Guanine Nucleotide Exchange Factor Trio Mediates Axonal Development in the Drosophila Embryo. *Neuron* **2000**, *26* (1), 93–106.
(117) Newsome, T. P.; Schmidt, S.; Dietzl, G.; Keleman, K.; Åsling, B.; Debant, A.; Dickson, B. J. Trio Combines with Dock to Regulate Pak Activity during Photoreceptor Axon Pathfinding in Drosophila. *Cell* **2000**, *101* (3), 283–294.
(118) Olson, P. F.; Fessler, L. I.; Nelson, R. E.; Sterne, R. E.; Campbell, A. G.; Fessler, J. H. Glutactin, a Novel Drosophila Basement Membrane-Related Glycoprotein with Sequence Similarity to Serine Esterases. *EMBO J.* **1990**, *9* (4), 1219–1227.

(119) Scholl, F. G.; Scheiffele, P. Making Connections: Cholinesterase-Domain Proteins in the CNS. *Trends Neurosci.* **2003**, *26* (11), 618–624.
(120) Inaki, M.; Yoshikawa, S.; Thomas, J. B.; Aburatani, H.; Nose, A. Wnt4 Is a Local Repulsive Cue That Determines Synaptic Target Specificity. *Curr. Biol. CB* **2007**, *17* (18), 1574–1579.
(121) Ball, E.; Ball, S. P.; Sparrow, J. C. A Mutation Affecting Larval Muscle Development in Drosophila Melanogaster. *Dev. Genet.* **1985**, *6* (2), 77–92.
(122) Krueger, N. X.; Reddy, R. S.; Johnson, K.; Bateman, J.; Kaufmann, N.; Scalice, D.; van Vactor, D.; Saito, H. Functions of the Ectodomain and Cytoplasmic Tyrosine Phosphatase Domains of Receptor Protein Tyrosine Phosphatase Dlar In Vivo. *Mol. Cell. Biol.* **2003**, *23* (19), 6909–6921.
(123) Clark, K. A.; Bland, J. M.; Beckerle, M. C. The Drosophila Muscle LIM Protein, Mlp84B, Cooperates with D-Titin to Maintain Muscle Structural Integrity. *J. Cell Sci.* **2007**, *120* (12), 2066–2077.
(124) Haines, N.; Seabrooke, S.; Stewart, B. A. Dystroglycan and Protein O-Mannosyltransferases 1 and 2 Are Required to Maintain Integrity of Drosophila Larval Muscles. *Mol. Biol. Cell* **2007**, *18* (12), 4721–4730.
(125) Pierschbacher, M. D.; Ruoslahti, E. Cell Attachment Activity of Fibronectin Can Be Duplicated by Small Synthetic Fragments of the Molecule. *Nature* **1984**, *309* (5963), 30–33.
(126) Pierschbacher, M.; Hayman, E. G.; Ruoslahti, E. Synthetic Peptide with Cell Attachment Activity of Fibronectin. *Proc. Natl. Acad. Sci.* **1983**, *80* (5), 1224–1227.
(127) Pankov, R.; Yamada, K. M. Fibronectin at a Glance. *J. Cell Sci.* **2002**, *115* (20), 3861–3863.
(128) Bork, P.; Doolittle, R. F. Proposed Acquisition of an Animal Protein Domain by Bacteria. *Proc. Natl. Acad. Sci. U. S. A.* **1992**, *89* (19), 8990–8994.
(129) Kvansakul, M.; Adams, J. C.; Hohenester, E. Structure of a Thrombospondin C-Terminal Fragment Reveals a Novel Calcium Core in the Type 3 Repeats. *EMBO J.* **2004**, *23* (6), 1223–1233.
(130) Blindauer, C. A.; Harvey, I.; Bunyan, K. E.; Stewart, A. J.; Sleep, D.; Harrison, D. J.; Berezenko, S.; Sadler, P. J. Structure, Properties, and Engineering of the Major Zinc Binding Site on Human Albumin. *J. Biol. Chem.* **2009**, *284* (34), 23116–23124.
(131) Leahy, D. J.; Aukhil, I.; Erickson, H. P. 2.0 Å Crystal Structure of a Four-Domain Segment of Human Fibronectin Encompassing the RGD Loop and Synergy Region. *Cell* **1996**, *84* (1), 155–164.
(132) Craig, D.; Gao, M.; Schulten, K.; Vogel, V. Tuning the Mechanical Stability of Fibronectin Type III Modules through Sequence Variations. *Structure* **2004**, *12* (1), 21–30.
(133) Cox, J.; Mann, M. MaxQuant Enables High Peptide Identification Rates, Individualized p.p.b.-Range Mass Accuracies and Proteome-Wide Protein Quantification. *Nat. Biotechnol.* **2008**, *26* (12), 1367–1372.

(134) Cox, J.; Hein, M. Y.; Luber, C. A.; Paron, I.; Nagaraj, N.; Mann, M. Accurate Proteome-Wide Label-Free Quantification by Delayed Normalization and Maximal Peptide Ratio Extraction, Termed MaxLFQ. *Mol. Cell. Proteomics* **2014**, *13* (9), 2513–2526.
(135) Pastor-Pareja, J. C.; Xu, T. Shaping Cells and Organs in Drosophila by Opposing Roles of Fat Body-Secreted Collagen IV and Perlecan. *Dev. Cell* **2011**, *21* (2), 245–256.
(136) Guiraud, S.; Migeon, T.; Ferry, A.; Chen, Z.; Ouchelouche, S.; Verpont, M.-C.; Sado, Y.; Allamand, V.; Ronco, P.; Plaisier, E. HANAC Col4a1 Mutation in Mice Leads to Skeletal Muscle Alterations Due to a Primary Vascular Defect. *Am. J. Pathol.* **2017**, *187* (3), 505–516.
(137) Kamimura, K.; Ueno, K.; Nakagawa, J.; Hamada, R.; Saitoe, M.; Maeda, N. Perlecan Regulates Bidirectional Wnt Signaling at the Drosophila Neuromuscular Junction. *J Cell Biol* **2013**, *200* (2), 219–233.
(138) Reynolds, B.; Roversi, P.; Laynes, R.; Kazi, S.; Boyd, R.; Goberdhan, D. C. I. Drosophila Expresses a CD98 Transporter with Evolutionarily Conserved Structure and Amino Acid Transport Properties. *Biochem. J.* **2009**, *420* (3), 363–372.
(139) Fenczik, C. A.; Sethi, T.; Ramos, J. W.; Hughes, P. E.; Ginsberg, M. H. Complementation of Dominant Suppression Implicates CD98 in Integrin Activation. *Nature* **1997**, *390* (6655), 81–85.
(140) Fenczik, C. A.; Zent, R.; Dellos, M.; Calderwood, D. A.; Satriano, J.; Kelly, C.; Ginsberg, M. H. Distinct Domains of CD98hc Regulate Integrins and Amino Acid Transport. *J. Biol. Chem.* **2001**, *276* (12), 8746–8752.
(141) Voulgaraki, D.; Mitnacht-Kraus, R.; Letarte, M.; Foster-Cuevas, M.; Brown, M. H.; Neil Barclay, A. Multivalent Recombinant Proteins for Probing Functions of Leucocyte Surface Proteins Such as the CD200 Receptor. *Immunology* **2005**, *115* (3), 337–346.
(142) Chen, C.-H.; Zhang, X.-Q.; Lo, C.-W.; Liu, P.-F.; Liu, Y.-T.; Gallo, R. L.; Hsieh, M.-F.; Schooley, R. T.; Huang, C.-M. The Essentiality of Alpha-2-Macroglobulin in Human Salivary Innate Immunity against New H1N1 Swine Origin Influenza A Virus. *Proteomics* **2010**, *10* (12), 2396–2401.
(143) Okroj, M.; Holmquist, E.; Sjölander, J.; Corrales, L.; Saxne, T.; Wisniewski, H.-G.; Blom, A. M. Heavy Chains of Inter Alpha Inhibitor (IαI) Inhibit the Human Complement System at Early Stages of the Cascade. *J. Biol. Chem.* **2012**, *287* (24), 20100–20110.
(144) Roney, K.; Holl, E.; Ting, J. Immune Plexins and Semaphorins: Old Proteins, New Immune Functions. *Protein Cell* **2013**, *4* (1), 17–26.
(145) Lopez, W.; Page, A. M.; Carlson, D. J.; Ericson, B. L.; Cserhati, M. F.; Guda, C.; Carlson, K. A. Analysis of Immune-Related Genes during Nora Virus Infection of Drosophila Melanogaster Using next Generation Sequencing. *AIMS Microbiol.* **2018**, *4* (1), 123–139.

(146) Pees, B.; Yang, W.; Zárate-Potes, A.; Schulenburg, H.; Dierking, K. High Innate Immune Specificity through Diversified C-Type Lectin-Like Domain Proteins in Invertebrates. *J. Innate Immun.* **2016**, *8* (2), 129–142.
(147) Hashimoto, N.; Feener, E. P.; Zhang, W. R.; Goldstein, B. J. Insulin Receptor Protein-Tyrosine Phosphatases. Leukocyte Common Antigen-Related Phosphatase Rapidly Deactivates the Insulin Receptor Kinase by Preferential Dephosphorylation of the Receptor Regulatory Domain. *J. Biol. Chem.* **1992**, *267* (20), 13811–13814.
(148) Långberg, E.-C.; Gu, H. F.; Nordman, S.; Efendic, S.; Östenson, C.-G. Genetic Variation in Receptor Protein Tyrosine Phosphatase σ Is Associated with Type 2 Diabetes in Swedish Caucasians. *Eur. J. Endocrinol.* **2007**, *157* (4), 459–464.
(149) Pei, Q.; Huang, Q.; Yang, G.; Zhao, Y.; Yin, J.; Song, M.; Zheng, Y.; Mo, Z.; Zhou, H.; Liu, Z. PPAR-Γ2 and PTPRD Gene Polymorphisms Influence Type 2 Diabetes Patients' Response to Pioglitazone in China. *Acta Pharmacol. Sin.* **2013**, *34* (2), 255–261.

VITA

Jessica Kawakami graduated from the University of Missouri-Kansas City in 2005 with a Bachelor of Science degree in Biology. She worked as a laboratory manager and technician at the University from 2005 – 2011 in the laboratories of Dr. George Thomas, Jr. and Dr. Julia Chekanova. During this time she published two journal articles with Dr. Jim Benevides and Dr. Thomas on mechanisms of drug-DNA and protein-DNA interactions.

In 2011 she began her Doctor of Philosophy degree in Molecular Biology and Biochemistry in the laboratories of Dr. Samuel Bouyain and Dr. Erika Geisbrecht. Her dissertation research was focused on conserved protein interactions of receptor tyrosine phosphatases in muscle tissue. She obtained a pre-doctoral fellowship from the American Heart Association and published one paper with Dr. Bouyain and Dr. Geisbrecht.